ELECTRONIC, MAGNETIC AND STRUCTURAL PROPERTIES OF TRANSITION METAL OXIDE

Thesis submitted for the degree of
Doctor of Philosophy (Science)

in

Physics (Theoretical)

by

Kapil Gupta

Department of Physics
Jadavpur University
November 2012

Dedicated to

My parents
who created me

Prabhat Sir
who moulded me

&

My wife
who nurtured me

CERTIFICATE FROM THE SUPERVISOR

This is to certify that the thesis entitled "**ELERCTRONIC, MAGNETIC AND STRUCTURAL PROPERTIES OF TRANSITION METAL OXIDE**", submitted by Sri **Kapil Gupta**, who got his name registered on August 10, 2009 for the award of the Ph.D. (Science) degree of Jadavpur University, is absolutely based upon his own work under the supervision of Dr. Priya Mahadevan at the S. N. Bose National Centre For Basic Sciences, Kolkata, India and that neither this thesis nor any part of it has been submitted for any degree/diploma or any other academic award anywhere before.

Priya Mahadevan
Associate Professor,
Department of Material Sciences,
S. N. B. National Centre For Basic Sciences,
JD Block, Sector III, Salt Lake City, Kolkata 700 098, India
Date :

Acknowledgments

"Musafir hun yaaro ...." more than a decade has passed since I heard this hindi song for the first time. And ever since I have been able to connect my ownself with this song in some or other way. This song talks about a continuous journey. Some take up a journey to reach some destination, some consider the journey as their destination, I am yet to know which one I am in pursuit of. Well, today a phase of my journey has reached its paramount as my doctorate dissertation has come into its existence.

In the inception, it was my M. Sc. Professor, Dr. Prabhat Kumar who sensitized that "scientific" part of me. It was him who inspired me to think and construct something. I take this opportunity to pay you my greatest of gratitude. Sir, Thanks for owning me.

Not just a customary *thank you* to the thesis supervisor, I intend to submit my sincere and utmost regards to my thesis supervisor Dr. Priya Mahadevan, first as a person and then as a supervisor. Thanks a lot ma'am, for being more than a guide. Your way to grow upon the initial scientific idea, and to cultivate real science out of it has taught me a lot. Moreover your enthusiasm, drive and dedication towards research was what prompted me to improvize upon my capacities. Your dilute doping has made me conducting.

I also thank Dr. Marjana Ležaić, from Peter Grünberg Institut, Forschungszentrum Jülich, Germany, with whom I had an active collaboration. Working with her helped me to widen my knowledge with certain computational tools, I also acknowledge her hospitality that I received during my stay in Jülich. I also thank Prof. Guang Yu Guo and Prof. Chong der Hu, whom I overlapped with during my visit to National Chengchi University and National Taiwan University, in Taipei Taiwan. I will cherish the excellent academic interactions with them as well as their hospitality during my stay over there.

Working in Priya Madam's group, which we call *pmg* fondly has been a great experience in the definitions of academics and otherwise. Hallmark treats in our group, and continuous search for a *reason* for them has always been a point of extreme interest!. My group senior Roby Cherian gave me my first computational lesson. Subhro da, great Ashis da, Abhinav, Hirak were the guys I started with in this group. Abhinav's VIBGYORic rapport with *iron*males, and Hirak's *lemon juice* episodes are quite an interesting events I am going to cherish with me. Then came the newer chaps: the Saikat, the Ruma, the Shishir, the Basudeb and their allotment of *projects* to each other, which were perhaps limited to allotment only most of the times. And yes their system of *G-ranking* for which I perhaps never qualified. Bipul *bhaiya* who never got to have a *mirinda*, at least on papers!. Basudeb's famous *court martial* and consequent nullification of his *G-rank*. And Saikat who whenever is out of country keeps calling back to ma'am at each single step he takes, to make sure that someone has not packed him up in one's suitcase. These are few of countless events which are worth mentioning here. And the latest addition, Azhar and Sagar. I thank all of you to add colours to my life here in S. N. Bose centre over all these years. Our *tea table* I will remember forever, though I seek my apology for being reclusive for a phase. Finally a big thanks to ma'am to bring this sense of "group" in us.

Prashant was the one with whom I landed up in Kolkata, a very good friend, my batch-mate, room-mate for initial years, with whom I shared a pretty good chemisty, until he found his *spin down*. Soumyajit the *gola*, ever gentle and witty Jena ji, Sujoy,Swastika, Sandeep's both the hotter and the cooler, Abhijit, Rajeev, I thank all of you from the very core of my heart for adding up those extra colours in my life. Amartya: who can speak on any topic possible on this earth, *Subhashis*: quite an

List of Publications

1. Strain-driven magnetism in $LaCoO_3$ thin films
   Kapil Gupta and Priya Mahadevan,
   Phys. Rev. B (Rapid Comm.), **79**, 020406(2009).
   Chapter-3 is based on this paper.

2. In search of a two-dimensional metallic oxide
   Priya Mahadevan and Kapil Gupta,
   in "Functional Metal Oxide Nanostructures", (Springer-Verlag)
   ed. J.Wu, W. Han, H. Kim, A. Janotti and J. Cao: ISBN No : 978144199306 (2010).

3. Strain induced ferromagnetic state in an otherwise nonmagnetic oxide
   Kapil Gupta and Priya Mahadevan,
   in "Simulation and characterization of Advanced Materials", (Research signpost)
   ed. Sudhir Kumar (2011)
   Chapter-3 is based on this paper.

4. Self-energy on the low- to high-energy electronic structure of correlated metal $SrVO_3$
   S. Aizaki, T. Yoshida, K. Yoshimatsu, M. Takizawa, M. Minohara, S. Ideta, A. Fujimori,
   K. Gupta, P. Mahadevan, K. Horiba, H. Kumigashira, M. Oshima
   Phys. Rev. Lett., **109**, 056401(2012).

5. Ferroelectric distortions in doped ferroelectrics: $BaTiO_3$:TM (TM=V-Fe)
   Hirak Kumar Chandra, Kapil Gupta, Ashis Kumar Nandy and Priya Mahadevan,
   Submitted

6. Orbital ordering induced ferroelectricity in metallic $SrCrO_3$
   Kapil Gupta, Priya Mahadevan, and Marjana Ležaić,
   Submitted
   Chapter-4 is based on this paper.

7. Strain induced metal-insulator transition in ultrathin films of $SrRuO_3$
   Kapil Gupta, and Priya Mahadevan,
   in preparation
   Chapter-5 is based on this paper.

8. A new route to ferromagnetic and ferroelectric insulator
   Kapil Gupta, and Priya Mahadevan,
   in preparation
   Chapter-6 is based on this paper.

Contents

List of Figures

List of Tables

Chapter 1

Introduction

1.1 Introduction to Transition Metal Oxides

Transition metal oxides are the building blocks of the technology of recent times. Realization of various efficient device applications, be it magnetic storage, magnetic reading, flat panel displays, fuel cells or others, has become possible by harnessing the multifaceted properties of transition metal oxides. Remarkable advances in the growth and characterization techniques have put transition metal oxides at par with the semiconductors, which dominated the technology solely for a long time. Transition metals stand distinct from other metals as they exihibit multiple valence states, allowing their oxides to have the spin, orbital and electronic degress of freedom active in the material. This in turn enables transition metal oxides to exhibit a wealth of functional properties such as superconductivity, piezoelectricity, giant magnetoresistance, spin and metal-insulator transitions. This has led to renewed interest in the transition metal oxides, specially in the perovskite type 3d transition metal oxides[1] .

Transition metal oxides exhibit a range of interesting features, though not all of them are fully understood. Their conductivity ranges from good metals to the insulators. There are Mott-Hubbard, Anderson localization induced insulators, charge-transfer or band insulators. Their magnetic behavior varies from ferromagnetism($SrRuO_3$, $Sr_4Co_3ReO_{12}$ [2], $La_{1/2}Ca_{1/2}MnO_3$[3]) to antiferromagnetism(NiO) to ferrimagnetism(La_2NiMnO_6) to paramagnetism ($SrRhO_3$[4]) to diamagnetism. They exhibit tem-

perature, pressure, applied field or doping tuned spin, orbital and magnetic state which is the origin of most of the functional properties in these oxides. Features of transition metal oxides are not limited to the fundamental physical properties, they show various technologically important properties such as giant magnetoresistance($La_{2/3}Ba_{1/3}MnO_x$ [5]), colossal magnetoresistance(Fe doped La(Ca)MnO$_3$ [6]), ferroelectricity(BaTiO$_3$, PbTiO$_3$), multiferroicity(BiFeO$_3$,TbMnO$_3$) or superconductivity ($La_{2-x}Sr_xCuO_4$) [7].

The wealth of phenomena that one finds in these materials has driven the studies over the past two-three decades. Initially unprecedented temperatures for superconductivity were observed in a family of cuprates [8]. This started the search for new systems in which superconductivity occurs at room temperature. There are other examples of transition metal oxides which show novel electronic and magnetic properties. A larger part of studies are about how one can control and tune these properties with external stimuli. Manganites [9, 10], for instance are examples which show a large change in the resistivity with applied magnetic field, and the phenomena is known as colossal magnetoresistive effect. Although the effect by itself is known since the pioneering work of van Santen and Jonker, the new aspect is the magnitude of the sensitivity. In metals for instance the effect emerges from a field dependent mean free path and is limited to just a few percent. There are other examples of systems where a phase transition is engineered by an electric field or a magnetic field, a very small energy scale in the problem. All this emerges from the fact that the 3d transition oxides comprise a set of systems where the spin, orbital and lattice degrees of freedom [11–15] are all equally important. These interaction strengths compete with each other, resulting in a phase diagram where sometimes a small change in the electronic interaction strengths leaves us in a part of the phase space with entirely different properties(Fig. 1.1).

Another important aspect to understand while examining phenomena in various transition metal oxides is the main electronic interaction which are responsible for their remarkable properties, and how they get modified. Apart from the hopping interaction strengths, key parameters determining the electronic properties of transition metal oxides are the coulomb correlation strength U between the electrons on the d site and the charge transfer energy Δ defined between the oxygen atom and the
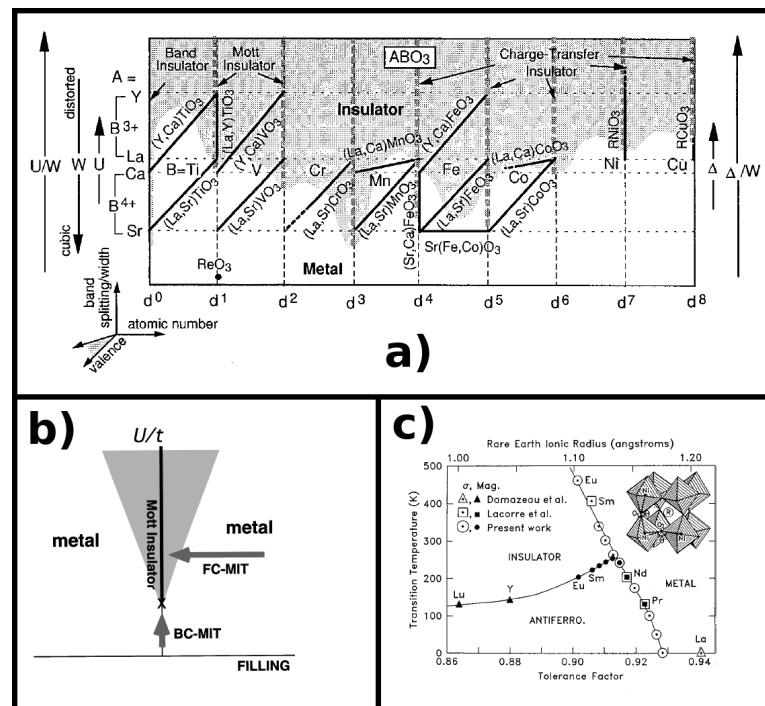
Figure 1.1 Phase diagrams for transition metal oxides with perovskite structure: a)schematic of metal to insulator transition, b) metal to insulator transition based on Hubbard model. Two routes for the MIT (metal-insulator transition) are shown: the FC-MIT (filling-control MIT) and the BC-MIT(bandwidth-control MIT). c) Phase diagram for $RNiO_3$, showing the phase transition with variation of R site ion and hence the tolerance factor.
Fig Ref: M. Imada *et. at.* Rev. Mod. Phys., **70**, 1039(1998).

transition metal atom. This was put on a firm footing by the seminal paper by Zannen, Sawatzky and Allen[16]. Within an Anderson impurity Hamiltonian it was shown that for $\Delta < U$, the bandgap scales with the smaller energy scale Δ and systems in this regime are called charge transfer insulators. For $\Delta > U$, the band gap scales with U and these systems are called Mott-Hubbard insulators.

The electron interaction strength can be controlled by modifying the lattice parameters or the chemical composition while essentially maintaining the original lattice structure. The on-site Coulomb interaction U is kept almost unchanged during the above procedure and hence control of electron correlation strength is usually achieved by control of the hopping interaction (t) or the one-electron bandwidth (W). One method of controlling W is the application of pressure. An application of hydrostatic pressure decreases the interatomic distance and hence increases the hopping strengths. Pressure-induced

Mott-insulator to metal transitions are observed typically for V_2O_3 and $RNiO_3$ (R:Pr and Nd). Hydrostatic pressure is an ideal perturbation that modifies W and that is suitable for investigating the critical behavior of the phase transition. Another method of W control is modification of the chemical composition. In the case of transition-metal oxides the electron correlation arises from a narrow d band. Another useful method of W control specially for a perovskite type compound (ABO_3) is modification of the ionic radius of the A site. The lattice distortion of the perovskite ABO_3 is governed by the so-called tolerance factor t (equation:1.2), leading to the rotation and tilts of the BO_6 octahedra, which is discussed in the following section in more detail. An advantage of using a distorted perovskite for W control is that the A site is not directly relevant to the electronic properties inherent in the B-O network and also that the W value can be varied to a considerable extent (by 30-40 %) by choice of different rare-earth or alkaline-earth cations as the A-site element. The best example of successful W control is the metal to insulator transition for $RNiO_3$ [24], with R being the trivalent rare-earth ions (La to Lu). The metal-insulator phase diagram for $RNiO_3$ driven by octahedral distortions is shown in Fig. (1.1-c)
.

Filling-control is also important to tune electronic strengths, as is evident from the discovery of high-temperature superconductivity as a function of filling in the layered cuprate compounds. The standard method of filling control is to utilize ternary or multinary compounds in which ionic sites other than the 3d (4d) or 2p electron related sites can be occupied by different valence ions. For example, the band filling of $La_{2-x}Sr_xCuO_4$ is controlled by substitution of divalent Sr on the trivalent La sites and is given by the relation; $n = 1 - x$. Similarly, a number of filling-controlled compounds can be made by forming the A-site mixed crystals of perovskites, such as $La_{1-x}Sr_xMO_3$, M being the 3d transition-metal element. Fig. (1.1-b) shows a schematic of bandwidth controlled (BC) and filling controlled (FC) metal-insulator transition.

Transition metal oxides show a tunable combination of electronic polarizability as a result of chemistry of the transition metal-oxygen bonds and the localized d electrons arising from strong correlation effects present. As a consequence of this combination various energy scales associated with the crystal field, Hund's exchange and the band width of the transition metal d orbitals compete with each other

resulting in a range of interesting properties in them with application of external stimuli such as doping, temperature of pressure. In other class of materials such as semiconductors or metals, one of these enegetics dominates and determines the macroscopic properties, while in transition metal oxides they compete with each other leading to strong lattice-electron, electron-spin and spin-orbit couplings [17]. As a result the ground state has more than one low energy phase which are highly susceptible to external perturbation [18].

With the remarkable advancement in experimental techniques, reducing the dimensionality by growing thin films of transition metal oxides(perovskite oxides in particular) provides an additional platform to have a handle on the delicate interplay among the interactions to produce unique collective phenomena. A dramatic change as well as enhancement in the properties of transition metal oxide thin films have been observed. Substrate induced strain in the film lead to an appearance of magnetism in otherwise nonmagnetic oxide films[19-21] or the activation of improper phase transitions[22]. Misfit strain also induces metal to insulator transitions in oxide thin films[23,24]. As thin films provide an appropriate architecture, it has been possible to achive electric field tuned electronic, magnetic and structural phase transitions which most importantly leads to technical device integration[25]. Substrate strain provides an extra handle to control the structure and the bandwidths consequently to manipulate localization effects.

The origin of many properties of transition metal oxides is not always clear, which is an important problem to attack in solid state physics. The difficulty arises from the fact that the valence electrons in these materials have a strong Coulomb interaction. To understand as well as predict the behavior of the electrons at a microscopic level becomes very important as both the physics and chemistry of the electrons drive the observed novel properties in these oxides. With the constant development of theoretical methods and the modern computational capacities, it has become much more convenient to handle a larger number of atoms along with several degrees of freedom associated with them. As a result computational material science has emerged as one of the foremost and very fertile research domain over the years.

In this thesis we have studied few of these transition metal oxides in the thin film and superlattice

geometries in first principle calculations. This thesis presents the work investigating the consequences of reducing the dimensionality from bulk to thin film or heterostructures on electronic, magnetic and structural properties of various transition metal oxides, consider a particular class which is know as perovskite oxides.

1.2 Crystal structure of perovskite oxides and related phonomena

The perovskite family of oxides is probably the best studied family of oxides. The interest in compounds belonging to this family of crystal structures arise in the large and ever surprising variety of properties exhibited and the flexibility to accommodate almost all of the elements in the periodic system. Pioneering structural work on perovskites were conducted by Goldschmidt *et al* in the 1920's that formed the basis for further exploration of the perovskite family of compounds [26]. Distorted perovskites have reduced symmetry, which is important for their magnetic and electric properties. Due to these properties, perovskites have great industrial importance, for instance the ferroelectric tetragonal form of $BaTiO_3$.

1.2.1 Crystal Structure

The ideal structure of perovskite-type oxides is cubic which occurs in space group $Pm\bar{3}m$ with the space group number 221. In the unit formula of perovskite-type oxides ABO_3, A is the larger cation and B is the smaller cation. In this structure, the B cation is 6-fold coordinated and the A cation is 12-fold coordinated with the oxygen anions, with three-dimensionally coordinated BO_6 octahedra resulting in a B-O-B angle equal to $180°$ in any .....B-O-B-O-B..... chain. The B sites are usually occupied by a transition metal ion. At the A sites, larger alkali metal or rare earth cations occupy the high symmetry positions of the cuboctahedral vacancies between the octahedra. Fig. 1.2 depicts the corner sharing octahedra that form the skeleton of the structure, in which the central position is occupied by the A cation. Alternatively, this structure can be viewed with the B cation placed in the center of the octahedron and the A cation is at the center of the cube. Some of the ABO_3 perovskite oxides crystalize

in this ideal structure, but in practice most of the perovskite oxides exhibit various structural distortions that lower the symmetry of the crystal system from that of the cubic one.
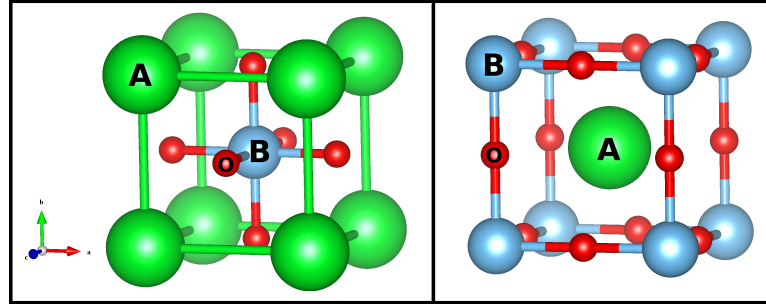
Figure 1.2 Cubic unit cell for the oxides with perovskite structure with a) A site atom at the body centre and b) B site atom at the body centre position.

1.2.2 Distortions in the unit cell

Distortions that occur most widely among this class of oxides are the rotations or the tilts of rigid oxygen octahedra around one or more high symmetry axes. In the ideal structure, where the atoms are touching one another, the cubic unit cell parameter is related to the ionic radii (r_A, r_B, r_O) by the relation

$$a = \sqrt{2}(r_A + r_O) = 2(r_B + r_O) \tag{1.1}$$

and the B-O distance is equal to a/2 the A-O distance is a/$\sqrt{2}$. However, it was found that the cubic structure was still retained in ABO_3 compounds, even though this equation is not exactly obeyed. As a measure of the deviation from the ideal situation, Goldschmidt [27] introduced a tolerance factor (t), defined by the equation

$$t = \frac{(r_A + r_O)}{\sqrt{2}(r_B + r_O)} \tag{1.2}$$

which is applicable at room temperature to the empirical ionic radii. Although for an ideal perovskite t is unity, this structure is also found for lower t-values ($0.75 < t < 1.0$). The ideal cubic perovskite structure appears in a few cases for t-values very close to 1 and at high temperatures. In

most cases, different distortions of the perovskite structure appear. The naturally occurring compound $CaTiO_3$ was originally thought to be cubic, but its true symmetry was later shown to be orthorhombic [28]. The ideal cubic perovskite $SrTiO_3$ has t = 1.00, r_A = 1.44 Å, r_B = 0.605 Å, and r_O = 1.40 Å. If the A ion is smaller than the ideal value(t=1) then t becomes smaller than 1. As a result the BO_6 octahedra will tilt in order to fill space, see Fig. 1.3. However, the cubic structure occurs if $0.89 < t < 1$ [29, 30]. Lower values of t will lower the symmetry of the crystal structure. For example $GdFeO_3$ with t = 0.81 is orthorhombic (r_A = 1.107 Å and r_B = 0.78 Å), see Fig-1.3(b).
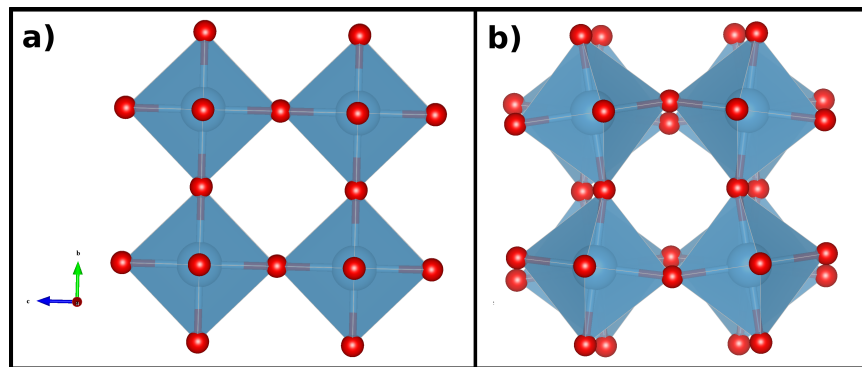
Figure 1.3 BO_6 octahedra in a) ideal cubic unit cell and b) in distorted unit cell with tilts and rotation of the octahedra.

In a distorted ABO_3 perovskite unit cell, rotation angles are given by $(90 - \theta)/2$, while tilt angles are given by $(180 - \phi)/2$, as shown in the Fig-1.4.

Glazer notation [31, 32] is used to denote various type of these distortions. In this notation a rotation pattern can be denoted as $a^*b^*c^*$ where superscripts represents whether the concerned octahedra rotates in-phase (ferrodistortively)(+) or out-of-phase (Antiferrodistortively)(-) or not at all (0). Few examples are, low temperature $SrTiO_3$ having $a^0a^0c^-$, rhombohedral $LaAlO_3$, $LaNiO_3$ and $BiFeO_3$ having $a^-a^-a^-$ and etc. Following are few examples of Glazer notation for distortions associated with various space groups: $a^-a^-c^-$ (15:C2/c or 14 P2$_1$/c), $a^-a^-c^+$ (62:Pnma), $a^+a^+c^-$ (137:P4$_2$/nmc), $a^-a^0c^0$ (69:Fmmm), $a^-a^-c^0$ (74:Imma), $a^0a^0c^0$ (221:Pm$\bar{3}$m), $a^+a^0c^0$ (55:Pbam), $a^+a^+c^0$ (139:I4/mmm), $a^0a^0c^-$ (140:I4/mcm), $a^0a^0c^+$ (127:P4/mbm), and $a^+a^+c^+$ (71:Immm).

If in this notation two letters are the same, then the magnitude of the octahedral distortions is same
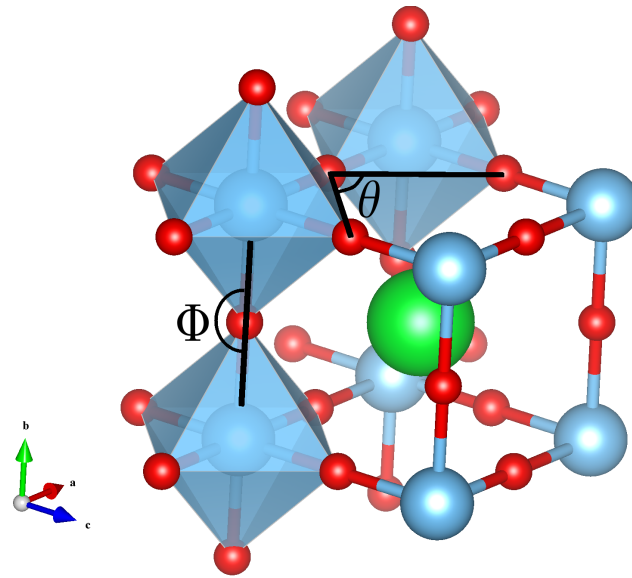
Figure 1.4 Angle of rotation and tilt in a distorted ABO_3 perovskite unit cell.

irrespective of whether the distortions are in or out of phase. Same letters should not be misunderstood with the corresponding lattice constant, they just represent that the nearest neighbor B site ion distances are same along that particular direction. Now as all the octahedra are connected to each other in three-dimensions, a rotation or tilt in one direction restricts the allowed rotation or tilt in other directions. Only 23 tilt systems can be obtained which belong to 15 unique space groups [33].

1.2.3 Implications of the distortions of the unit cell on the chemistry of perovskite oxide

The geometry defining the transition metal and the oxygen environment around it has direct implications on the chemistry of the d orbitals associated with the transition metal, and consequently controls the behavior of the transition metal oxides. Transition metal oxides exhibit various geometries of oxygen cage around the transition metal *viz* octahedral, tetrahedral, trigonal bipyramidal, square planar, square pyramidal, pentagonal bipyramidal, square antiprismatic etc. Not all of the d orbitals behave in a similar manner under the influence of this field. It is the geometry of the oxygen cage around the transition metal that dictates the behavior of the d orbitals associated with the transition metal. In most of the perovskite oxides, the six oxygens around the transition metal form an octahedron around the

transition metal. In a cubic unit cell of perovskite oxides, if the transition metal ion is sitting at the body centre position and the six oxygens at the face centre positions, the five fold degenerate d orbitals split into lower lying three fold t_{2g} orbitals and two fold e_g orbitals lying higher in energy. The $d_{x^2-y^2}$ and d_{3z^2} orbitals with e_g symmetry on the transition metal oxides will point directly towards the oxygen atoms, while the d_{xy}, d_{yz} and d_{xz} with t_{2g} symmetry will be pointing in between the oxygen atoms. As a result of the larger electrostatic repulsion, the e_g orbitals move up higher in energy than the t_{2g} orbitals. The strength of this spliting is known as crystal field splitting. This splitting depends upon the nature of the transition metal, its oxidation state (a higher oxidation state leads to larger splitting), geometry of the ligand oxygens around it, the nature of the ligand oxygens(greater effect of ligands leads to larger splitting). Moreover partial occupancy of these t_{2g} and e_g orbitals results in further lifting of degeneracy which is more pronounced in the case of e_g orbitals. The transition metal-oxygen octrahedral cage distorts in either of the two manners as shown in the Fig. 1.5, removing the degeneracy of the d orbitals and thus gaining energy to stabilize the structure. This is known as the Jahn-Teller effect [34].
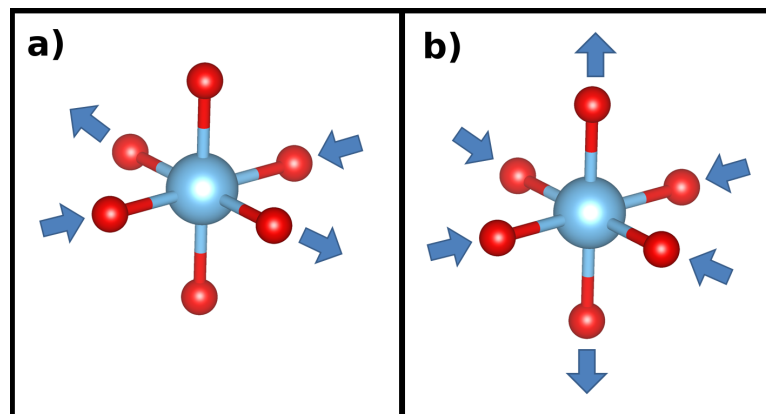
Figure 1.5 Schematic for the possible Jahn-Teller modes in an octahedral environment of oxygens around a transition metal. Blue spheres are transition metal while the red ones are oxygens.

Jahn-Teller distorions can be further divided into first and second-order Jahn-Teller distortions. When an electronic degeneracy usually associated with the d-electrons on the B site cation can be removed by an appropriate structural distortion, such distortions are called first-order Jahn-Teller distortions [35, 36]. This typically manifests as an elongation of some B-O bonds and a shortening of

others. While relative displacements of cations and ions that result in polar ferroelectric distortions further lower the crystal symmetry into a polar space group [41]. Since these distortions can be described to second order in perturbation theory they are often referred to as second-order Jahn-Teller effects[37-40]. As discussed earlier the octahedral rotations and tilts, are driven mainly by geometric and electrostatic effects, on the other hand, first- and second-order Jahn-Teller distortions are driven by electronic effects.

1.3 Motivation of the present thesis

In **chapter-2** we introduce and discuss the basics of density functional theory, on which the calculations we have carried out throughout the thesis are based on. We start with a many particle Hamiltonian, show how it is constructed and then discuss various approximations which are made to solve it in practice.

One of the foremost examples depicting the different spin-states associated with an ion and the transition from one to the other has been extensively discussed in, is cobaltates. As discussed earlier transition metal ions exhibit multiple oxidation states, cobalt ion is typically either divalent $Co^{2+}(3d^7)$ or trivalent $Co^{3+}(3d^6)$. Co in $LaCoO_3$ is trivalent, in this case there are three possible spin-states. First, a low spin-state with S=0, where all the six electrons are paired and occupy the t_{2g} orbitals in both up- and down-spin channels resulting in a configuration $t_{2g}^6 e_g^0$. This arises when the crystal field energy is larger than the Hund's exchange energy. Second a high-spin state with S=2, where five electrons occupy up-spin channels of t_{2g} and e_g orbitals and sixth electron sits in the down-spin channel of t_{2g} orbitals, resulting in a configuration $t_{2g}^4 e_g^2$. This arises when the Hund's exchange energy is larger than the crystal field energy. Third an intermediate-spin state with S=1, where five electrons occupy the t_{2g} orbitals and the sixth electron sits in the e_g up-spin channel resulting in a configuration of $t_{2g}^5 e_g^1$. This arises when Hund's exchange energy competes with the crystal field energy. $LaCoO_3$ is a system which exhibits a transition from one to another spin states as discussed above, which has a nonmagnetic insulating ground state at low temperature and becomes paramagnetic with increasing temperature and beyond 500 K it becomes metallic. Earlier this was interpreted as a gradual population of a high spin

state from a low spin-state. Korotin *et al.* [42] first proposed that this gradual transition is instead to an intermediate-spin state from a low-spin state rather than from low to high spin state. But Haverkort *et al.* [43] in 2006 from their X-Ray absorption studies, again established the low- to high-spin state. The puzzle of this spin-state transition from low-high [44–48] or low-intermediate [49–62] spin state is still not solved, despite a large number of papers on it.

In this transition its only the resistivity of $LaCoO_3$ that changes, the system still remains non-magnetic in the variation of temperature. In 2007, Fuch *et al.*[19,63] grew thin films of $LaCoO_3$ on different substrates. Ferromagnetism has been found with a T_c(Curie temperature) of 85K on $(LaAlO_3)_{0.3}(SrAlTaO_6)_{0.7}$ (LSAT) substrate, in addition to a strain dependent T_c. The origin of the ferromagnetism is however not clear, with a significant role played by the rotation of the CoO_6 octahedra being offered as one of the reasons [19,63]. In **chapter-3** we investigate the electronic structure and origin of the strain tuned ferromagnetism in thin films of nonmagnetic material $LaCoO_3$ and what is the spin-state favored in its ground state.

Multiferroics are materials that exhibit more than one primary ferroic order such as ferromagnetism, ferroelectricity, and ferroelasticity [94]. Additionally systems which show one primary order parameter and one non-primary order parameter, in a combination such as antiferromagnetism and ferrimagnetism, are also considered as multiferroics [65, 66]. There are very few systems which are magnetic or ferroelectric can exhibit both magnetic and electric order parameters simultaneously[67]. In this distinct category of materials, applied magnetic field can tune the magnetization as well as induce ferroelectricity, or an applied electric field can change the orientation of the polarization as well as the spins. Such cross coupled order parameters add up an extra degree of freedom and provides the possibility to fabricate new devices based on these materials. Most of the ferroelectrics are d^0 systems and ferromagnetism requires transition metals with unpaired 3d electrons. Hence due to mutual exclusivity of the mechanisms of the magnetic and electric order parameter, the possible candidate multiferroic systems are scarce, in particular ferromagnetic-ferroelectic systems as shown in Fig-1.6.

The magnetoelectric multiferroic compounds must be simultaneously both ferromagnetic and ferroelectric. Because multiferroicity is determined by a number of factors, including crystal structural
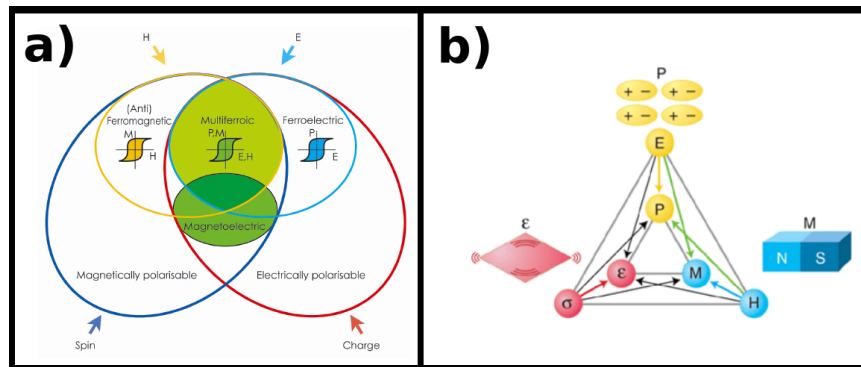
Figure 1.6 Schematics showing coupling between various order parameters and very few possible candidates which could have a combination of them.
Fig ref: a)http://www.esrf.eu /UsersAndScience/Publications/Highlights/2009/elecstrmag and b) Science 309, 391 (2005).

symmetry, electronic properties, and chemical properties, there are only thirteen point groups that can give rise to multiferroic behaviour[66,67,79]. There are examples of systems which exhibit both orders among finite d^n systems, however the magnitudes of polarization are usually small in such cases. In addition to it, there have been reports that the simultaneous presence of electric and magnetic ordering does not guarantee strong coupling between the two, as microscopic mechanisms of ferroelectricity and magnetism are quite different and do not strongly interfere with each other[69,70].

An avenue that has been explored in great detail to achieve alternate methods to the design of multiferroics is in the thin film regime where film thickness and substrate imposed strain has been used as a handle to modify propeties which are dramatically different from their bulk counterpart. Design of new materials depends upon extensive experimentations, but in recent times first principle studies have reached a level of predictive capabilities. Such studies theoretically predict new routes to design a range of novel systems which could show multiferroic behavior and effects as magnetostructural coupling. Fennie *et al.* predicted that in EuTiO$_3$ [71], the expitaxial strain can drive a ferromagnetic and ferroelectric phase to co-exist at the same temperature. Strong magnetostructural coupling was the origin of the multiferroic behavior in this system. Later on Lee *et al.* confirmed this prediction in their experiments[72], when they grew thin films of EuTiO$_3$ on DyScO$_3$ substrates. Although the transition temperatures are quite low, below 5 K, the discovery is indeed remarkable as it creates possibilities

of designing multiferroic materials by the application of the external stimuli such as strain. Similar predictions of multiferroic behavior have been made by first principle calculation for other systems $SrMnO_3$ [73] and $SrCoO_3$ [74], though they are still not verified in experimets. An important consequence of these studies was that ferroelectric polarization as large as that found in d^0 ferroelectrics was predicted in these oxides. In contrast the observed ferroelectric polarization in most multiferroics is at least one or more orders of magnitude lower[75-77]. Nevertheless, the design of materials using these approaches open new opportunities for the tailoring of devices, important from the device perspective because devices use such materials in thin film form and strain in such systems can be effectively used to induce hitherto unobserved effects. In **chapter-4** we explore a new route to realize an orbital ordering assisted d^0-type displacive ferroelectricity in a non-d^0 system through ultrathin films of transition metal oxides $SrVO_3$ and $SrCrO_3$.

Most of the multiferroics and magnetoelectric system can be divided into two types: single(all the examples discussed so far) and two phase systems. Two components systems are mainly artificially grown superlattice heterostructures, composites consisting of more than one materials. A lot of efforts have been made to grow artificial layers and tailor their structures suitable for a possible multiferroic in various systems such as $BaTiO_3$-$CoFe_2O_4$[78,79], $Pr_{0.85}Ca_{0.15}MnO_3$/$Ba_{0.6}Sr_{0.4}TiO_3$[80], $BaTiO_3$/$SrTiO_3$[81], $PbTiO_3$/$SrTiO_3$[82],$BiFeO_3$/$SrTiO_3$[84,85]. Superlattice structures have been an alternate route to circumvent the scarcity of single phase multiferroics, which can have cross-coupled ferroic order parameters. A diverse range of functional properties can be achieved in these heterostructures, with variation in the choice of the constituent materials, and the order in which they are fabricated as well as the epitaxial strain that is imposed by the substrate. In some cases these properties can be explained by understanding how the electrical and mechanical boundary conditions of the superlattice drive the behavior of the ingredient materials, while in some instances these properties are directly associated with the way the atomic and electronic structure get modied at the interfaces[86]. In **chapter-5** we have studied the heterostructures of $BaVO_3$/$BaTiO_3$ and $BaCrO_3$/$BaTiO_3$. The former is found to be a ferromagnetic-ferroelectric while the later is antiferromagnetic-ferroelectric. Calculated polarization are comparable to that in the bulk prototypes.

SrRuO$_3$ is another interesting perovskite oxide. Ru is a 4d transition metal, hence SrRuO$_3$ is moderately correlated system as compared to 3d systems. In Ruthenates corelation effects are less effective as due to the larger spread of wavefunctions corresponding to 4d orbitals, and hence increased hybridization results into more effective screening and a reduced coulumb repulsion energy U. It permits the epitaxial growth of essentially single-crystal films, it is widely studied as a conducting electrode layer [87, 88] in epitaxial heterostructures in conjunction with a range of other oxides. SrRuO$_3$ is a popular choice since among perovskite oxides, it is one of the more conductive metallic oxides with good thermal properties [89].

In the thin film regime SrRuO$_3$ has been studied extensively to explore possiblities to realize field effect devices [90, 91]. Moreover this system has drawn a lot of attention in the area of spintronics [92, 93] and even multiferroics [94, 95]. This is again assisted by device applications which have become possible by engineering interface phenomena [96–99] in heterostructures. But due to the inceased resistivity in ultrathin films of transition metal oxides these device applications are limited. Thin films of SrRuO$_3$ also show metal to insulator transitions at the thickness of four monolayers[100,101]. There are first principle studies carried out to understand the observed metal to insulator transition in thin films of SrRuO$_3$ Rondinelli et.al.[102] suggested indirect experimental factors or structural defects as a possible reason behind this metal-insulator transition. They found that including correlations with an effective Hubbard U of 0.6 eV or correction of the self-interaction error gives good agreement for bulk orthorhombic SrRuO$_3$ with the experimental spectroscopic data. The addition of the octahedral distortions leads to a narrowing of the majority spin Ru t$_{2g}$ and O 2p states, however the exchange splitting is small with respect to these bandwidths and consequently a fully insulating ground state was not obtained. A half-metallic ground state was shown to be stable by including moderate electron-electron correlation effects of U=2 eV, which has not been observed experimentally. Zayak et.al.[103] studied how structural and magnetic behavior depends upon the strain. Though the phenomena of metal-insulator transition was not addressed. Mahadevan *et al.*[104] succesfully explained mechanism of experimentally observed metal-insulator transition in thin films of SrRuO$_3$. Films were found to become an antiferromagnetic insulator compared to their ferromagnetic metallic state in bulk from, driven

by a low-spin to high-spin state transition. For thicker films an antiferromagnetic insulating solution coexists with a metallic solution corresponding to an antiferromagnetic surface and a ferromagnetic bulk. Films beyond four-monolayers were found to be metallic as observed in the bulk, though the magnetic state does not evolve to be like a bulk ferrromagnetic state. The bulk shows ferromagnetism while the surface remains antiferromagnetic. In this work only rotations of RuO_6 octahedra were considered. In **chapter-6** we study the epitaxial thin films of $SrRuO_3$ cosidering both rotations as well as tilts of the RuO_6 octahedra. We discuss how we find a regime where anisotropic intra-atomic exchange interactions drive the insulating state. Using strain as a parameter, we can move away from this regime into one where Jahn-Teller effects dominate, hence manipulating interaction strengths at the atomic level. We also explore avenues to realize a two-dimensional electron gas in three monolayers limit.

Modification of electronic properties of transition metal oxides in reduced dimensionality such as thin films, heterostructures and superlattices with very precise interfaces at atomic level is one of the foremost areas of material research at present[105-107]. A systematic tuning of various phenomena, such as ferroelectricity, magnetic order and superconductivity has been achieved by several control parameters which includes the overlayer thickness, composition along with the substrate imposed epitaxial strain. The role played by static lattice distortions occuring at the interface affect some of these phenomena and this has been studied already in literature[108-111]. It is not just the physical properties of systems that evolve as a function of thickness, one finds that the structure also evolves as a function of thickness. The substrate constrains the lattice constant of the overlayers and this in turn results in the realization of crystal structures which have not been observed in the bulk. An additional dimension comes in when one has few monolayers. This is an increase in the degree of localization of the electrons as the full bandwidth is not formed. This takes the system which is metallic in the bulk in addition to having full cubic symmetry to one in which electron-phonon couplings get enhanced, resulting in structural distortions not observed in the bulk. The dynamical electron-phonon interaction tuned electronic properties of artificial layered structures and thin films have not been studied in detail yet. Though their crucial role in phase behavior of bulk transition metal oxides has been suggested[112-114].

In **chapter-7** we have explored the dimensional crossover driven metal to insulator transition in the

ultrathin films of a metallic oxide $SrVO_3$, and we find strong structural modifications arising from the surface effects. Additionaly the terminating layer as well as the substrate structure plays an important role in the structural effects in the $SrVO_3$ overlayers.

Bibliography

[1] M. Imada, A. Fujimori and Y. Tokura, Rev. Mod. Phys. **70**, 1039 (1998).

[2] Abanti Nag, J. Manjanna, R. M. Tiwari and J. Gopalakrishnan, Chem. Mater., **20**, 4420(2008).

[3] J. C. Loudon, N. D. Mathur and P. A. Midgley, Nature **420**, 797(2002).

[4] K. Yamaura, E. Takayama-Muromachi, Phys. Rev. B, **64**, 224424(2001).

[5] R. von Helmolt, J. Wecker, B. Holzapfel, L. Schultz, and K. Samwer, Phys. Rev. Lett. **71**, 2331 (1993).

[6] K. H. Ahn, X. W. Wu, K. Liu, and C. L. Chien, Phys. Rev. B, **54**, 15299(1996).

[7] Z. A. Xu, N. P. Ong, Y. Wang, T. Kakeshita and S. Uchida, Nature **406**, 486 (2000).

[8] J. G. Bednorz and K. A. Muller, Z. Phys. B **64**, 189 (1986).

[9] S. Jin, T. H. Tiefel, M. McCormack, R. A. Fastnacht, R. Ramesh and L. H. Chen, Science **264**, 413 (1994).

[10] S. Jin, M. McCormack, T. H. Tiefel, and R. Ramesh, J. App. Phys., **76**, 6929(1994).

[11] M. Dawber, K. M. Rabe, and J. F. Scott, Rev. Mod. Phys. 77, 1083 (2005).

[12] V. Laukhin, V. Skumryev, X. Marti, D. Hrabovsky, F. Sanchez, M. V. Garcia Cuenca, C. Ferrater, M. Varela, U. Lüders, J. F. Bobo, and J. Fontcuberta, Phys. Rev. Lett. **97**, 227201 (2006).

[13] C. Thiele, K. Dörr, O. Bilani, J. Rödel, and L. Schultz, Phys. Rev. B **75**, 054408(2007).

[14] A. D. Rata, A. Herklotz, K. Nenkov, L. Schultz, and K. Dörr, Phys. Rev. Lett. **100**, 076401 (2008).

[15] J. H. vanSanten and G. H. Jonker, Physica **16**, 337 (1950).

[16] J. Zaanen and G. A. Sawatzky and J. W. Allen, Phys. Rev. Lett. **55**, 418 (1985).

[17] J. M. Rondinelli and N. A. Spaldin, Adv. Mater., **23**, 3363 (2011).

[18] E. Dagotto , Science, **309**, 257(2005).

[19] D. Fuchs, C. Pinta, T. Schwarz, P. Schweiss, P. Nagel, S. Schuppler, R. Schneider, M. Merz, G. Roth, H. von Löhneysen, Phys. Rev. B , **75**, 144402(2007).

[20] K. Gupta and P. Mahadevan, Phys. Rev. B, **79**, 020406,(2009).

[21] J. M. Rondinelli and N. A. Spaldin, Phys. Rev. B **79**, 054409 (2009).

[22] E. Bousquet, M. Dawber, N. Stucki, C. Lichtensteiger, P. Hermet, S. Gariglio, J. M. Triscone, P. Ghosez, Nature , **452**, 732(2008).

[23] A. Tiwari, C. Jin, and J. Narayan, Appl. Phys. Lett. **80**, 4039 (2002).

[24] R. Scherwitzl, S. Gariglio, M. Gabay, P. Zubko, M. Gibert, and J. M. Triscone, Phys. Rev. Lett. **106**, 246403 (2011).

[25] J. Mannhart, D. Schlom, Science, **327**, 1607(2010).

[26] A. S. Bhalla, R. Guo and R. Roy, Mat. Res. Innovat. **4**, 3(2000), and references therein.

[27] Goldschmidt, V. M. Skr. Nor. Viedenk.-Akad., Kl. I: Mater.- Naturvidensk. Kl. 1926, No. 8.

[28] H. D. Megaw Proc. Phys. Soc. **58**, 133(1946).

[29] A.F. Wells, Structural Inorganic Chemsitry, Oxford Science publications. (1995).

[30] U. M*ü*ller, Inorganic Structural Chemistry, Wiley & Sons Ltd. (1993).

[31] A. M. Glazer , Acta Crystallogr. Sect.B **28**, 3384(1972).

[32] A. M. Glazer , Acta Crystallogr. Sect.A **31**, 756(1976).

[33] C. J. Howard, H. T. Stokes, Acta Crystallogr. Sect. B ,**54** , 782(1998).

[34] H. Jahn and E. Teller, Proc. Roy. Soc. A **161**, 220 (1937).

[35] J. B. Goodenough , Ann. Rev. Mater. Res. **28** , 1(1998).

[36] M. B. Salamon , M. Jaime , Rev. Mod. Phys., **73**, 583(2001).

[37] J. K. Burdett , Inorg. Chem.,**20**, 1959(1981).

[38] R. G. Pearson , J. Mol. Struct.: THEOCHEM, **103** , 25(1983).

[39] I. B. Bersuker , Chem. Rev., **101**, 1067(2001).

[40] J. M. Rondinelli , A. S. Eidelson , N. A. Spaldin , Phys. Rev. B, **79**, 205119(2009).

[41] H. T. Stokes , E. H. Kisi , D. M. Hatch , C. J. Howard , Acta Crystallogr. Sect.B, **58**, 934(2002).

[42] M. A. Korotin, S. Y. Ezhov, I. V. Solovyev, V. I. Anisimov, D. I. Khomskii, and G. A. Sawatzky,Physical Review B **54**, 5309 (1996).

[43] M. W. Haverkort, Z. Hu, J. C. Cezar, T. Burnus, H. Hartmann, M. Reuther, C. Zobel, T. Lorenz, A. Tanaka, N. B. Brookes, H.- H. Hsieh, H.-J. Lin, C.-T. Chen, and L. H. Tjeng, Physical Review Letters **97**, 176405 (2006).

[44] M. Zhuang, W. Zhang, and N. Ming, Phys. Rev. B **57**, 10705(1998).

[45] S. Noguchi, S. Kawamata, K. Okuda, H. Nojiri and M. Motokawa, Phys. Rev. B **66**, 094404 (2002).

[46] T. KyoËĘmen, Y. Asaka, and M. Itoh, Phys. Rev. B **67**, 144424 (2003).

[47] Z. Ropka and R. J. Radwanski, Phys. Rev. B **67**, 172401 (2003).

[48] T. Kyomen, Y. Asaka, and M. Itoh, Phys. Rev. B **71**, 024418 (2005).

[49] T. Saitoh, T. Mizokawa, A. Fujimori, M. Abbate, Y. Takeda, M. Takano, Phys. Rev. B **55**, 4257 (1997); **56**, 1290(1997).

[50] Svein Stolen, Fredrik Gronvold, Hendrik Brinks, Tooru Atake and Hideki Mori, Phys. Rev. B **55**, 14103 (1997).

[51] K. Asai et al., J. Phys. Soc. Jpn. **67**, 290 (1998).

[52] J. Okamoto et al., Phys. Rev. B **62**, 4455 (2000).

[53] P. Ravindran et al., J. Appl. Phys. **91**, 291 (2002).

[54] C. Zobel et al., Phys. Rev. B **66**, 020402(R) (2002).

[55] P. G. Radaelli and S.-W. Cheong, Phys. Rev. B **66**, 094408(2002).

[56] T. Vogt, J. A. Hriljac, N. C. Hyatt, and P. Woodward, Phys. Rev. B **67**, 140401(R) (2003).

[57] I. A. Nekrasov, S. V. Streltsov, M. A. Korotin, and V. I. Anisimov, Phys. Rev. B **68**, 235113 (2003).

[58] D. Louca and J. L. Sarrao, Phys. Rev. Lett. **91**, 155501(2003).

[59] G. Maris et al., Phys. Rev. B **67**, 224423 (2003).

[60] A. Ishikawa, J. Nohara, and S. Sugai, Phys. Rev. Lett. **93**,136401 (2004).

[61] M. Magnuson et al., Europhys. Lett. **68**, 289 (2004).

[62] K. Knizek, P. Novak, and Z. Jirak, Phys. Rev. B **71**, 054420 (2005).

[63] D. Fuchs, E. Arac, C. Pinta, S. Schuppler, R. Schneider, and H. v. Löhneysen, Phys. Rev. B **77**, 014434 (2008).

[64] Y. Tokura and S. Seki, Adv. Mater. **22**, 1554 (2010).

[65] K. F. Wang, J. M. Liu, and Z. F. Ren, Adv. Phys. **58**, 321(2009).

[66] J. van den Brink and D. Khomskii, J. Phys. Cond Mat. **20**, 434217 (2008).

[67] T. Kimura, Annu. Rev. Mater. Res. **37**, 387 (2007).

[68] K. F. Wang, J. M. Liu, and Z. F. Ren, Adv. Phys. **58**, 321 (2009).

[69] D. I. Khomskii, Bull. Am. Phys. Soc. C 21, 002 (2001).

[70] T. Katsufuji, S. Mori, M. Masaki, Y. Moritomo, N. Yamamoto, and H. Takagi Phys. Rev. B **64**, 104419 (2001).

[71] C. J. Fennie and K. M. Rabe, Phys. Rev. Lett., **97**, 267602(2006).

[72] J. H. Lee, L. Fang, E. Vlahos *et al.*, Nature, **466**,954(2010).

[73] J. H. Lee and K. M. Rabe, Phys. Rev. Lett., **104**, 207204(2010).

[74] J. H. Lee and K. M. Rabe, Phys. Rev. Lett. **107**, 067601(2011).

[75] T. Kimura, T. Goto, H. Shintani, Y. Tokura, Nature **55**,426 (2003).

[76] L. C. Chapon *et al.*, Phys. Rev. Lett. **93**, 177402 (2004).

[77] G. Lawes *et al* Phys. Rev. Lett. **95** 087205, (2005).

[78] H. Zheng, J. Wang, S. E. Lo and, W. Ma, L. Mohaddes-Ardabili, T. Zhao, L. Salmanca- Riba, S.R. Shinde, S. B. Ogale, F. Bai, D. Viehland, Y. Jia; D. G. Schlom, M. Wuttig, A. Roytburd, and R. Ramesh, Science **303**, 661 (2004).

[79] K. S. Wang, M. A. Aronova, C. L. Lin, M. Murakami, M. H. Yu, J. Hattrick-Simpers, O. O. Famodu, S. Y. Lee, R. Ramesh, M. Wuttig, I. Takeuchi, C. Gao, and L.A. Bendersky, Appl. Phys. Lett. **84**, 3091 (2004).

[80] P. Murugavel, D. Saurel, W. Prellier, Ch. Simon, and B. Raveau, Appl. Phys. Lett. 85, 4424(2004).

[81] J. B. Neaton and K. M. Rabe, Appl. Phys. Lett. **82**, 1586 (2003).

[82] K. Johnston, X. Huang, J. B. Neaton, and K. M. Rabe, Phys. Rev. B **71**, 100103(R) (2005).

[83] M. Dawber, C. Lichtensteiger, M. Cantoni, M. Veithen, P. Ghosez, K. Johnston, K. M. Rabe, and J.-M. Triscone, Phys. Rev. Lett, **95**, 177601 (2005).

[84] R. Ranjith, B. Kundys, and W. Prellier, Appl. Phys. Lett. **91**, 222904 (2007).

[85] S. Bose and S. B. Krupanidhi, Appl. Phys. Lett. **90**, 212902 (2007).

[86] X. Wu, M. Stengel, K. M. Rabe, and D. Vanderbilt, Phys. Rev. Lett. **101**, 087601 (2008).

[87] F. L. Marrec, A. Demuer, D. Jaccard, J. M. Triscone, M. K. Lee, and C. B. Eom, Appl. Phys. Lett. **80**, 2338 (2002).

[88] K. S. Takahashi, A. Sawa, Y. Ishii, H. Akoh, M. Kawasaki, and Y. Tokura, Phys. Rev. B **67**, 094413(2003).

[89] H. N. Lee, H. M. Christen, M. F. Chisholm, C. M. Rouleau, and D. H. Lowndes, Appl. Phys. Lett. **84**, 4107 (2004).

[90] 5C. H. Ahn, R. H. Hammond, T. H. Geballe, M. R. Beasley, J.-M. Triscone, M. Decroux, O. Fischer, L. Antognazza, and K. Char, Appl. Phys. Lett. **70**, 206 (1997).

[91] K. S. Takahashi, M. Gabay, D. Jaccard, K. Shibuya, T. Ohnishi, M. Lippmaa, and J.-M. Triscone, Nature London **441**, 195 (2006).

[92] I. Zutic, J. Fabian, and S. D. Sarma, Rev. Mod. Phys. **76**, 232 (2005).

[93] D. Awschalom and M. Flatte, Nat. Phys. **3**, 153 (2007).

[94] N. A. Spaldin and M. Fiebig, Science **309**, 391 (2005).

[95] R. Ramesh and N. A. Spaldin, Nature Mater. **6**, 21(2007).

[96] A. Ohtomo, D. A. Muller, J. L. Grazul, and H. Y. Hwang, Nature London **419**, 378 (2002).

[97] A. Ohtomo and H. Y. Hwang, Nature (London) **427**, 423 (2004).

[98] H. Y. Hwang, Science **313**, 1895 (2006).

[99] H. Yamada, Y. Ogawa, Y. Ishii, H. Sato, M. Kawasaki, H. Akoh, and Y. Tokura, Science **305**, 646 (2004).

[100] D. Toyota *et al.*, Appl. Phys. Lett. **87**, 162508(2005).

[101] J. Xia, W. Siemons, G. Koster, M. R. Beasley, and A. Kapitulnik, Phys. Rev. B **79**, 140407(R) (2009).

[102] J. Rondinelli, N. Caffrey, S. Sanvito, N. Spaldin, Phys. Rev. B ,**78**, 155107(2008).

[103] A. T. Zayak, X. Huang, J. B. Neaton, and Karin M. Rabe, Phys. Rev. B, **74**, 094104(2006).

[104] P. Mahadevan, F. Aryasetiawan, A. Janotti, and T. Sasaki, Phys. Rev. B, **80**, 035106 (2009).

[105] J. Mannhart and D. G. Schlom, Science, **327** 1607 (2010).

[106] H. Y. Hwang, Y. Iwasa, M. Kawasaki, B. Keimer, N. Nagaosa and Y. Tokura, Nature Materials, **11**, 103 (2012).

[107] P. Yu, W. Luo, D. Yi, J. X. Zhang, M. D. Rossell, C.-H. Yang, L. You, G. Singh-Bhalla, S. Y. Yang, Q. He, Q. M. Ramasse, R. Erni, L. W. Martin, Y. H. Chu, S. T. Pantelides, S. J. Pennycook and R. Ramesh, PNAS, **109**, 9710 (2012).

[108] S. A. Pauli, S. J. Leake, B. Delley, M. Björck, C. W. Schneider, C. M. SchlepÃijtz, D. Martoccia, S. Paetel, J. Mannhart, and P. R. Willmott, Phys. Rev. Lett., **106**, 036101 (2011).

[109] V. Y. Butko, Natasha Bozovic, Z. Radovic and I. Bozovic, Advanced Materials **21**, 3644(2009).

[110] J. Hoppler, J. Stahn, Ch. Niedermayer, V. K. Malik, H. Bouyanfif, A. J. Drew, M. Rössle, A. Buzdin, G. Cristiani, H.-U. Habermeier, B. Keimer and C. Bernhard, Nature Materials, **8** 315(2009).

[111] R. Pentcheva, and W. E. Pickett, Phys. Rev. Lett. **102** 107602 (2009).

[112] D. M. Edwards, Adv. Phys., **51** 1259 (2002).

[113] E. Dagotto, T. Hotta, and A. Moreo, Phys. Rep., **344**, 1-153 (2001).

[114] O. Gunnarsson, and O. Rösch, J. Phys. Condens. Matter **20**, 043201 (2008).

Chapter 2

Theory of electronic structure calculations

2.1 Introduction

Last century has seen an enormous development of theoretical physics. The inception took place when the wave-particle nature was verified through the work of Louis de Broglie, Albert Einstein and many others. Prediction of chemical or physical properties of a material requires quantum mechanical treatment of the many-body system of electrons and nuclei with their basic electrostatic coulumb interactions.

A real physical system is a combination of heavier positively charged particle *nuclei* and lighter negatively charged particle *electrons*. If N_n and N_e being number of nuclei and the electrons surrounding them respectively, then the problem we are dealing here is in fact a many body problem and can be described by the following Hamiltonian

$$H = -\frac{\hbar^2}{2m_e}\sum_{i=1}^{N_e}\nabla^2_{\mathbf{r_i}} - \frac{\hbar^2}{2M_I}\sum_{I=1}^{N_n}\nabla^2_{\mathbf{R_I}} - \sum_{i,I}\frac{Z_I e^2}{|\mathbf{R_I}-\mathbf{r_i}|} + \sum_{i>j}\frac{e^2}{|\mathbf{r_i}-\mathbf{r_j}|} + \sum_{I>J}\frac{Z_I Z_J e^2}{|\mathbf{R_I}-\mathbf{R_J}|} \qquad (2.1)$$

where r_i is the position of the ith electron. R_I is the position of the Ith nucleus, Z_I is the atomic number of the nucleus, m_e is the mass of the ith electron and M_I is the mass of the Ith nucleus respectively. The first term of equation 2.1 is the kinetic energy operator for the electrons while the second one is for the nuclei. The last three terms describe the Coulomb interaction between electrons and

nuclei, between electrons and other electrons and between nuclei and other nuclei respectively. It is almost impossible to solve the stationary Schrödinger equation even by using the fastest and the largest computers, for the many body hamiltonian 2.1 above, as most of the systems consists of a large number of atoms. This requires simplifications to the Hamiltonian which involves several approximations. The simplification of the Schrödinger equation is fundamental to the electronic structure theory.

The first approximation is the Born-Oppenheimer [1] or adiabatic approximation. The Born-Oppenheimer takes advantage of the fact that since the nucleus is heavier in mass compared to the electron, its motion can be ignored while solving the electronic Schrödinger equation; that is, the nucleus is assumed to be stationary while electrons move. This makes the nuclei kinetic energy term negligible in the Schrödinger equation. This approximation reduces the many body problem to the dynamics of the electrons with some frozen-ion configuration of the nuclei. The ion-ion interaction term is also a constant. The constant term, called the Madelung Energy is calculated classically. So under this approximation the many body Hamiltonian for a N electron system(we shall be dealing with electrons only so N_e changes to N)moving in the field of fixed ion cores, reduces to the following form

$$H = -\sum_{i=1}^{N} \frac{\hbar^2}{2m_e} \nabla_{\mathbf{r_i}}^2 - \frac{1}{4\pi\varepsilon_0} \sum_{i,I} \frac{Z_I e^2}{|\mathbf{R_I} - \mathbf{r_i}|} + \frac{1}{2}\frac{1}{4\pi\varepsilon_0} \sum_{i,j} \frac{e^2}{|\mathbf{r_i} - \mathbf{r_j}|} \tag{2.2}$$

2.2 Single-particle approximation

Even the task of solving the Schrödinger equation for a system with more than one electron is formidable because of electron-electron interactions. Several approaches have been developed to deal with such kinds of problems, though the more accurate ones can handle only few electron-systems. One approach is the single-electron approach. It assumes that the electron-electron contributions can be dealt with by a clever choice of periodic potential V(r) in the one-electron Schrödinger equation below,

$$[T_{elec} + V(r)]\psi_k(r) = \varepsilon(k)\psi_k(r) \tag{2.3}$$

The subscript k is a wave vector and r denotes the position of the electron. However a problem arises in describing a system of more than one electron. The potential V(r) must be chosen to describe the interaction of periodic ions and the interactions of other electrons, but in order to establish this, equation 2.2 is needed to be solved for all other electrons first. Which means that in order to know the potential one needs to know the solution, but to discover the solution one needs to know the potential. Various approximations have been adopted in solving this. In 1920 Douglas Hartree [2]developed an approach named after himself called the Hartree approximation.

The Hartree approximation is capable of solving the multi-electron Schrödinger equation of the wave function of the form $\psi(r_1 s_1, r_2 s_2, \ldots\ldots, r_n s_n)$, where r_i and s_i are spatial and spin coordinates. This approximation defines the potential by separating it into an electronic part (V_{elec}) and an ionic part, V_{ion}. The electron-electron interaction term is approximated so that each electron moves in the electric field of the other electrons which are assumed to be stationary. This leads to the remaining electrons being treated as a static distribution of negative charge with their charge density defined as follows,

$$\rho_i(r) = -e \sum_i |\psi_i(r)|^2 \tag{2.4}$$

This subscript *i* assumes that electrons are uncorrelated and obey the Pauli exclusion principle. The electronic potential can be modified by substituting the charge density 2.2 as follows,

$$V_{elec} = e^2 \sum_i \int dr' |\psi_i(r')|^2 \frac{1}{|r - r'|} \tag{2.5}$$

Then, substituting the above equation and the ordinary ionic potential (V_{ion}) in the equation 2.2 we obtain the Hartree equation

$$\varepsilon_i \psi_i(r) = [T_{elec} + V_{ion}(r) + V_{elec}(r)] \psi_i(r). \tag{2.6}$$

The Hartree approximation fails to work when the electron is removed from the averaged N electrons, and it is only capable of describing the field experienced by the electron from the other remaining

electrons. It also does not take into account the antisymmetric nature of the fermionic wavefunction. In the next section we focus on the Hartree-Fock approximation which involves the inclusion of the exchange term in the Hartree equation.

2.3 Wave function based approaches

2.3.1 Hartree-Fock Approximation

The main purpose of the Hartree-Fock approximation [3] is to correct the failure of the Hartree approximation. This approach is also based on the independent electron approximation. The independent electron approximation is given by the sum of a single one-electron Hamiltonian as follows:

$$H_{app} = \sum_{i=1}^{N} [T_{elec} + V(r_i)]. \tag{2.7}$$

$V(r_i)$ is the new electronic potential energy in the field of all the nuclei and N is the number of electrons in the system. The solution of the Schrödinger equation is a product of one-electron states and is expressed as follows:

$$\psi(x_1, ... x_n) = \psi_1(x_1)\psi_2(x_2).......\psi_N(x_N) \tag{2.8}$$

Where $\psi_1, \psi_2.......\psi_N$ are eigenstates of the one-electron Schrödinger equation. These eigenstates are orthogonal and uncorrelated due to the fact that each particle is independent of the other. The terms x_i are the combination of spin s_i and orbital co-ordinate position r_i and are written as follows:

$$x_i = (r_i, s_i) \tag{2.9}$$

The probability density of finding the electrons in the orbital co-ordinates is given by

$$\rho(x_1, x_2, ... x_N) = |\psi_1(x_1)|^2 |\psi_2(x_2)|^2 ...... |\psi_N(x_N)|^2 \tag{2.10}$$

This equation is the product of one electron probability densities and is uncorrelated. A state $\psi(x_i)$ with the permutation of x_i is also a solution of the Schrödinger equation, but we require the state to be antisymmetric with the interchange of any two electrons in order to satisfy the Pauli's exclusion principle. The solution of the Schrödinger equation can be determined by replacing the trivial wave function $\psi(r)$ by a Slater determinant [4] of one-electron wave functions.

$$\psi(x_1, x_2, \ldots\ldots, x_N) = \frac{1}{\sqrt{N!}} \begin{vmatrix} \psi_1(\mathbf{r_1}) & \psi_1(\mathbf{r_2}) & \cdots & \psi_1(\mathbf{r_N}) \\ \psi_2(\mathbf{r_1}) & \psi_2(\mathbf{r_2}) & \cdots & \psi_2(\mathbf{r_N}) \\ \vdots & \vdots & \ddots & \vdots \\ \psi_N(\mathbf{r_1}) & \psi_N(\mathbf{r_2}) & \cdots & \psi_N(\mathbf{r_N}) \end{vmatrix}. \tag{2.11}$$

The Slater determinant above is helpful in obtaining the exchange term

$$-\frac{1}{2} \sum_j \int d^3r' \, \psi_j^*(r') \psi_i(r') \frac{1}{|\mathbf{r} - \mathbf{r'}|} \psi_j(r) \tag{2.12}$$

that acts between electrons of the same spin. Applying this third term to the Hartree equation leads to the Hartree-Fock equation. The latter equation is written as follows:

$$H\psi(r) = [T_{elec} + V_{ion}(r) + V_{elec}] \psi_i(r) - \frac{1}{2} \sum_j \int d^3r' \, \psi_j^*(r') \psi_i(r') \frac{1}{|\mathbf{r} - \mathbf{r'}|} \psi_j(r) \tag{2.13}$$

The exchange term introduces some complications to the Hartree equation and causes the Hartree-Fock equation to be difficult to solve because of its non-local nature. This approximation fails due to the ignored Coulomb repulsion of the electrons.

2.3.2 Density Functional Theory

Density functional theory (DFT) is one of the most important tools for predicting the ground-state properties of electronic systems (metals, semiconductors and insulators). The reason for the widespread use of this tool is its reasonable accuracy and high computational efficiency. DFT started to be popular in the 1970s and in 1998, one of its developers, Walter Kohn, was honoured with the Nobel Prize in

Chemistry. To date it is still one of the leading tools for calculations of the electronic structure in solid state physics and chemistry. DFT yields results regarding electronic structure which in several instances are in agreement with experimental results. In contrast to the Hartree Fock method which focuses on the many body wavefunctions as the fundamental variable of the system, DFT describes the entire number of interacting electrons through their density. The Hartree Fock approximation is computationally very costly and fails particularly for metals.

DFT separates the total energy into three terms, starting with the kinetic energy term, the (coulomb energy term which includes the classical electrostatic interactions between the electrons and nuclei in the system) and the exchange-correlation term that includes the many body interactions. Although DFT is significant, it fails to properly describe the van der Waals forces in sparse materials. It also underestimates the band gaps of semiconductors and some other electronic properties of highly correlated systems and this is related to aspects of formalism that we discuss below. It is still a current focus of improvement in research.

Hohenberg and Kohn proposed the Density Functional Theory (DFT) [5, 6] to deal with many-electron problems more efficiently. In DFT one ignores the precise details of the many-electron wave function $\psi(\mathbf{r_1}, \mathbf{r_2}, \ldots, \mathbf{r_N})$ and considers the density of electrons in the system

$$\rho(\mathbf{r}) = N \int \psi^*(\mathbf{r}, \mathbf{r_2}, \ldots, \mathbf{r_N}) \, \psi(\mathbf{r}, \mathbf{r_2}, \cdots, \mathbf{r_N}) \, d\mathbf{r_2} d\mathbf{r_3} \ldots d\mathbf{r_N}$$

as the basic variable. The main result of DFT is that the ground state properties of a many electron system are uniquely determined by its electron density distribution. In other words, all ground state properties of the many electron system are functional of its ground state electron density distribution. When the ground state electron density distribution of the many electron system is determined, its external potential is also uniquely determined.

2.3.2.1   Basic theorems of DFT and Kohn-Sham equation

Density functional theorem can be expressed in terms of two basic theorems:

Theorem I : There is a one-to-one correspondence between the ground-state density $\rho(\mathbf{r})$ of a many-electron system and the external potential V_{ext}. An immediate consequence is that the ground-state expectation value of any observable $\hat{O}$ is a unique functional of the exact ground-state electron density:

$$\langle \Psi | \hat{O} | \Psi \rangle = O[\rho]$$

Few steps of calculation can prove the above statement. Let us consider two N-electron systems, characterised by two different external potentials (differing by more than an additive constant), $V_1(r)$ and $V_2(r)$. Let us consider that corresponding two wavefunctions ψ_1 and ψ_2, yield the same electron density $\rho(\mathbf{r})$. One can use the variational principle and write for the energy the results:

$$
\begin{aligned}
E_1 &= \langle \psi_1 | H_1 | \psi_1 \rangle \\
&< \langle \psi_2 | H_1 | \psi_2 \rangle = \langle \psi_2 | H_2 | \psi_2 \rangle + \langle \psi_1 | [H_1 - H_2] | \psi_1 \rangle \\
&< E_2 + \int dr \rho(r) [V_1(r) - V_2(r)]
\end{aligned}
$$

On interchange of the suffixes, one also has the result

$$E_2 < E_1 + \int dr \rho(r) [V_2(r) - V_1(r)]$$

Summation of the two inequalities leads to the contradiction

$$E_1 + E_2 < E_2 + E_1$$

Hence the assumption of identical density arising from two different external potentials is wrong. This automatically implies the following:

A given $\rho(\mathbf{r})$ can correspond to only one $v(\mathbf{r})$

$$\Downarrow$$

Since $V(\mathbf{r})$ is fixed, the Hamiltonian and hence the wave-function are also fixed by the density.

$$\Downarrow$$

Since the wave-function is a functional of density, the energy functional $E_V[\rho]$ for a given external potential $V(\mathbf{r})$ is a unique functional of the density.

Theorem II : For $\hat{O}$ being the Hamiltonian $\hat{H}$, the ground-state total energy functional $H[\rho] \equiv E_{V_{ext}}[\rho]$ is of the form

$$E_{V_{ext}}[\rho] = \underbrace{\left\langle \Psi|\hat{T}+\hat{V}|\Psi \right\rangle}_{F_{HK}} + \left\langle \Psi|\hat{V}_{ext}|\Psi \right\rangle \tag{2.14}$$

$$= F_{HK}[\rho] + \int \rho(\mathbf{r}) V_{ext}(\mathbf{r}) d\mathbf{r} \tag{2.15}$$

where the Hohenberg-Kohn density functional $F_{HK}[\rho]$ is universal for any many-electron system. $E_{V_{ext}}[\rho]$ reaches its minimal value (equal to the ground-state total energy) for the ground state density corresponding to V_{ext}.

The Hohenberg-Kohn variational theorem states that if the functional $E_{V_{ext}}[\rho]$ is varied with respect to $\rho(\mathbf{r})$, then $E_{V_{ext}}[\rho_0]$ takes the lowest value, corresponding to the ground state, with the correct ground state density $\rho_0(\mathbf{r})$, i.e. $E_{V_{ext}}[\rho_0] \leq E_{V_{ext}}[\rho]$. The equations of Kohn and Sham, published in 1965, turn DFT into a practical tool [6]. We can rewrite the Hohenberg-Kohn functional in the following way :

$$F_{HK} = T + V + T_0 - T_0$$

$$= T_0 + V + \underbrace{T - T_0}_{V_C}$$

$$= T_0 + V_H + V_C + \underbrace{V - V_H}_{V_X}$$

$$= T_0 + V_H + \underbrace{V_C + V_X}_{E_{XC}}$$

Here T and V are the exact kinetic and electron-electron potential energy functionals, T_0 is the functional for the kinetic energy of a non-interacting electron gas, V_H stands for the Hartree contribution and V_X for the exchange contribution. Here E_{XC} is the exchange-correlation energy functional. We can write explicitly the energy functional as following

$$E_{V_{ext}}[\rho] = T_0[\rho] + V_H[\rho] + E_{XC}[\rho] + V_{ext}[\rho] \tag{2.16}$$

The above expression can also be viewed from a different perspective as the energy functional of a non-interacting classical electron gas, subject to two external potentials. One due to the nuclei, and other due to exchange and correlation effects. The corresponding Hamiltonian - called the Kohn-Sham Hamiltonian is

$$\hat{H}_{KS} = \hat{T}_0 + \hat{V}_H + \hat{V}_{XC} + \hat{V}_{ext} \tag{2.17}$$
$$= -\frac{\hbar^2}{2m_e}\nabla_i^2 + \frac{e^2}{4\pi\varepsilon_0}\int\frac{\rho(\acute{\mathbf{r}})}{|\mathbf{r}-\acute{\mathbf{r}}|}d\acute{\mathbf{r}} + \hat{V}_{XC} + \hat{V}_{ext}$$

where the exchange-correlation potential is given by the functional derivative

$$\hat{V}_{XC} = \frac{\delta E_{XC}[\rho]}{\delta\rho} \tag{2.18}$$

The minimization of E_{KS} ($E_{V_{ext}}$ in Eq.2.16) is carried out subject to the constraint of normalized density $\int\rho(\mathbf{r})d\mathbf{r} = N$. Application of the variational principle of the Kohn-Sham theory requires that for the ground state

$$\frac{\delta}{\delta\rho}\{E_{KS}[\rho] - \lambda N\} = 0 \tag{2.19}$$

λ is the Lagrange multiplier. Using Eq.2.16, one gets,

$$\frac{\delta T_0[\rho]}{\delta\rho(\mathbf{r})} + V_{KS}(\mathbf{r}) = \lambda \tag{2.20}$$

where

$$V_{KS}(\mathbf{r}) = v(\mathbf{r}) + V_H(\mathbf{r}) + V_{XC}(\mathbf{r}) = v(\mathbf{r}) + \frac{e^2}{4\pi\varepsilon_0}\int\frac{\rho(\acute{\mathbf{r}})}{|\mathbf{r}-\acute{\mathbf{r}}|}d\acute{\mathbf{r}} + \frac{\delta E_{XC}}{\delta\rho(\mathbf{r})}$$

Kohn and Sham showed that solving Eq.2.20 is equivalent to solving the following set of single-particle Schrödinger-like equations for the variational wave-functions of fictitious non-interacting electrons

$$\left[-\frac{\hbar^2}{2m_e}\nabla^2 + V_{KS}(\mathbf{r})\right]\phi_i = \varepsilon_i\phi_i \tag{2.21}$$

where ϕ_i and ε_i are the single-particle wave-functions and eigenvalues, respectively, such that $\rho(\mathbf{r}) = \sum_i^N\phi(\mathbf{r})^*\phi(\mathbf{r})$. The Eq.2.21, therefore, represents the set of Kohn-Sham self-consistent equations. Since $V_H(\mathbf{r})$ and $V_{XC}(\mathbf{r})$ depend on ρ, which depend on ϕ_i, which in turn depend on $V_{KS}(\mathbf{r})$, the problem of solving the Khon-Sham equations is not a straight-forward one. The usual way of solving such

problems is the iterative procedure, *i.e.* to start with an initial guess for $\rho(\mathbf{r})$, calculate the corresponding $V_{KS}(\mathbf{r})$, and then solve the differential equation (Eq.2.21) for the ϕ_i. From these one calculates a new density, and starts again. The process is repeated until it converges. Thus the procedure is called self-consistent cycle.

2.3.2.2   Exchange-correlation functional

Basically we know that the electrons are indistinguishable (Fermions) which means that the wavefunctions of the many body electron system must always be antisymmetric. If they are not it means the electrons have the same spin and by the Pauli exclusion principle those electrons are avoiding each other by a certain distance which reduces the coulomb interaction. The energy gained during the reduction is called exchange energy. Considering the electrons of opposite spin, their energy difference is termed the correlation energy E_{cor}. This energy difference is caused by the small decrease in the coulomb energy due to the small separation of the electrons of different spin caused by their charges. In terms of the explanation above, the correlation energy is always less than the exchange energy. The correlation energy helps in defining the length and the strength of interatomic bonds. In a sparse material the correlation is merely approximate since it is difficult to calculate exactly because correlation affects both kinetic and potential energy. The exchange-correlation energy is a combination of the exchange energy and correlation energy.

$$E_{xc} = E_x + E_c \tag{2.22}$$

In detailed form, the exchange corelation energy can be expresed as a function of charge density $\rho(r)$. The exchange-correlation energy has been successfully calculated by many approaches including quantum Monte Carlo methods. Considering the situation of two electrons of opposite spin satisfying the exchange correlation principle, then the exchange correlation energy is written as follows:

$$E_{xc}[\rho(r)] = \frac{1}{2} \int \int \rho(r_1)\rho(r_2)V(r_1 - r_2)d^3r_1 d^3r_2 \tag{2.23}$$

This exchange-correlation energy $E_{xc}[\rho(r)]$ is required for evaluating the total energy $E[\rho(r)]$ of the system and is related to the exchange-correlation potential by,

$$V_{xc} \quad = \quad \frac{\delta E_{xc}}{\delta \rho(r)} \tag{2.24}$$

This exchange correlation potential V_{xc} is useful in solving the density functional Kohn Sham equations.

2.3.3 Approximations to the exchange-correlation potential

As the form of the exchange-correlation functional are not known, approximations have to be made and this is the part which makes DFT an approximate theory. There are several approximations to the exchange correlation, namely local density approximation(LDA), generalised gradient approximation (GGA), Meta GGA and Hybrid functionals. In this section we focus in detail on the LDA and GGA.

2.3.3.1 Local density approximation (LDA)

In the local density approximation, the electron density $\rho(r)$ which specifies that electron density locally (over a distance comparable to the inverse Fermi wavevector k) varies smoothly. We consider the electron density $\rho(r)$ at each point r in the system and assume that the electron at that point r experiences the same effect from the combination of the surrounding electrons as if the density of the surrounding electrons had possessed the same values throughout the entire space. We may approximate the exchange-correlation energy as the summation (integral) of the electron contribution from a volume which depends on the electron density $\rho(r)$.

$$E_{xc} \quad = \quad \int \rho(r)\varepsilon_{xc}[\rho(r)]d^3r \tag{2.25}$$

Where ε_{xc} is the exchange-correlation energy per particle of a homogenous electron gas which can successfully and accurately be measured experimentally. From a theoretical point of view, ε_{xc}

is parameterized by Hedin and Lundqvist [8]. In some of the work where LDA is applied instead of GGA, the Perdew and Zunger [9] parameterization is employed. LDA is found to be exact for transition metals due to the fact that the electron density varies smoothly. The reason that the LDA is exact is to fulfil the correct sum rule for the exchange correlation hole. The said hole is explained as electrons avoiding each other at a point r, thus obeying the Pauli exclusion principle. Their exchange-correlation energy includes the coulomb interaction of each electron

$$E_{xc}[\rho(r)] \quad = \quad \frac{1}{2} \int \int \rho(r)\rho_{xc}(r,r')v(r-r')d^3r d^3r' \qquad (2.26)$$

The density $\rho_{xc}(r,r')$ is regarded as the conditional density due to the fact that if the separation between these two particles approaches zero, it disappears and leaves a hole which is called the exchange-correlation hole.

2.3.3.2   Generalized gradient approximation (GGA)

The generalized gradient approximation is another form of exchange correlation which is non local. GGA takes into account the density of the electron and its gradient at each point in the space. GGA is constructed by starting from the second order density gradient expansion for the exchange correlation hole surrounding the electron in a system by slowly varying the densities [11]. several GGA functionals like Perdew-Wang 1991 [12] and Perdew, Burke and Ernzerhof (PBE) [13] are the most popular. It is exceptionally successful for small molecules but fails for delocalized electrons in simple metals. It takes a form which includes the gradient density

$$E_{xc} \quad = \quad \int \varepsilon_{xc} f[\rho, \bigtriangledown \rho]\rho(r)d^3r \qquad (2.27)$$

This equation depends only on the general feature of the real space construction where f is a parametrized analytic function, and $\bigtriangledown$ is the gradient density of the electrons. The equation above is only based on the systems of non-spin electrons. If we consider the system containing electrons with

different spins, the system exhibits magnetism and is a straightforward spin polarised material. Now the equation above will take the form of spin densities,

$$E_{xc}[\rho \uparrow, \rho \downarrow] \quad = \quad \int \varepsilon_{xc} f[\rho, \rho, \bigtriangledown \rho \uparrow, \bigtriangledown \rho \downarrow] \rho(r) d^3 r \qquad (2.28)$$

GGA in most cases improves upon the LDA in the description of atoms and solids [15] and it also tends to improve the total energies and atomization energies [6, 17]. The local density approximation (LDA) underestimates the lattice constants by 1% while the GGA overestimates the lattice parameters by 1%. It also reduces the chronic overbinding of the local density approximations [51]. It tends to improve the energy band gap between valence and conduction bands in the cases of semiconductor and insulator materials[114]. The generalised gradient approximation is efficient in computational cost and is numerically accurate and quite reliable. We can conclude that GGA tends to satisfy the demands of quantum mechanics and solid state physics.

2.4   The Plane Wave Formalism

In a solid or crystal, the wavefunctions $\psi(r)$ of the free electrons can be extended in terms of plane waves. By ignoring the potentials caused by ions, the plane waves become exact solutions of the Kohn Sham equations. An atom possessing one electron has a potential which is relatively smooth and is treated as a perturbation. Taking the example of the hydrogen atom which has potential $-\frac{1}{r}$, its wavefunction diverges at the origin and decays exponentially with increasing distance. However in systems containing more than one atom their wavefunctions in the core states are highly complicated and the potential is not smooth. Because of such complications, the plane waves become difficult to implement due to the requirements of the plane wave components. Two types of plane waves that are used, Augmented and Orthogonalised.

The augmented plane wave is based on the solution of the Schrödinger [20] equation for the atom with a spherical region around it. This solution to the atomic problem was implemented in 1937 by Slater [4]. The augmentation solution of the augmented plane wave solution assumes the potential

to be symmetric inside the spheres and zero outside. The construction of the augmented plane wave makes it identical to the original plane wave outside the sphere. The augmented plane wave solution is constructed so that its wavefunction is continuous at the radius $r = R$ whereby,

$$\phi(r) = e^{ikr} \tag{2.29}$$

Since the wavefunction is continuous at $r = R$, the requirements of the Schrödinger equation of the system are not clearly met and its wavefunctions do not join smoothly. The expansion of the augmented plane waves gives the correct approximation of the Schrödinger equation. The wavefunction of the expanded augmented plane waves can be written in terms of the reciprocal lattice vectors G

$$\psi(r) = \sum_G c_G e^{i(k+G)r} \tag{2.30}$$

This plane wave is the one which is applicable in most computational calculations nowadays and is highly accurate in terms of energy values. The second type of plane wave is the orthogonal plane wave which was introduced by Herring in 1940 [21] . This method is not accurate because it lacks the other terms but is better in approximating the bands in the materials, especially in sp-bonded metals.

2.5   Crystal Lattices

Crystalline solids can be described as a Bravais lattice in which small units are repeated in a periodic array. The units may be atoms, ions or molecules and the crystal may be described as primitive, Wigner-seitz, conventional unit cells etc. This crystalline solid can contain a large number of electrons (approximately 10^{23}) moving in a field produced by a similarly large number of ions. This large number of electrons is extremely difficult to use in computations. Bloch's theorem is employed to reduce this large number to as little as half the number of electrons in the unit cell of the crystal.

2.5.1 Bloch's Theorem

The Bloch's theorem can be stated as follows: In a periodic solid, the eigenstates $\psi_i(r)$ of an electron are given in the form of plane waves times the cell-periodic $g_i(r)$,

$$\psi_i(r) = e^{ik.r} g_i(r) \tag{2.31}$$

The Bloch's theorem introduces wave vectors k which are always in the primitive cell of the reciprocal lattice and satisfy the expression $e^{ik.r} = 1$ for all lattice points. The potential $g_i(r)$ is cell periodic and can be expressed as a fourier expansion of plane waves whose wave vectors are reciprocal lattice vectors of the crystal

$$g_i(r) = \sum_q c_{i,q} e^{ik.r} \tag{2.32}$$

Where q is the reciprocal lattice vectors defined by the reciprocal of lattice vector l as follows,

$$q.l = 2\pi n \tag{2.33}$$

and n is any integer. Now each electronic wavefunction can be expressed as the sum of all plane waves,

$$\psi_i(r) = \sum_q c_{i,k+q} e^{i(k+q).r} \tag{2.34}$$

The $c_{i,(k+q)}$ are the coefficients for the plane waves that need to be solved and depend on the kinetic energy cut-off.

2.6 The plane wave energy cut-off

In a crystal, the wavefunction at each k-point can be expanded as a plane wave basis and the convergence of kinetic energy cut-off E_{cut} can be obtained. The Fourier coefficients $C_{i,(k+q)}$ with small kinetic

energies are large and become small when the kinetic energy increases. The plane wave expansion can be truncated to contain the plane waves that consist of the kinetic energy less than the energy cut-off.

$$\frac{\hbar^2}{2m}|k+q|^2 < E_{cut} \tag{2.35}$$

However the truncation of the plane wave expansion at a small energy cutoff will lead to an error when computing the total energies of the system. This error may decrease when the energy cut-off increases. The expansion of the electronic wavefunctions in terms of the plane waves basis set allows the Kohn-Sham equations to be represented in a reciprocal space. The electronic wavefunction expressed in terms of all plane waves equation 2.5.1 is substituted into the Kohn Sham equation 2.21 and, integrated over the region r, gives the equation

$$\sum_{q'}[\frac{\hbar^2}{2m}|k+q|^2\sigma_{qq'} + V_{ion}(q-q') + V_H(q-q') + V_{xc}(q-q')]c_{i,k+q} = \varepsilon_i c_{i,k+q} \tag{2.36}$$

In this equation, the kinetic energy is diagonal and the potentials are expressed in terms of their Fourier components. The Hamiltonian matrix in the square brackets of this equation is diagonal: the size of the matrix was determined by the energy cut-off

$$E_{cut} = \frac{\hbar^2}{2m}|k+q|^2 \tag{2.37}$$

2.7 k-point sampling

Since any point in an integrated Brillouin zone can represent a k-point, there are an infinite number of discrete k-vectors well qualified to be a wave function. Fortunately, the wave function and other properties in most cases vary smoothly over the integrated Brillouin zone so that we can just sample only a finite number of k-points that represent each small region. Thus, the electronic energy and other properties can be evaluated for the occupied Kohn-Sham eigenstates only on these selected points.

The electronic states calculated at a set of k-points contribute to the electronic potential of the solid system and are determined by the shape of the Brillouin zone. This is done since the electronic wavefunctions at the k-points that are close together will be identical, which causes the electronic wavefunctions to be represented over a region of reciprocal space at a single k-point. This enables us to calculate the electronic potential and the total energy of the solid system at a finite number of k-points. The error occurring during calculations can be made small by choosing a heavier set of k-points in the Brillouin zone. For example in a metallic system, dense k-points are needed since it is very difficult to define the Fermi surface with a few points. The dense k-points still make the computational time lenthly and still offer a challenge in research.

Sampling a set of special k-points in the integrated Brillouin zone is a critical part of the Density Functional Theory flow and must fulfill two important goals: select as few as possible to reduce the calculation time and, at the same time, select enough so that they can represent the actual quantities adequately. For a large system with hundreds of atoms, for example, the integrated Brillouin zone volume becomes very small, and a few k-points can describe the variation across the zone accurately. For another example, a supercell of a slab often adopted for the study of surfaces and thin films in this thesis has a long dimension in z-direction (perpendicular to the surface), which includes a thick layer of vacuum in which the wave functions decay to zero. Then only a single k-point is sufficient in z-direction.

Remember that each k-point contains rather rich information about the wave at that point:

- The wave vector k (wave's magnitude and direction), wave length ($\lambda = 2\pi/k$), and kinetic energy (for example, $E = \mathbf{k}^2/2$ for a plane wave)

- The plane that the particular wave permitted to exist, imposing a particular condition on the wave function to be a solution to the wave equation.

- If we plot all the incoming energies on each k-point, it will form the band structure, the energy dispersion.

The whole bulk material is now narrowed down to a handful of sampled k-points for calculation. A

standard method for the generation of a k-point mesh will be discussed next.

2.7.1 Standard k-points method in the Brillouin zone

Now we consider the special k-point method of choosing the sets of points in the Bril- louin zone, which makes the calculation simple and accurate. This method is based on an integrated function (3.58) averaged over a Brillouin zone.

$$F(r) = \frac{\Omega}{(2\pi)^3} \int_{BZ} f(k)d^3k \tag{2.38}$$

where $f(k)$ is the Fourier transformation of $F(r)$ and the function represent complete symmetry of the lattice. Ω is the volume of the unit cell. The Fourier transform may be written in terms of $A_m(k)$ as follows:

$$f(k) = f_o + \sum_{m=1} A_m(k) \tag{2.39}$$

where $A_m(k)$ is the transformation expression defined by,

$$A_m(k) = \sum e^{ik.r} \tag{2.40}$$

where m is any integer. The expression $A_m(k)$ is associated with any shell of the lattice vector and is a real function. This method obtains an approximate value for the integral in the equation $F(r)$. The approximated value can be exact if the term $A_m(k)$ is zero,

$$A_m(k) = 0 \tag{2.41}$$

These sets of points are identical with the ones generated by Monkhorst and Pack [81], and this method is an unbiased one for choosing the set of k-points for sampling the Brillouin zone in fractional

co-ordinates. It gives the points in a rectangular grid of points, *i.e* (k_x, k_y, k_z). The Monkhorst and Pack k-points are sometimes called k-meshes. When the k-meshes are large, the sampling is expected to be fine and accurate. The selection of points depends on the type of crystal. Simple cubic has k-points different to those of body centred cubic (bcc). In the face centred cube (fcc) structure, a good choice for starting points $k = (k_x, k_y, k_z)$ is to select $(1/2, 1/2, 0)$ and $(1/2, 1/2, 1/2)$. These chosen points can satisfy the expression $A_m(k)$ for the infinite set of nearest-neighbour shells represented by the lattice vectors.

2.8 Basis sets

Regardless of whether it is k-space approach or real-space approach, one has to choose an appropriate basis set to expand the single-particle wave-functions and depending on the choice of basis functions, different schemes, therefore, can be broadly grouped into two categories: (*i*) methods using energy independent basis sets or fixed basis sets, like tight binding method using linear combination of atomic orbitals (LCAO) type basis [22], orthogonalized plane wave (OPW) method using plane waves orthogonalized to core states as the basis set [23], pseudopotential method using plane wave basis [24], and (*ii*) methods using energy dependent basis set, like cellular method [25], augmented plane wave (APW) method [26] and the Korringa-Kohn-Rostocker (KKR) Green's function method [27], which use partial waves as basis set. In this thesis, we mainly used pseudopotential method along with plane wave basis, as implemented in the Vienna *ab initio* simulation package (VASP) [28].

2.9 Band structure methods

2.9.1 Pseudopotential Method

It is well known that electrons in the outermost shell of atoms, the so called valence electrons, actively participate in determining the most of the chemical and physical properties of molecules and solids. This leads to the idea behind the pseudopotential theory. Here we will develop the basic concept of

pseudopotential by a simple transformation of single-particle Kohn-Sham equation (2.21) for an atom where core and valence states are denoted as ψ^c and ψ^v respectively. A new set of single-particle valence states $\tilde{\phi}^v$ can be defined as

$$\psi^v(\mathbf{r}) = \tilde{\phi}^v + \sum_c \alpha_c \psi^c(\mathbf{r}) \tag{2.42}$$

where α_c are determined from the condition that ψ^v and ψ^c are orthogonal to each other *i.e* $\langle \psi^v | \psi^c \rangle = 0$ which gives $\alpha_c = - \langle \psi^c | \tilde{\phi}^v \rangle$. Eqn. (2.21) then can be manipulated, with the help of Eqn. (2.42), to

$$\left[T_S + V_{KS} + \sum_c (\varepsilon^v - \varepsilon^c) | \psi^c \rangle \langle \psi^c | \right] \tilde{\phi}^v = \varepsilon^v \tilde{\phi}^v \tag{2.43}$$

with ε^c as the eigenvalue of the core state. Considering $V_R = \sum_c (\varepsilon^v - \varepsilon^c) | \psi^c \rangle \langle \psi^c |$ which is a repulsive potential operator (as $\varepsilon^v > \varepsilon^c$, making ε^v - ε^c positive), Eqn. (2.43) can be written as

$$[T_S + V_{PS}] \tilde{\phi}^v = \varepsilon^v \tilde{\phi}^v \tag{2.44}$$

The operator

$$V_{PS} = V_{KS} + \sum_c (\varepsilon^v - \varepsilon^c) | \psi^c \rangle \langle \psi^c | \tag{2.45}$$

represents a weak attractive potential, denoting the balance between the attractive potential V_{KS} and the repulsive potential V_R, and is called a pseudopotential. While the new states $\tilde{\phi}^v$ obey a single-particle equation with a modified potential, but have the same eigenvalues ε^v as the original valence state ψ^v, are called pseudo-wavefunctions. These new valence states project out of the valence wavefunctions any overlap they have with the core wavefunctions, thereby having zero overlap with the core states. In other words, through the pseudopotential formulation, we have created a new set of valence states, which experience a weaker potential near the atomic nucleus, but the proper ionic potential away from the core region. Since it is this region in which the valence electrons interact to form bonds that hold the solid together, the pseudo-wavefunctions preserve all the important physics relevant to the behavior of the solid.

Since then several methods have been used to generate more accurate as well as more efficient pseudopotentials, keeping the basic principles same. In norm-conserving pseudopotential [29], the all electron

(AE) wave function is replaced by a soft nodeless pseudo (PS) wave function, with the restriction to the PS wave function that within the chosen core radius the norm of the PS wave function have to be the same with the AE wave function and outside the core radius both the wave functions are just identical. Good transferability of constructed pseudopotential requires a core radius around the outermost maximum of the AE wavefunction, because only then the charge distribution and moments of the AE wavefunctions are well produced by the PS wavefunctions. Therefore, for elements with strongly localized orbitals like first-row, 3d and rare-earth elements, the resulting pseudopotentials require a large plane-wave basis set. To work around this, compromises are often made by increasing the core radius significantly beyond the outermost maximum in the AE wave-function. But this is usually not a satisfactory solution because the transferability is always adversely affected when the core radius is increased, and for any new chemical environment, additional tests are required to establish the reliability of such soft PS potentials. This was improved by Vanderbilt [30], where the norm-conservation constraint was relaxed and localized atom centered augmentation charges were introduced to make up the charge deficit. These augmentation charges are defined as the charge density difference between the AE and the PS wavefunction, but for convenience, they are pseudized to allow an efficient treatment of the augmentation charges on a regular grid. Only for the augmentation charges, a small cutoff radius must be used to restore the moments and the charge distribution of the AE wavefunction accurately.

The success of this approach is partly hampered by rather difficult construction of the pseudopotential. Later Blöchl [31] has developed the projector-augmented- wave (PAW) method, which combines idea from the LAPW method with the plane wave pseudopotential approach, and finally turns out computationally elegant, transferable and accurate method for electronic structure calculation of transition metals and oxides. Below we have outlined the idea behind the PAW method.

In the PAW method, the AE wavefunction Ψ_n (which is a full one-electron Kohn-Sham wavefunction) is derived from the PS wavefunction $|\tilde{\Psi}_n\rangle$ by means of a linear transformation:

$$|\Psi_n\rangle = |\tilde{\Psi}_n\rangle + \sum_i (|\phi_i\rangle - |\tilde{\phi}_i\rangle)\langle\tilde{p}_i|\tilde{\Psi}_n\rangle \qquad (2.46)$$

The index i is a shorthand for the atomic site $\mathbf{R}$, the angular momentum numbers $L = (l,m)$ and an additional index k referring to the reference energy ε_{kl}. The all electron partial waves ϕ_i are the solutions of the radial Schrödinger equation for the isolated atom, and the PS partial waves $\tilde{\phi}_i$ are are equivalent to the AE partial waves outside a core radius r_c^l and match with value and derivative at r_c^l. The core radius r_c^l is usually chosen approximately around half the nearest-neighbor distance. The projector function $\tilde{p}_i$ for each PS partial wave localized within the core radius, obeys the relation $\langle \tilde{p}_i | \tilde{\phi}_i \rangle = \delta_{ij}$. Starting from Eqn. (2.46), it is possible to show that in the PAW method, the AE charge density is given by

$$\rho(\mathbf{r}) = \tilde{\rho}(\mathbf{r}) + \rho^1(\mathbf{r}) - \tilde{\rho}^1(\mathbf{r}) \tag{2.47}$$

where $\tilde{\rho}$ is the soft pseudo-charge density calculated directly from the pseudo wavefunctions on a plane wave grid:

$$\tilde{\rho}(\mathbf{r}) = \sum_n f_n \langle \tilde{\Psi}_n | \mathbf{r} \rangle \langle \mathbf{r} | \tilde{\Psi}_n \rangle \tag{2.48}$$

The on-site charge densities ρ^1 and $\tilde{\rho}^1$ are treated on a radial support grids localized around each atom. They are defined as

$$\rho^1(\mathbf{r}) = \sum_{n,(ij)} f_n \langle \tilde{\Psi}_n | \tilde{p}_i \rangle \langle \phi_i | \mathbf{r} \rangle \langle \mathbf{r} | \phi_j \rangle \langle \tilde{p}_j | \tilde{\Psi}_n \rangle \tag{2.49}$$

and

$$\tilde{\rho}^1(\mathbf{r}) = \sum_{n,(ij)} f_n \langle \tilde{\Psi}_n | \tilde{p}_i \rangle \langle \tilde{\phi}_i | \mathbf{r} \rangle \langle \mathbf{r} | \tilde{\phi}_j \rangle \langle \tilde{p}_j | \tilde{\Psi}_n \rangle \tag{2.50}$$

It is to be noted that the charge density $\tilde{\rho}^1$ is exactly the same as $\tilde{\rho}$ within the augmentation spheres around each atom. In PAW approach, an additional density, called compensation charge density is added to both auxiliary densities $\tilde{\rho}$ and $\tilde{\rho}^1$ so that the multi-pole moments of the terms $\rho^1(\mathbf{r})$ - $\tilde{\rho}^1(\mathbf{r})$ in Eqn. (2.47) vanish. Thus the electrostatic potential due to these terms vanishes outside the augmentation spheres around each atom, just as is accomplished in LAPW method. Like density, the energy can also be written as a sum of three terms and by functional derivatives of the total energy, one can derive the expressions of Kohn-Sham equations.

2.9.2 The Projector-Augmented-Wave Formalism

P. E. Blöchl in 1994, developed the projector-augmented- wave (PAW) method, which combines the linear augmented plane wave method with the plane wave pseudopotential approach. This method turned out to be computationally elegant, transferable and accurate method for electronic structure calculation. Later Kresse and Joubert [32] modified this PAW method and implemented within the plane wave code of VASP.

In this formalism, the AE wavefunction Ψ_n is derived from the PS wavefunction $\tilde{\Psi}_n$ by means of a linear transformation:

$$|\Psi_n\rangle = |\tilde{\Psi}_n\rangle + \sum_i \left(|\phi_i\rangle - |\tilde{\phi}_i\rangle \right) \langle \tilde{p}_i | \tilde{\Psi}_n \rangle \tag{2.51}$$

The index i is a shorthand for the atomic site at $\vec{R}_i$. The all electron partial waves ϕ_i are the solutions of the radial Schrödinger equation for the isolated atom. The PS partial waves $\tilde{\phi}_i$ are equivalent to the AE partial waves outside a core radius r_c^l. Of course these two wavefunctions match both in value and slope at the boundary r_c^l. The projector function $\tilde{p}_i$ for each PS partial wave localized within the core radius, obeys the relation $\langle \tilde{p}_i | \tilde{\phi}_j \rangle = \delta_{ij}$. From Eq.2.51, the AE charge density in PAW method can be written as,

$$\rho(\vec{r}) = \tilde{\rho}(\vec{r}) + \rho^1(\vec{r}) - \tilde{\rho}^1(\vec{r}) \tag{2.52}$$

where $\tilde{\rho}$ is the soft pseudo-charge density calculated directly from the pseudo wavefunctions on a plane wave grid. The on-site charge densities ρ^1 and $\tilde{\rho}^1$ are treated on radial support grids localized around each atom. It should be mentioned that the charge density $\tilde{\rho}^1$ is exactly the same as ρ^1 within the augmentation spheres around each atom. In PAW approach, an additional density, called compensation charge density is added to both auxiliary densities ρ^1 and $\tilde{\rho}^1$ so that the multi-pole moments of the terms $\rho^1 - \tilde{\rho}^1$ in Eq.2.52 vanish. Thus the electrostatic potential due to these terms vanishes outside the augmentation spheres around each atom, just as is accomplished in LAPW method. Like density, the energy can also be written as a sum of three terms and by functional derivatives of the total energy, one can derive the expressions of Kohn-Sham equations.

2.9.3   The tight-binding method (LCAO method)

For a periodic system, the tight-binding Hamiltonian is given by

$$\mathbf{H} \;=\; \sum_{il_1\sigma}\varepsilon_{l_1}a^{\dagger}_{il_1\sigma}a_{il_1\sigma}+\sum_{ij}\sum_{l_1,l_2,\sigma}(t^{l_1l_2}_{ij}a^{\dagger}_{il_1\sigma}a_{jl_2\sigma}+h.c.) \tag{2.53}$$

where, the electron with spin σ is able to hop from the orbitals labelled l_1 with onsite energies equal

to ε_{l_1} in the ith unit cell to those labelled l_2 in the jth unit cell, with the summations l_1 and l_2 running

over all the orbitals considered on the atoms in a unit cell, and i and j over all the unit cells in the solid.

Thus, any orbital in the solid can be defined with the two indices, i and l_1, henceforth referred to as the

set (i, l_1). The hopping interaction strength $(t^{l_1l_2}_{ij})$ depends on the nature of the orbitals involved as well

as on the geometry of the lattice [22]. Since the hopping integrals are expected to fall off rapidly with

distance [33], it is sufficient to consider those terms in the Hamiltonian which allow the electron to hop

to orbitals on nearest neighbor atoms. Further, since the Hamiltonian is independent of the spin (σ), in

the rest of the discussion the spin indices of the Fermion operators will not be retained explicitly. The

Hamiltonian can be cast into the momentum space by a Fourier transformation of the operators given

by

$$a^{\dagger}_{il_1} \;=\; \frac{1}{\sqrt{N}}\sum_{k}a^{\dagger}_{kl_1}e^{i\mathbf{k}.\mathbf{r}_{il_1}}$$

so that,

$$\mathbf{H} \;=\; \sum_{il_1}\varepsilon_{l_1}a^{\dagger}_{il_1}a_{il_1}+\sum_{<ij>}\sum_{l_1,l_2}(t^{l_1l_2}_{ij}a^{\dagger}_{il_1}a_{jl_2}+h.c.)$$

$$=\; \frac{1}{N}\sum_{il_1}\sum_{kk'}\varepsilon_{l_1}a^{\dagger}_{kl_1}a_{k'l_1}e^{i\mathbf{k}.\mathbf{r}_{il_1}}e^{-i\mathbf{k}'.\mathbf{r}_{il_1}}$$

$$+\frac{1}{N}\sum_{<ij>}\sum_{l_1,l_2,k,k'}(t^{l_1l_2}_{ij}a^{\dagger}_{kl_1}a_{k'l_2}e^{i\mathbf{k}.\mathbf{r}_{il_1}}e^{-i\mathbf{k}'.\mathbf{r}_{jl_2}}+h.c.)$$

An advantage of this representation is that the Hamiltonian breaks into distinct blocks for each $\mathbf{k}$ value,

thereby simplifying the problem. In order to realize this, we first define a set of vectors $\mathbf{R}^{l_1l_2}_{\alpha}$ for the

orbital (i, l_1), that connect it to the orbitals (j, l_2) on nearest neighbor atoms, $\mathbf{r}_{jl_2} = \mathbf{r}_{il_1} + \mathbf{R}^{l_1l_2}_{\alpha}$. As a

result of the periodicity of the lattice, the set of vectors $\mathbf{R}^{l_1l_2}_{\alpha}$ are the same for every (i, l_1) ndependent

of the unit cell index, i. As the hopping integrals, between orbitals (i, l_1) and (j, l_2) depend only on the

vector $\mathbf{R}_\alpha^{l_1 l_2}$ connecting the two orbitals involved, the quantities $t_{ij}^{l_1 l_2}$ in the Hamiltonian can be replaced with $t_\alpha^{l_1 l_2}$. Therefore, the simplified Hamiltonian becomes,

$$
\begin{aligned}
\mathbf{H} &= \frac{1}{N}\sum_{il_1}\sum_{kk'}\varepsilon_{l_1} a_{kl_1}^\dagger a_{k'l_1} e^{i\mathbf{k}.\mathbf{r}_{il_1}} e^{-i\mathbf{k}'.\mathbf{r}_{il_1}} \\
&+ \frac{1}{N}\sum_\alpha \sum_{i,l_1,l_2,k,k'} (t_\alpha^{l_1 l_2} a_{kl_1}^\dagger a_{k'l_2} e^{i\mathbf{k}.\mathbf{r}_{il_1}} e^{-i\mathbf{k}'.(\mathbf{r}_{il_1}+\mathbf{R}_\alpha^{l_1 l_2})} + h.c) \\
&= \frac{1}{N}\sum_{il_1}\sum_{kk'}\varepsilon_{l_1} a_{kl_1}^\dagger a_{k'l_1} e^{i(\mathbf{k}-\mathbf{k}').r}_{il_1} + \frac{1}{N}\sum_\alpha \sum_{i,l_1,l_2,k,k'} (t_\alpha^{l_1 l_2} a_{kl_1}^\dagger a_{k'l_2} e^{i(\mathbf{k}-\mathbf{k}').\mathbf{r}_{il_1}} e^{-i\mathbf{k}'.\mathbf{R}_\alpha^{l_1 l_2}} + h.c) \\
&= \sum_{l_1}\sum_{kk'}\varepsilon_{l_1} a_{kl_1}^\dagger a_{k'l_1}\delta(k-k') + \sum_\alpha \sum_{l_1,l_2,k,k'} (t_\alpha^{l_1 l_2} a_{kl_1}^\dagger a_{k'l_2}\delta(k-k') e^{-i\mathbf{k}'.\mathbf{R}_\alpha^{l_1 l_2}} + h.c.) \\
&= \sum_{l_1}\sum_k \varepsilon_{l_1} a_{kl_1}^\dagger a_{kl_1} + \sum_\alpha \sum_{kl_1 l_2} (t_\alpha^{l_1 l_2} a_{kl_1}^\dagger a_{kl_2} e^{-i\mathbf{k}.\mathbf{R}_\alpha^{l_1 l_2}} + h.c.)
\end{aligned}
$$

From the above expression, it is seen that the Hamiltonian involves terms connecting different orbitals which may be on the same or on different atoms at a **k** point. Thus, the problem of electronic structure determination reduces to one of solving the Hamiltonian at each **k** point in the Brillouin zone. This has to be performed numerically in most cases, with the size of the matrix equal to the total number of orbitals considered on all the atoms in the unit cell.

The eigenfunctions of the Hamiltonian, **H**, correspond to linear combinations of the atomic orbitals, $\phi_j(r)$, given by,

$$
\Psi_i(r) = \sum_j x_{ij}\phi_j(r)
$$

It is seen that the different atomic orbitals located on neighboring atoms are not necessarily orthogonal to each other. However, since the formalism of second quantization requires an orthogonal basis for the proper definition of fermion creation and annihilation operators and their associated Fock space, the Löwdin transformation [34] which is outlined below has been used to transform the orbitals into an orthogonal basis set. If the spatial overlap between orbitals on neighboring atoms is given by

$$
S_{\alpha\beta} = \int dr \phi_\alpha^*(r)\phi_\beta(r) - \delta_{\alpha\beta}
$$

it is then seen that the coefficients x_{ij} must satisfy the matrix equation

$$
\mathbf{Hx} = (\mathbf{1}+\mathbf{S})\mathbf{x}\mathbf{E}
$$

$$
\text{where,} \qquad \mathbf{x}^\dagger(\mathbf{1}+\mathbf{S})\mathbf{x} = \mathbf{1}
$$

involving $\mathbf{x}$ and $\mathbf{E}$, which are the matrices formed by the expansion coefficients x_{ij} and the eigenvalues E_j respectively. In order to represent the Hamiltonian in an orthogonal basis, given by $\mathbf{c}$, the matrix $\mathbf{x}$ is replaced by $\mathbf{c}$ according to the relation,

$$\mathbf{x} \;=\; (\mathbf{1}+\mathbf{S})^{-1/2}\mathbf{c}$$

By this substitution, the eigenvalue problem is reduced to the form,

$$\mathbf{H}'\mathbf{c} \;=\; \mathbf{E}\mathbf{c}$$

$$\mathbf{c}^{\dagger}\mathbf{c} \;=\; 1$$

where $\mathbf{H}'$ is the Hamiltonian in the orthogonal basis. $\mathbf{H}'$ is related to the Hamiltonian set up in the non-orthogonal basis by the expression,

$$\mathbf{H}' \;=\; (\mathbf{1}+\mathbf{S})^{-1/2}\mathbf{H}(\mathbf{1}+\mathbf{S})^{-1/2}$$

In order to evaluate $(\mathbf{1}+\mathbf{S})^{-1/2}$, the matrix $(\mathbf{1}+\mathbf{S})$ is first diagonalized by a unitary transformation $\mathbf{U}$ to yield a diagonal matrix $\mathbf{D}$,

$$\mathbf{U}^{\dagger}(\mathbf{1}+\mathbf{S})\mathbf{U} \;=\; \mathbf{D}$$

As the eigenvalues of $(\mathbf{1}+\mathbf{S})$ are positive, a new matrix $\mathbf{D}^{-1/2}$ can be formed from $\mathbf{D}$ by replacing each diagonal element by its inverse square root. So, $(\mathbf{1}+\mathbf{S})^{-1/2}$ can be evaluated using the following relation

$$(\mathbf{1}+\mathbf{S})^{-1/2} = \mathbf{U}\mathbf{D}^{-1/2}\mathbf{U}^{\dagger}$$

Once $(\mathbf{1}+\mathbf{S})^{-1/2}$ is known, the Hamiltonian can be set up in the orthogonal basis and solved.

2.10   Practical algorithm for Density Functional Theorem runs

After going through the topics covered so far, we can make the conclusion that the level of a DFT run in terms of accuracy and efficiency crucially depends on three choices:

- The choice of and XC functional

- The choice of a pseudopotential

- The choice of a basis set for the expansion of the KS orbitals.

Assuming that we have made best choices for the above factors, in this section we add one more element : the algorithms adopted for solving the Kohn-Sham equations. Remember that a DFT calculation must repeatedly treat large nonlinear eigenvalue problems to reach the electronic ground state of a solid. At a given computer power, hence the rest depends on the calculation algorithms implemented. Not that calculating the charge density or energy terms is of minor importance, but the diagonalization of the Kohn-Sham Hamiltonian takes about 70% of overall computer time.

2.10.1   Electronic minimizations

The electonic minimization or electronic relaxation or static relaxation means finding the ground state of electrons at the fixed atom positions and it can be achieved by diagonalization for the *H* matrix either directly or iteratively. For the full minimization of the system, an ionic minimization must follow after each electonic minimization.

2.10.1.1   Direct diagonalization

The conjugate gradient and CP algorithms belong to this category. Note, however that we only need those of the lowest occupied orbitals ($\sim n/2$) for the total energy at the end. Therefore, the direct method is not suitable for materials calculations which normally require large matrix elements of plane waves (10^4-10^5).

2.10.1.2   Iterative Davidson method

Rarely with normal matrix-matrix operations do we find the eigenvalues of large martrices. Rather, the methods always involve a variety of algorithms, manipulations, and tricks to speed up the diagonalization: the Hamiltonian matrix is projected, approximated to smaller sizes, preconditioned, or spanned in subspace. In this iterative diagonalization (normally in conjuction with the charge density mixing),

matrix elements are preconditioned and thus the needed number of orbitals can be reduced to slightly more than $n/2$. Furthermore, the orbitals other than the ground states will be removed along the iteratiin process. The most notable iterative algorithms along this line are the blocked Davodson(1975)(Kresse and Furthmüller 1996) and the residual minimization/direct inversion in the interative subspace (RMM-DIIS) methods. All these are algebraic manipulations to solve the matrix problem efficiently.

The Davidson method provides an efficient way for solving eigenvalue matrix problems of a very large size, iteratively and self-consistently. The Davidson algorithm is considered to be slower, but it is very reliable in a crude convergence of the wave function at the initial stage of iteration. Normally, by combining sets of bands into blocks, energy minimization is performed iteratively in parallel.

2.10.1.3 RMM-DIIS method

The RMM-DIIS method (Pulay 1980; Wood and Zunger 1985) also provides an efficient and fast way of solving eigenvalue matrix problems iteratively and self-consistently. The diagonalization is carried out iteratively with respect to plane wave coefficeints, inproving the orbitals (and thus charge densities). The actual calculation, however does not handle the orbitals directly but instead minimizes the residual vector R, which is generally written as:

$$R = (\hat{H} - \varepsilon)\phi \tag{2.54}$$

In this residuum minimization approach, R becomes smaller and smaller as iteration proceeds and eventually vanishes to zero at convergence. It also involves subspace diagonalization and plays with residuum (actually the norm of the residual vector), the difference between input and calculated wave functions. The convergence is achieved when the residual becomes zero. Note that working with the residual vector (the norm of the residual vector is clearly positive) removes the orthogonality reqirement because the norm of the residual vector has an unconstrained local minimum at each eigenvector, which can speed up the calculation significantly. After updating all wave functions, orthoginalization is then carried conveniently by subspace diagonalization.

Its parallel implementation is also possible based on a band-by-band optimization of wave functions

(information about other bands is not required). Thus, the RMM-DIIS algorithm is considered to be fast and efficient for large systems but sometimes is apt to miss the right wave function at the initial stage of iteration. (If the initial set of wave functions does not span the real ground state, it might happen that, in the final solution, some eigenvectors will be missing.) this fact naturally suggests the optimal option for us: starting with the Davidson method, followed by the RMM-DIIS method.

2.10.2 Ionic minimizations

The DFT calculation aims for a system fully relaxed both electronically and structurally. All topics up to now have concerned minimizing the electronic energy, with the inner Self consistent loop at fixed ionic positions. After each electronic relaxation, the forces acting on each ion are calculated, and ions are driven to downward directions of forces for the next electronic relaxation. This outer loop, the ionic minimization, includes relaxations of ionic positions and/or unit cell shape/size. After successive minimization of electronic and atomic energies, the system will reach the minimum-energy configuration at which the forces at each atom vanish close to zero (normally $< 0.01 - 0.05$ eV/Å). We first see how the forces at each atom are calculated and then move to three algorithms that are commonly implemented for this ionic minimization: the quasi-Newton method, the conjugate gradient (CG) method, and the damped MD method.

2.10.2.1 Hellmann-Feynman forces

Forces on atoms arise from both atomic and electronic sources, and the Hellmann-Feynman theorem (Feynman 1939; Hellmann 1937) provides an efficient way to account for them, which does not require any additional effort, other than normal electronic minimization. The theorem states that, if an exact $\hat{H}$ and the corresponding ϕ_i are calculated, the force on an atom is the expectation value of the partial derivative of $\hat{H}$ with respect to atomic position r_I. Since only two potential terms are related to r_I, the theorem leads to

$$F_I = -\frac{dE}{dr_I} = -\left\langle \phi_i \mid \frac{\partial \hat{H}}{\partial r_I} \mid \phi_i \right\rangle = -\frac{\partial U_{IJ}}{\partial r_I} - \int \frac{\partial U_{ext}}{\partial r_I} \rho(r) dr \qquad (2.55)$$

Therefore after an electronic iteration, the forces can be calculated accordingly by taking simple derivatice operations on two potential terms. This is why the force calculations, which are so fast, are almost unnoticed in a normal DFT run. Based on these calculated forces, we can direct in which direction and how much the atoms should move. One remark should be made here. If the basis set depends upon atomic positions, the Hellmann-Feynman equation has an extra term Pulay forces. The PW approach has no such problem as it is nonlocal.

Three commonly implemented schemes for ionic minimization are the conjugate gradient, the quasi-Newton and the damped MD methods.

Bibliography

[1] M. Born and J. R. Oppenheimer, "Zur Quantentheorie der Molekeln", Ann. Physik **84**, 457 (1927).

[2] D. R. Hartree, "The wave mechanics of an atom with non-coulombic central field: parts I, II, III", Proc. Cambridge Phil. Soc. **24**, 89, 111, 426 (1928).

[3] V. Fock, "Naherungsmethode zur Losung des quanten-mechanischen Mehrkorperprobleme", Z. Phys. **61**, 126 (1930).

[4] J. C. Slater, "The Theory of Complex Spectra", Phys. Rev. **34**, 1293 (1929).

[5] W. Kohn and L. J. Sham, Phys. Rev. **140**, A1133 (1965).

[6] P. Hohenberg and W. Kohn, Phys. Rev. **136**, B864 (1964).

[7] E. Kaxiras, Atomic and Electronic Structure of Solids; Cambridge University Press, UK, p. 62-65, (2003).

[8] L. Hedin and B. I. Lundqvist. J.Phys.C, **4**, 2064 (1971).

[9] . Perdew and A. Zunger. Phys.Rev.B, **23**, 5048 (1981).

[10] D. M. Ceperley and B. J. Alder, Phys. Rev. Lett. **45**, 566 (1980).

[11] D. C. Langreth and M. J. Mehl. Phys.Rev. A, **38**, 3098 (1983).

[12] J.P. Perdew and Y. Wang, Phys. Rev. B **45**, 13244 (1992).

[13] J. P. Perdew, K. Burke, and M. Ernzerhof, Phys. Rev. Lett. **77**, 3865 (1996).

[14] A. D. Becke. Phys.Rev.Lett, **77**,18 (1988).

[15] J. Perdew, K. Burke, and M. Ernzerhof. Phys. Rev. Lett, **77**, 18 (1996).

[16] Y. Zhang and W. Yang. Phys. Rev. Lett, **80**, 890 (1998).

[17] B. Hammer, L. B. Hansen, and J. K. Norskov. Phys. Rev. B, **59**, 7413 (1999).

[18] W. Kohn and L. J. Sham. Phys. Rev, **140** A1133, (1965).

[19] Z. Wu and R. E Cohen. Phys. Rev. B, **73**, 235116, (2006).

[20] E. Schrodinger. Phys. Rev, **28**, 1049 (1926).

[21] W. C. Herring. Phys. Rev. Lett, **57**, 1169,(1940).

[22] J. C. Slater and G. F. Koster, Phys. Rev. **94**, 1498 (1954).

[23] W. C. Herring, Phys. Rev. **57**, 1169 (1940); W. C. Herring and A. G. Hill, Phys. Rev. **58**, 132 (1940).

[24] J. C. Phillips and L. Kleinman, Phys. Rev. **116**, 287 (1959).

[25] E. P. Wigner and F. Seitz, Phys. Rev. **46**, 509 (1934).

[26] T. L. Loucks, *Augmented Plane Wave Methods*, (Benjamin, New York, 1967).

[27] J. Korringa, Physica **13**, 392 (1947); J. Korringa, Phys. Rev. **238**, 341 (1994).

[28] G. Kresse and J. Hafner, Phys. Rev. B **47**, 558 (1993); G. Kresse and J. Furthmuller, Phys. Rev. B **54**, 11169 (1996)

[29] D. R. Hamann, M. Schlüter, and C. Chiang, Phys. Rev. Lett. **43**, 1494 (1979).

[30] D. Vanderbilt, Phys. Rev. B **41**, 7892 (1985).

[31] P. E. Blöchl, Phys. Rev. B **50**, 17953 (1994).

[32] G. Kresse and D. Joubert, Phys. Rev. B 59, 1758 (1999).

[33] Walter A. Harrison, *Electronic Structure and Properties of Solids* (Dover, 1989).

[34] Per-Olov Löwdin, J. Chem. Phys. **18**, 365 (1950).

Chapter 3

Strained induced magnetism in a nonmagnetic oxide LaCoO$_3$

3.1 Introduction

Recent Advances in growth technology have led to the growth of oxide with the same quality that was earlier possible with semiconductors. This has led to renewed interest in the transition metal oxides specially in 3d transition metal oxides[1]. The wealth of phenomena that one finds in these materials has driven the studies over the past two-three decades. Initially unprecedented temperatures for superconductivity were observed in a family of cuprates [2]. This began the search for new members, especially examples exhibiting superconductivity near room temperature. The search is still on, and over the years other classes of materials have been synthesized as candidate high temperature superconductors. It is not just the cuprates but other members of the transition metal oxide family which exhibit very interesting electronic and magnetic properties. A crucial aspect that has emerged is the tunability of several phenomena with external parameters. One such example is the colossal magnetoresistive effect where a large change in the resistance is found in the manganite [3, 4] in the presence of a magnetic field. Although the effect by itself is known since the pioneering work of van Santen and Jonker [5], the new aspect is the magnitude of the sensitivity. In metals for instance the effect emerges

from a field dependent mean free path and is limited to just a few percent. There are other examples of systems where a phase transition is engineered by an electric field or a magnetic field, a very small energy scale in the problem. All this emerges from the fact that the 3d transition oxides comprise a set of systems where the spin, orbital and lattice degrees of freedom[6-10] are all equally important. These interaction strengths compete with each other, resulting in a phase diagram where sometimes a small change in the electronic interaction strengths leaves us in a part of the phase space with entirely different properties. With the emergence of thin film technology improvements in the context of oxides, substrate strain has emerged as an important parameter to tune electronic interaction strengths as well as the structure of the material. This sometimes results in properties not observed in the bulk form for these materials. For instance an antiferromagnetic insulating phase is found in $SrRuO_3$[11] which is otherwise metallic and ferromagnetic in the bulk. $LaCoO_3$ which does not exhibit any type of long-range order in the bulk form, is found to exhibit ferromagnetism in epitaxially grown thin films of the material[12,13]. The bulk nickelates which have a very interesting phase diagram which can be tuned with a change in the $Ni - O - Ni$ angle[14], also are an interesting system in the thin film form where they exhibit metal insulator transitions[15-18] as a function of thickness. After an introduction to the properties in the transition metal oxides land, the next question we asked was what were the principal electronic strengths and how do they get modified. Apart from the hopping interaction strengths, key parameters determining the electronic properties of transition metal oxides are the coulomb correlation strength U between the electrons on the d site and the charge transfer energy delta (Δ) defined between the oxygen and the transition metal atom. This was put on a firm footing by the seminal paper by Zannen, Sawatzky and Allen[19]. Within an Anderson impurity Hamiltonian it was shown that for Δ < U, the bandgap scales with the smaller energy scale Δ and systems in this regime are called charge transfer insulators. For Δ > U, the band gap scales with U and these systems are called Mott-Hubbard insulators. An extension of their work was carried out by Nimkar [20] and co-workers who included translational symmetry in the problem which allowed them to discuss periodic systems in addition to describing magnetism. Their model found another interesting phase called the covalent insulator, negative delta insulator for negative values of Δ. Extending the work to a multiband model, Mahadevan

and co-workers [21] showed that one had very interesting phase transitions within such a model for the transition metal oxides with re entrant transitions as well as multicritical behavior. Strain allows us to tune the electronic interaction strengths. Usually one finds that the films grow epitaxially for a few monolayers to several tens of monolayers depending on the imposed lattice strain. This growth mode therefore imposes the substrate lattice constant on the overlayers. The hopping interaction strengths scale with the bondlengths and a good approximation for this scaling is given by Harrison's scaling law [22] which says that if l and l' are the angular momenta of the orbitals between which one is discussing the hopping interaction strength, then hopping interaction strength t scales as $\frac{1}{r^{l+l'+1}}$ where r is the distance between the two atoms. A change in the bondlength is not the only change that the substrate imposes. In most transition metal oxides one has additionally a change in the structure. This leads to very interesting consequences and we shall consider one example, that of $LaCoO_3$ and continue the rest of the discussion for this material. $LaCoO_3$ is a perovskite oxide of the form ABO_3. In an ideal perovskite structure as shown in Fig.3.1, one has a cube in which the A site atom which is usually a rare-earth or an alkali metal atom sits at the body-centered position. The B site atom is usually a transition metal atom and this sits at the corners of the cube. The oxygen atoms sit at the centre of the cube edges as shown. As a result each transition metal atom is surrounded by six oxygens, and the structural motif (octahedron) formed by the central transition metal site and six oxygens is an important part of the structural distortions that one finds in these systems. All transition metal-oxygen bondlengths are equal in the ideal perovskite structure.

Most transition metal oxides, however exhibit structural distortions and their structures deviate from the ideal perovskite structure. The two most commonly encountered distortions are the Jahn-Teller distortion and the $GdFeO_3$ distortion [23]. As a knowledge of both of these distortions are needed for our subsequent analysis of the properties of $LaCoO_3$, we provide a brief overview here. The bandwidths in most $3d$ transition metal oxides are narrow compared to the compounds formed by the first and second row elements. As a result in systems where the d bands are partially occupied, Jahn-Teller distortions play an important role in lifting the orbital degeneracy and lowering the energy of the system. The octahedral environment of the oxygens however affects different d orbitals in a different
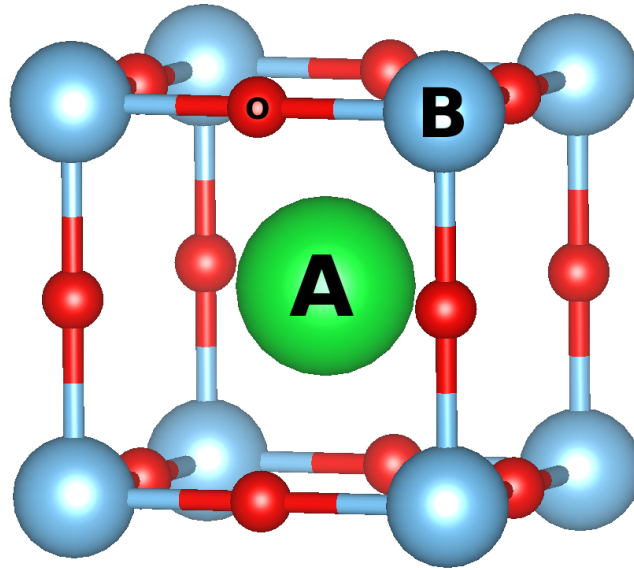
Figure 3.1 An ideal unit cell for ABO$_3$ perovskite oxide.

manner. The electrons on those d orbitals which are oriented towards the oxygens (e_g), the $d_{x^2-y^2}$ & $d_{3z^2-r^2}$ orbitals, experience a larger repulsion from the electrons on the oxygens than those electrons on the d orbitals which are oriented away from the oxygens (t_{2g}). As a result the degeneracy of the d orbitals is lifted and we have the energy of the t_{2g} orbitals to be lower than the energies of the e_g orbitals as shown schematically in Fig. 3.2. There is no Jahn-Teller activity when the t_{2g} levels are completely filled or when the e_g levels are completely filled. Introducing the spin degree of freedom, the exchange splitting becomes an additional parameter and depending on the splitting between the t_{2g} and e_g states (crystal field splitting) and the exchange splitting (splitting between up and down spin states of the same symmetry), one has different occupancy configurations realized. Even if the t_{2g} levels in one spin channel, or the e_g levels in one spin channel are completely occupied, there is no Jahn-Teller activity. Partially occupied t_{2g} levels tend to be less Jahn-Teller active than partially occupied eg levels.

Another important structural distortion is the $GdFeO_3$ distortion [23]. This is usually triggered by a small cation sitting at the *A*-site. A small cation at the *A* site can occupy a smaller unit cell than a larger cation. As a result, the transtition metal-oxygen bondlengths also decrease. This results in an increase in the repulsion between the electrons on the transition metal atom and the oxygens. To overcome
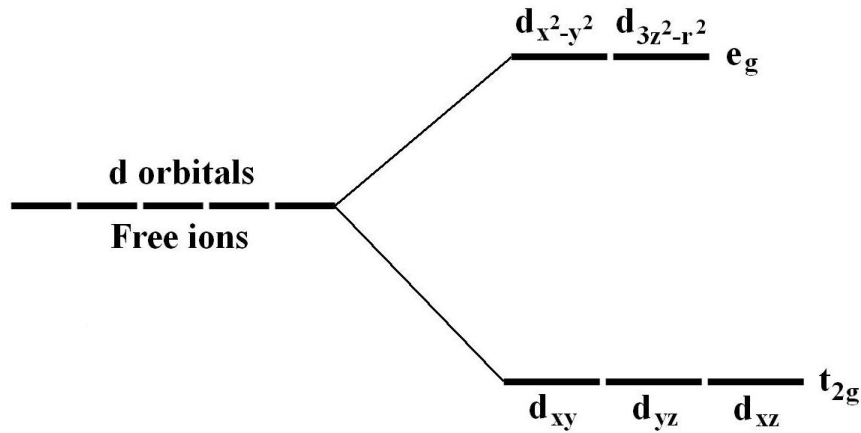
Figure 3.2 Splitting of five fold degenerate orbitals under octahedral environment of oxygens.

this, the system distorts with a rotation of its BO_6 octahedra along the $< 110 >$ axis. As a result of this distortion the B-O bondlength becomes longer and a part of the energy stabilization comes from this increase. This distortion also makes the $B - O - B$ angle deviate from $180°$ and so the effective hopping between the B sites, however, decreases with distortion. Now substrate strain offers a unique handle on the structural distortions as the transition metal-transition metal distance is determined by the substrate. As a result, there has been a lot of speculation that the substrate strain may be able to modify the $GdFeO_3$ distortion, so that for a perovskite oxide which usually has a distorted structure, the $M - O - M$ angle may be varied all the way to $180°$. The study of the $LaCoO_3$ gained considerable interest due to its unusual magnetic and transport properties, caused by the puzzling nature of the two transitions in this compound. The ground state of $LaCoO_3$ is a nonmagnetic insulator and there is no long range magnetic order at all temperatures. The spin singlet ground state is attributed to Co^{3+} ions in a low-spin (LS) state due to the crystal field splitting slightly larger than the Hund's-rule coupling [24]. At low temperatures, the magnetic susceptibility increases exponentially with temperature showing a maximum near 100 K. At higher temperatures, a second anomaly is observed around 500 K which is accompanied by a semiconductor to metal transition. The peak at 100 K was initially ascribed to a change of the spin state in the Co^{3+} ions, i.e. a transition from a LS nonmagnetic ground state $(t_{2g}^6, S = 0)$ to a high-spin (HS) state $(t_{2g}^4 e_g^2, S = 2)$ [24–28]. In the more recent literature[30-34], new

scenarios including an intermediate-spin state (IS) ($t_{2g}^5 e_g^1$, $S = 1$) have been proposed. The evolution of the magnetic and transport properties of the parent compound, *LaCoO$_3$*, with doping is similar to the manganites [35]. By doping with a small amount of Sr (less than 5 %), the susceptibility is similar to the undoped compound [27, 33]. With increasing Sr content, first a spin-glass state occurs and above 18% doping, a ferromagnetic metallic state is obtained. The insulator to metal transition can be understood to be obtained by the suppression of orbital ordering, as it was demonstrated for the *La$_{1-x}$Ca$_x$MnO$_3$*[36] . The electronic configurations for the three states of the Co ions, i.e. LS, IS and HS, are represented schematically in Fig. 3.3.
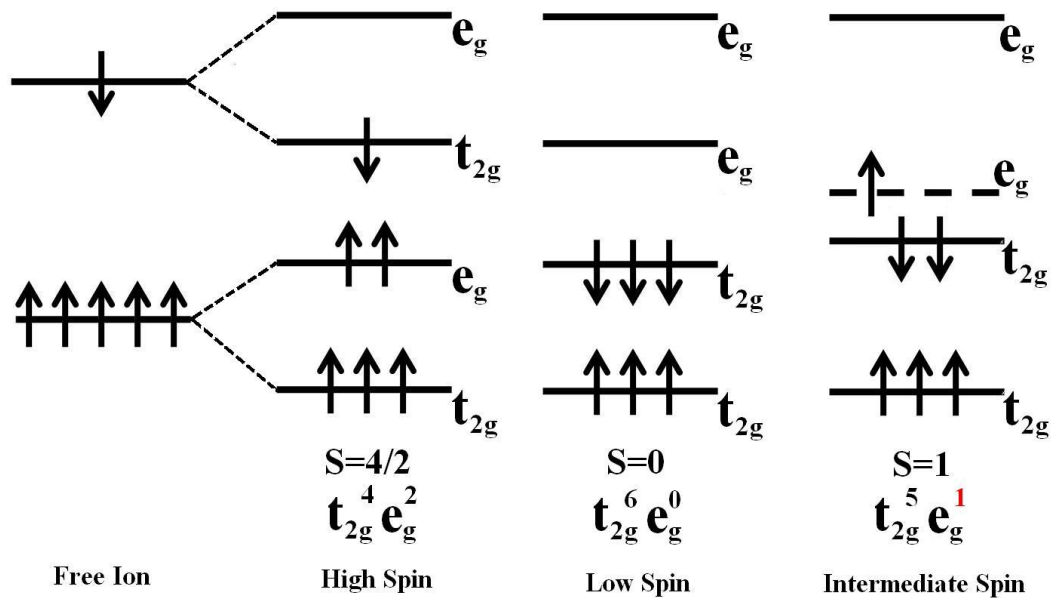
Figure 3.3 Distribution of electrons in high, low and intermediate spin state for Co^{3+}.

Due to the partially filled e$_g$ level, the IS state is Jahn-Teller (JT) active. The degeneracy of the e$_g$ orbitals of Co^{3+} ions in the LS state is expected to be lifted in the IS state by a JT distortion. Using LDA+U calculations, Korotin *et al.* [30] proposed the stabilization of the IS state due to the large hybridization between the Co-e$_g$ and O-2p levels as well as the orbital ordering effect. The authors found that the IS state lies somewhat higher in energy than the LS ground state, while the HS state lies at significantly higher energy. Furthermore, they proposed that the second transition at ≈ 500 K to a

metallic state can be associated with the disappearance of the orbital ordering within the IS state.

Susceptibility data [37] show a maximum at 90 K followed by a Curie-Weiss-type decrease at higher temperatures. This has been interpreted as arising from a spin state transition taking place as a function of temperature. The nature of the transition, however, is still very controversial with the debate [30, 38–40, 40–43] being whether it is a low spin to high spin transition or one to an intermediate spin state. This crossover takes place as a result of a delicate interplay between the crystal-field splitting and the intra-atomic exchange interaction. The temperature dependence is brought about by the dependence of the crystal-field splitting on the bond length which in turn changes with temperature. This naturally suggests epitaxial strain as an alternate handle to tune the spin state transition and therefore change the magnetism.

Recently Fuchs *et al*[12,13] have grown thin films of LCO on different substrates. Ferromagnetism has been found with a T_c(Curie temperature) of 85K on $(LaAlO_3)_{0.3}(SrAlTaO_6)_{0.7}$ (LSAT) substrate, in addition to a strain dependent T_c. The origin of the ferromagnetism is however not clear, with a significant role played by the rotation of the CoO_6 octahedra being offered as one of the reasons[12,13]. To address this issue we have considered tetragonal unit cells of LCO where the inplane and out of plane lattice constants have been kept fixed to the experimental values[12,13]. We however allowed for a rotation of the CoO_6 octahedra which is a commonly observed lattice distortion in perovskite oxides[23] and optimized the total energy as a function of the angle. The paper by Fuchs *et al*[12,13] speculated that the $Co - O - Co$ angle strongly deviated from $180°$ for thin films grown on $LaAlO_3$(LAO) and LCO substrate. However, the angles they speculated reached a value close to $180°$ in the films grown on LSAT and $SrTiO_3$(STO). Thus the strong angle dependence of strain drove the spin state transition and hence gave rise to ferromagnetism. Contrary to their speculations we find that there is a very slight angle dependence of the strained films. This therefore cannot be the reason for the spin state transition observed by us in our calculations. We therefore conclude that it is the strain induced pseudo tetragonal structure which is responsible for the spin state transition. Further as support to the model proposed by us, we are able to explain the temperature dependence of the *X* ray absorption spectra within our calculations. Experimentally it was found that the films of LCO grown on LCO showed a strong temperature

dependence of the O K edge as well as the Co L edge *X* ray absorption spectra [44]. The L edge *X* ray absorption spectra of the transition metal atom is strongly sensitive to crystal field and spin state effects. Hence the temperature dependence has been compared with cluster calculations for CoO$_6$ clusters and interpreted as arising from spin state transitions. LCO films grown on LSAT substrate however did not show any significant temperature dependence. Comparing the total energies obtained by us from calculations for different magnetic states, we find that for LCO on LCO the nonmagnetic solution as well as the other magnetic solutions lie very close in energy. The magnetic solutions correspond to an intermediate spin state. Temperature effects we show change the relative concentrations of low spin and intermediate spin states. Hence explaining the temperature dependence of the spectra. However as the substrate strain is varied, the intermediate spin state gets frozen in as the ground state, the low spin state lies much higher in energy and hence there is no temperature dependence.

3.2   Methodology

We have performed *ab initio* calculations for the electronic structure of thin films of LCO using a plane wave pseudopotential implementation of density functional theory as implemented in VASP[45]. PAW potentials[46] have been used, in addition to the GGA approximation. In order to calculate the properties of thin films of *LaCoO$_3$* we considered an ideal perovskite unit cell of *LaCoO$_3$*. A $\sqrt{2} \times \sqrt{2} \times 2$ supercell was constructed from the primitive cell that we had. The effect of the substrate was simulated by fixing the in-plane lattice constant to that of the substrate. There were experimental values available for the out of plane lattice constants. We fixed our out of plane lattice constants to these values. *LaCoO$_3$* in its bulk form has *GdFeO$_3$*-type distortions. In order to simulate this we started with a structure in which the octahedra in the plane were rotated by an angle $+\theta/-\theta$ alternately in the x-y plane, as well as in the z-direction. The axis of rotation was $< 110 >$ direction and the total energy was minimized as a function of the angle. A k point mesh of $4 \times 4 \times 4$ was considered for the total energy calculations, but increased to $8 \times 8 \times 8$ for the density of states calculations using the tetrahedron method. Spheres of radii 1.3Å, 1.2Å and 1.2Å were considered on La, Co and O for evaluating the

magnetic moment and the orbital projected density of states.

3.3   Results & Discussion

In Fig. 3.4 we have plotted the variation of the magnetic moment on the Co site as a function of the in-plane lattice parameter. For LCO films on LCO we show both the nonmagnetic moment as well as the moment for the structure exhibiting the ferromagnetic state. The dependence on the in-plane lattice constant is nonmonotonic. It should be noted that LCO exhibits a pseudotetragonal unit cell for all values of the substrate lattice constant except for LCO on LCO where it is pseudocubic. In the case of all other substrates LCO is found to be pseudotetragonal. LCO on LAO represents compressive strain while LCO on STO or LSAT represents tensile strain. From Table-3.1, if we look at the total energy values we find that the ferromagnetic state is the ground state in every case except for LCO on LCO where all magnetic states as well as nonmagnetic state lie very close to each other in energy.

Table 3.1 Energies in eV for 4 formula units of LCO grown on different substrates for different magnetic configurations.

	LCO/LCO	LCO/LAO	LCO/LSAT	LCO/STO
Non-magnetic	-152.761	-152.742	-152.875	-152.793
A-type	-152.746	-152.719	-152.827	-152.845
C-type	-152.761	-152.736	-152.862	-152.793
Ferro-magnetic	-152.742	-152.781	-152.953	-152.939

The $Co - O - Co$ angle variations for the ground-state structure as a function of the in-plane and out-of-plane lattice constants are given in Table-3.2. Earlier reports suggest that a change in the angle drives the spin state transition. The in-plane angle changes are small and cannot explain the stabilization of the ferromagnetic state for finite strain. The out-of- plane $Co - O - Co$ angles are found to decrease with the strain in contrast to earlier speculations where angles were expected to approach $180°$ for films of LCO on LSAT/STO. Hence it is primarily the change in bond lengths as a result of substrate strain
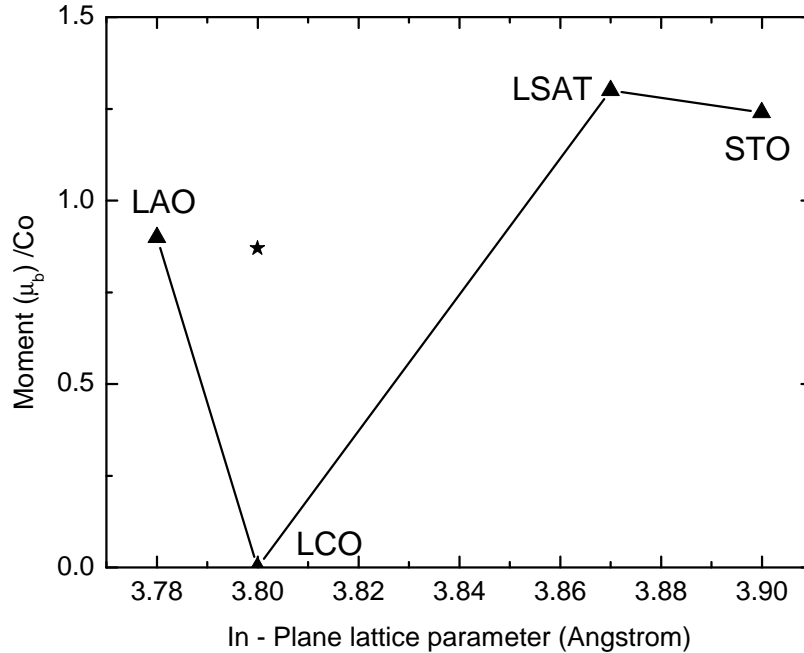
Figure 3.4 The variation of the magnetic moment (triangles) on the Co site as a function of the in-plane lattice parameter for the ground state. The nature of the substrate has also been indicated. For LCO on LCO we also provide the moment of the ferromagnetic state (star) which lies close in energy to the nonmagnetic states.

which drives the system into the ferromagnetic state.

As discussed earlier when one has a smaller ion at the A site, the volume of the unit cell becomes smaller and the B-O bond lengths become smaller. As a result there is an increased repulsion between the electrons on the B site and O. In order to minimize its energy, the system distorts with a rotation of the BO$_6$ octahedra about the $< 110 >$ axis. Thin films allow us to externally control the B-O bond-length with the use of a substrate. So in a situation from perfect cubic case to tetragonal unit cell for a tensile case where in-plane lattice constant is larger than the out-of-plane lattice constant there will be a lesser repulsion between the electrons on the Co and O sites, while it will be larger in out-of-plane direction because of smaller lattice constant. And we must expect an in-plane $Co - O - Co$ angle close

Table 3.2 Co-O-Co angle(degree) in x- y- and z- directions for LCO grown on different substrates. In- and out- of plane lattice constants are also given.

Substrate	Lattice Constant		Co-O-Co Angle		
	Inplane	Out of plane	x direction	y direction	z direction
LAO	3.78	3.87	163.3°	163.3°	160.9°
LCO	3.8	3.8	162.2°	162.2°	158.3°
LSAT	3.87	3.8	163.2°	163.2°	157.6°
STO	3.9	3.79	163.1°	163.1°	156.7°

to 180° with larger strain while angles deviated from 180° in out-of-plane direction. Our calculations as shown in Table-3.2 support this. On contrary earlier reports speculated angles close to 180° for thin films of LCO on LSAT/STO.

The next we probed was the spin state stabilized in the ferromagnetic state. To address this we have plotted the Co d projected up and down spin partial density of states for t_{2g} and e_g symmetries in Fig. 3.5, for LCO on LSAT. In the tetragonal case there is a further splitting of the t_{2g} orbitals into doubly degenerate d_{xz} and d_{yz} as well as singly degenerate d_{xy} orbital. Similarly there is a splitting of the e_g orbitals into singly degenerate $d_{x^2-y^2}$ and $d_{3z^2-r^2}$ orbitals. However these splittings are small and so we choose to still discuss the electronic structure in terms of the nomenclature valid for the cubic case. From the density of states(Fig 3.5) we find that the up spin t_{2g} states are fully occupied while the down spin t_{2g} states are partially occupied. In addition the up spin e_g states are partially occupied(Fig 3.5). For a high spin configuration we would have the t_{2g} and e_g up spin states fully occupied before the t_{2g} down spin states are filled. Hence an intermediate spin state($t_{2g\uparrow}^3 t_{2g\downarrow}^2 e_{g\uparrow}^1$) is stabilized on Co for LCO on LSAT. This is seen to be the case even for LCO on LCO for the ferromagnetic case (Fig. 3.6). The partial occupancy of the t_{2g} down spin levels as well as the e_g up spin levels favors a ferromagnetic state as the ground state for LCO on LSAT and STO.

Recent X ray absorption experiments [44] carried out at the Co $L_{2,3}$ edge for the epitaxial films showed a strong temperature dependence for LCO on LCO. This was absent for LCO films grown
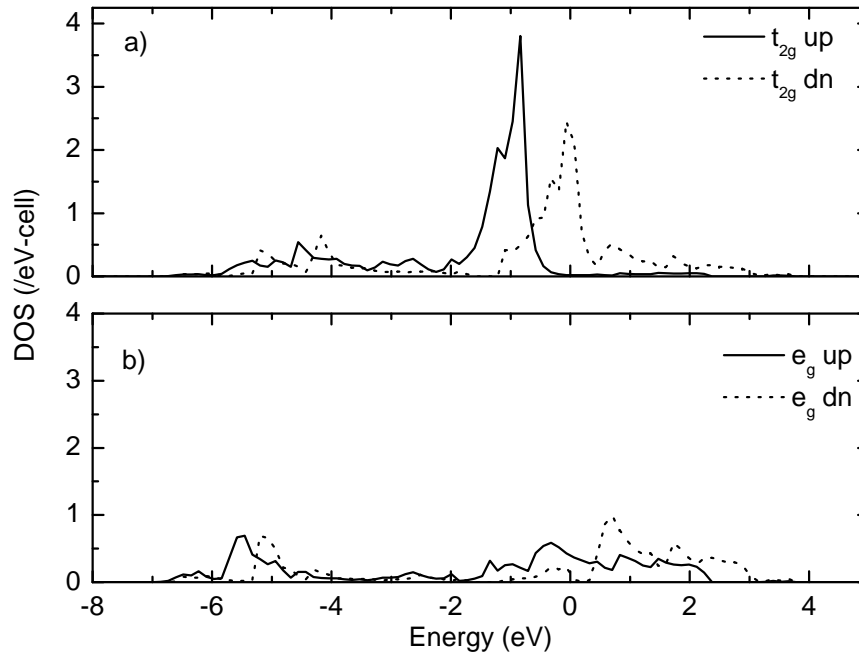
Figure 3.5 Co *d* projected up and down spin partial density of states for t_{2g} and e_g symmetries for LCO on LSAT

on LSAT. They interpreted the results in terms of a spin state transition taking place as a function of temperature for LCO on LCO films. Our total energy calculations for magnetic and nonmagnetic solution indicate that the solutions lie very close in energy for LCO on LCO while the difference is large in all other cases considered by us. The effect of temperature is simulated by us by considering pseudocubic unit cells with a uniform expansion of the unit cell volume. We have computed the total energies for different magnetic configurations and we find that for an expansion of 1% of the lattice constant, the ferromagnetic state gets stabilized by 60 meV. Thus as a function of temperature the relative weight of intermediate and low spin state in the ground state wavefunction changes giving rise to the temperature dependence. Plotting the Co *d* projected partial density of states for LCO on LCO considering the nonmagnetic and ferromagnetic solutions we find that the density of states are very different in the two cases(Fig 3.6). The nonmagnetic solution(Fig 3.6a) has the low spin stabilized
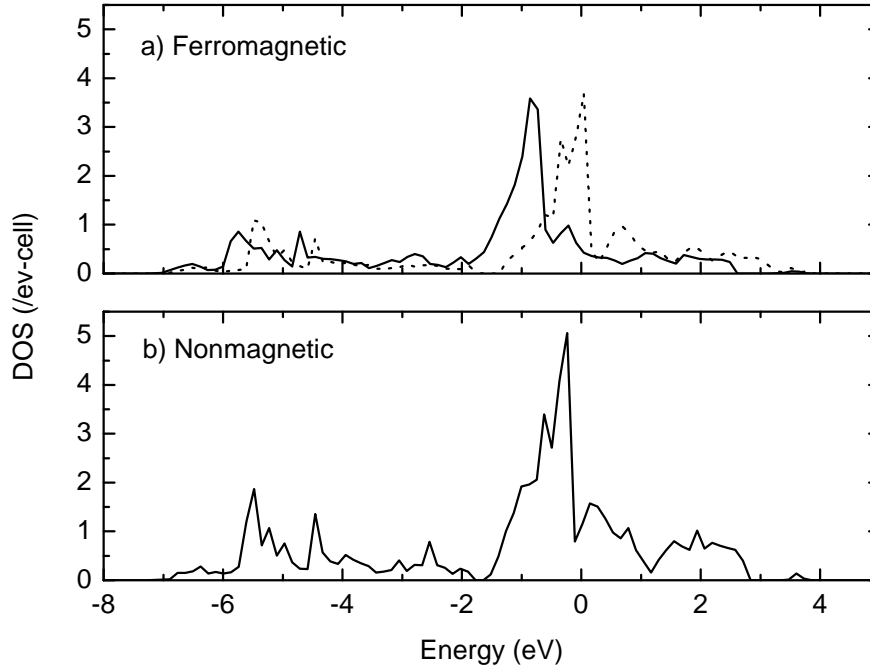
Figure 3.6 Co *d* projected partial density of states for (a)ferromagnetic case and (b)nonmagnetic case for films of LCO grown on LCO

while the ferromagnetic solution(Fig 3.6b) has the intermediate spin stabilized. The partial density of states are consequently different in the two cases. Although multiplets are important in the description of the *X* ray absorption spectra at the $L_{2,3}$ edge, these results indicate that the final states are different and can therefore explain the temperature dependence seen in experiment.

It is for this reason that we choose to explain the O K edge x-ray absorption spectra where initial-state core hole effects as well as multiplet effects are not important. The experimental spectrum corresponds to transitions from the oxygen 1s level to the unoccupied oxygen states with 2p character. Hence the experimental spectrum may be compared to the broadened O p partial density of states, with the broadening accounting for instrumental resolution among other effects. The results of such a comparison are shown in Fig. 3.7, considering the calculated O p densities of states for the ferromagnetic case as well as the nonmagnetic case. There is transfer of spectral weight in the low energy region from

the nonmagnetic to the ferromagnetic spectral function. A similar transfer of spectral weight is seen in the high energy region around 3.0-4.0 eV. This could explain the trend seen in experiments for LCO on LCO as a function of temperature.
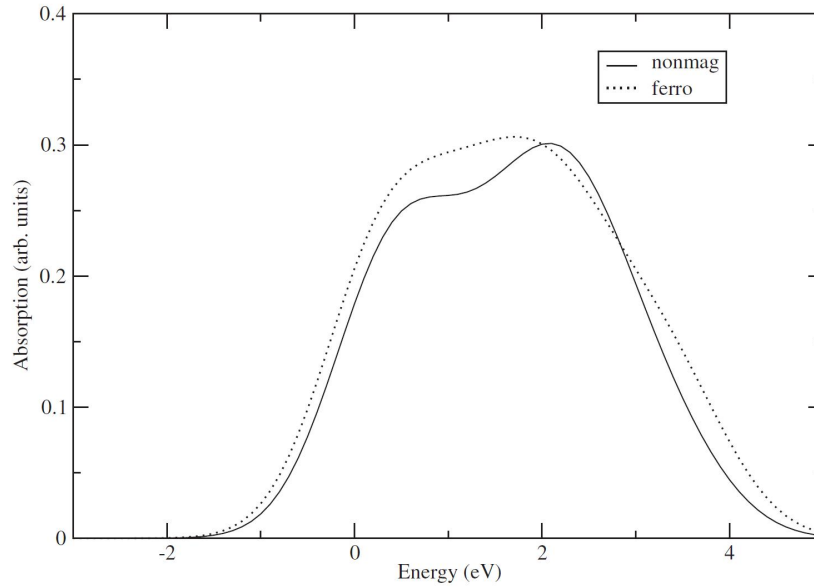
Figure 3.7 Calculated O K edge x-ray absorption spectra for nonmagnetic solid line as well as ferromagnetic cases dashed line.

In the results discussed until now we have analyzed the results from bulk calculations for *LaCoO$_3$* where the effect of the substrate is taken in defining the in-plane lattice constants. The electronic and magnetic structures could strongly deviate at the interface as well as at the surface. In order to analyze this we have considered films of *LaCoO$_3$* grown on STO substrate consisting of 16 layers of LCO grown in a symmetric slab arrangement on STO. At the surface as well as at the interface we find a significant reduction in the moment from bulklike values. However no significant moment or occupancy of the Ti layers is found.

3.4   Conclusion

First principle electronic structure calculations have been carried out for epitaxial films of *LaCoO$_3$* grown on various substrates. We find that the intermediate spin is frozen in for the cases in which

a pseudotetragonal structure is stabilized and the films are subject to compressive or tensile strain. The stabilization of the intermediate spin state also makes the ferromagnetic state to have lowest energy. LCO on LCO is found to have a pseudocubic structure. Total-energy calculations reveal that the nonmagnetic and magnetic solutions lie close in energy for the ground-state lattice constant with the energy difference changing for a uniformly expanded or contracted case, thus explaining the temperature dependence observed in the x-ray absorption spectra. As concept of switching the magnetic state of a material specially in thin film geometry by some external parameter is very important in the memory(MRAM) device application, present work motivates one to explore more such avenues.

Bibliography

[1] M. Imada, A. Fujimori and Y. Tokura, Rev. Mod. Phys. **70**, 1039 (1998).

[2] J. G. Bednorz and K. A. Muller, Z. Phys. B **64**, 189 (1986).

[3] S. Jin, T. H. Tiefel, M. McCormack, R. A. Fastnacht, R. Ramesh and L. H. Chen, Science **264**, 413 (1994).

[4] S. Jin, M. McCormack, T. H. Tiefel, and R. Ramesh, J. App. Phys., **76**, 6929 (1994).

[5] J. H. van Santen and G. H. Jonker, Physica **16**, 599 (1950).

[6] M. Dawber, K. M. Rabe, and J. F. Scott, Rev. Mod. Phys. 77, 1083 (2005).

[7] V. Laukhin, V. Skumryev, X. Marti, D. Hrabovsky, F. Sanchez, M. V. Garcia Cuenca, C. Ferrater, M. Varela, U. Luders, J. F. Bobo, and J. Fontcuberta, Phys. Rev. Lett. **97**, 227201 (2006).

[8] C. Thiele, K. Dorr, O. Bilani, J. Rodel, and L. Schultz, Phys. Rev. B **75**, 054408 (2007).

[9] A. D. Rata, A. Herklotz, K. Nenkov, L. Schultz, and K. Dãűrr, Phys. Rev. Lett. **100**, 076401 (2008).

[10] J. H. vanSanten and G. H. Jonker, Physica **16**, 337 (1950).

[11] P. Mahadevan, F. Aryasetiawan, A. Janotti and T. Sasaki, Phys. Rev. B **80**, 035106 (2009).

[12] D. Fuchs, C. Pinta, T. Schwarz, P. Schweiss, P. Nagel, S. Schuppler, R. Schneider, M. Merz, G. Roth, and H. v. Lohneysen, Phys. Rev. B **75**, 144402 (2007).

[13] D. Fuchs, E. Arac, C. Pinta, S. Schuppler, R. Schneider, and H. v. Lãűhneysen, Phys. Rev. B **77**, 014434 (2008).

[14] Jian Liu, M. Kareev, B. Gray, J. W. Kim, P. Ryan, B. Dabrowski, J. W. Freeland, and J. Chakhalian, Appl. Phys. Lett. **97**, 142110 (2010).

[15] J. L. Garcia-Munoz, J. Rodriguez-Carvajal and P. Lacorre, Phys. Rev. B **50**, 978 (1994).

[16] J. L. Garcia-Munoz, J. Rodriguez-Carvajal, P. Lacorre and J. B. Torrance, Phys. Rev. B **46**, 4414 (1992).

[17] X. Obradors, L. M. Paulius, M. B. Maple, J. B. Torrance, A. I. Nazzal, J. Fontcuberta and X. Granados, Phys. Rev. B **47**, 12353 (1993).

[18] P. C. Canfield, J. D. Thompson, S-W. Cheong and L. W. Rupp, Phys. Rev. B **47**, 12357(1993).

[19] J. Zaanen and G. A. Sawatzky and J. W. Allen, Phys. Rev. Lett. **55**, 418 (1985).

[20] S. Nimkar, D. D. Sarma, H. R. Krishnamurthy and S. Ramasesha Phys. Rev. B **48**, 7355âĂŞ7363 (1993).

[21] P. Mahadevan, K. Sheshadri, D. D. Sarma, H. R. Krishnamurthy and Rahul Pandit, Phys. Rev. B **55**, 9203 (1997).

[22] W. A. Harrison, *Electronic Structure and the Properties of Solids*.

[23] T. Mizokawa and A. Fujimori, Phys. Rev. B **54**, 5368 (1996).

[24] P. M. Raccah and J. B. Goodenough, Phys. Rev. **155**, 932 (1967).

[25] K. Asai, O. Yokokura and N. Nishimori, Phys. Rev. B **50**, 3025 (1994).

[26] M. Itoh, I. Natori, S. Kubota and K. Motoya, J. Phys. Soc. Japan **63**, 1486 (1994).

[27] S. Yamaguchi, Y. Okimoto, H. Taniguchi and Y. Tokura, Phys. Rev. B **53**, 2926 (1996).

[28] M. A. Senaris Rodriguez and J. B. Goodenough, J. Sol. State Chem. **116**, 224 (1995).

[29] R. H. Potze, M. Abbate and G. A. Sawatzky, Phys. Rev. B **51**, 11501 (1995).

[30] M. A. Korotin, S. Yu. Ezhov, I. V. Solovyev, V. I. Anisimov, D. I. Khomskii, and G. A. Sawatzky, Phys. Rev. B **54**, 5309 (1996).

[31] T. Saitoh, T.Mizokawa, M. Abbate, Y. Takeda, M. Takano and A. Fujimori, Phys. Rev. B **55**, 4257 (1997).

[32] K. Asai, A. Yoneda, O. Yokokura, J. M. Tranquada, G. Shirane and K. Kohn, J. Phys. Soc. Japan **67**, 290 (1998).

[33] S. Yamaguchi, Y. Okimoto and Y. Tokura, Phys. Rev. B **55**, 8666 (1997).

[34] Y. Kobayashi, N. Fujiwara, S. Murata, K. Asai and H. Yasuoka, Phys. Rev. B **62**, 410 (2000).

[35] M. R. Ibarra, R. Mahendiran, C. Marquina, B. Garcialanda, and J. Blasco, Phys. Rev. B **57**, R3217 (1998).

[36] B. B. van Aken, A. Meetsma, Y. Tomioka, T. Tokura, and T. T. M. Palstra, Phys. Rev. Lett. **90**, 66403 (2003).

[37] C. Zobel, M. Kriener, D. Bruns, J. Baier, M. GrÃijninger, T. Lorenz, P. Reutler, and A. Revcolevschi, Phys. Rev. B **66**, 020402 R (2002).

[38] S. R. Barman and D. D. Sarma, Phys. Rev. B **49**, 13979 1994;

[39] M. Abbate, R. Potze, G. A. Sawatzky, and A. Fujimori, Phys. Rev. B **49**, 7210 (1994).

[40] Y. Takeda, and M. Takano, Phys. Rev. B **55**, 4257 1997.

[41] M. W. Haverkort, Z. Hu, J. C. Cezar, T. Burnus, H. Hartmann, M. Reuther, C. Zobel, T. Lorenz, A. Tanaka, N. B. Brookes, H. H. Hsieh, H. J. Lin, C. T. Chen, and L. H. Tjeng, Phys. Rev. Lett. **97**, 176405 (2006).

[42] A. Podlesnyak, S. Streule, J. Mesot, M. Medarde, E. Pomjakushina, K. Conder, A. Tanaka, M. W. Haverkort, and D. I. Khomskii, Phys. Rev. Lett. **97**, 247208(2006).

[43] R.F. Klie, J. C. Zheng, Y. Zhu, M. Varela, J. Wu and C. Leighton, Phys. Rev. Lett. **99**, 047203 (2007).

[44] C. Pinta, D. Fuchs, M. Merz, M. Wissinger, E. Arac, A. Samartsev, P. Nagel, S. Schuppler,Phys. Rev, B **78** 174402 (2008).

[45] G. Kresse, and J. Furthm*ü*ller, Phys. Rev. B. **54**, 11169 (1996); G. Kresse, and J. Furthm*ü*ller, Comput. Mat. Sci. **6**, 15 (1996).

[46] G. Kresse, and J. Joubert,Phys. Rev. B **59**, 1758 (1999).

Chapter 4

Orbital ordering induced ferroelectricity in metallic SrCrO$_3$

4.1 Introduction

Magnetism and ferroelectricity are very much essential to academic interest as well as for some of the most important technologies of modern age. The continuous search for the multiferroic materials where these two parameters can co-exist and are coupled with each other become very important for the scientific community. Furthermore recent advances in the growth of oxide thin films have allowed one to engineer both electronic and magnetic functionalities in oxides, very different from their bulk counterparts[1-11]. Strain leads to a spectrum of novel properties in extensively studied epitaxial thin films of multiferroic BiFeO$_3$. Strain tuned critical temperatures [12], transitions to a structure which exihibit giant axial ratio and polarization [13, 14], a phase transition that leads to interpenetrated arrays of vortices and antivortices when thin films are grown in the [$\bar{1}$10] in place of the usual [001] direction [15], photoelectric effect [16, 17] and most importantly almost co-occurence of a ferroelectric and a magnetic transition near room temperature [18, 19] as well as enhancement of magnetoelectric coefficients [20, 21] are example of such exciting properties. This additional dimension of oxide research has opened up the possibility of generating cross-correlated electronic couplings which could be

interchangeably controlled by both electric as well as magnetic fields, generating new classes of multiferroics. In contrast, there are very few examples among bulk materials which are both magnetic as well as ferroelectric. This is because the largest ferroelectric polarizations are usually found in d^0 systems and d^0-ness is not compatiable with magnetic order[22,23]. There are examples of systems which exhibit both orders among finite d^n systems, however the magnitudes of polarization are usually small in such cases. In addition to it, there have been reports that the simultaneous presence of electric and magnetic ordering does not guarantee strong coupling between the two, as microscopic mechanisms of ferroelectricity and magnetism are quite different and do not strongly interfere with each other [24,25].

An avenue that has been quite successful as a route to new ferroelectrics in thin films is one where substrate strain and overlayer thickness have been used as handles to modify properties resulting in behavior very different from the bulk. The work by Haeni *et al.*[27] showed that substrate strain could be used to engineer a ferroelectric ground state in $SrTiO_3$, a d^0 paraelectric. While it was not obvious that this route should work for multiferroics also, first-principles calculations [27] predict that the strain induced by merely depositing the room-temperature ferrimagnetic double perovskites Bi_2NiReO_6 and Bi_2MnReO_6 on a substrate should turn their antipolar bulk ground state into a ferroelectric one. S. Bhattacharjee *et al.* [28] showed theoretically that by increasing the lattice constant of $CaMnO_3$, a polar mode becomes soft and almost degenerate with an antipolar mode. Similar observations were made in epitaxially strained simple binary oxides such as BaO, EuO [29] as well as $BaMnO_3$ [30]. Design of new materials on a larger part depends upon experiments, but with a remarkable development in theoretical tools, first principle calculations have been successful in understanding and predicting several unusual phenomena. Such studies theoretically predict new routes to design a range of novel systems which could show multiferroic behavior and effects as magnetostructural coupling. For example one of such first principle calculations predicted that in epitaxial thin films of $EuTiO_3$ [32], the substrate imposed strain can drive a ferromagnetic and ferroelectric phase to co-exist at the same temperature. In these thin films, a strong magnetostructural coupling has been offered as the origin of multiferroic behavior. These speculations were confirmed in experiments[33] when Lee *et al.* grew thin films of $EuTiO_3$ on $DyScO_3$ substrates. Although the transition temperatures are quite low, below 5 K, the dis-

covery is indeed remarkable as it creates possibilities of designing multiferroic materials by application of external stimuli such as strain. Similar predictions of multiferroic behavior have been made by first principle calculation for other systems $SrMnO_3$[31] and $SrCoO_3$, though they are still not verified in experiments. An important consequence of these studies was that ferroelectric polarization as large as that found in d^0 ferroelectrics was predicted in these oxides. Nevertheless, design of materials using these approaches open new opportunities for the tailoring of devices, important from the device perspective because devices use such materials in thin film form and strain in such system can be effectively used to induce several unobserved effects.

All these examples were band insulators. Therefore, Jahn-Teller effects were irrelevant in these systems, allowing, under strain, for the manifestation of the pseudo Jahn-Teller effects, which are usually associated with non-centrosymmetric distortions. An important consequence of these studies was that ferroelectric polarization as large as that found in d^0 ferroelectrics was predicted in these oxides. In contrast the observed ferroelectric polarization in most multiferroics is at least one or more orders of magnitude lower [34–36]. This route to a high polarization and possibly magnetism associated with the same atom opens up interesting possibilities.

Orbital ordering has recently emerged as an alternate route to ferroelectricity. First principle calculations for epitaxial thin films of $BiFeO_3$ and $PbTiO_3$ have been reported to show existence of orbital ordering along with a large in-plane polarization for a tensile strain $\simeq 5\%$[37]. Role of orbital ordering was also realized in films of doped manganites on a high-index surface of the substrate [38]. This has resulted in an orbital ordering with an axis tilted away from the substrate normal, which led to the off-centring. Again in this case the examples considered were bulk insulators, which we show in the present work need not be a limitation in the choice of materials. We start by considering the example of $SrVO_3$ and $SrCrO_3$, both of which are metallic in the bulk. In this work we explore a new route to non-d^0 ferroelectricity through ultrathin films of transition metal oxides which, as discussed earlier, were found to be insulating. In contrast to the examples listed above, in the cases we investigate, the transition-metal cation is Jahn-Teller active in bulk. A further important difference is that strain (although it could be present) does not play a crucial role in the induced ferroelectricity.

Ultrathin films (just two monolayers) of SrVO$_3$ on SrTiO$_3$ (001) as well as films comprising of two monolayers of SrCrO$_3$ on SrTiO$_3$ (001) are considered. Examining the electronic structure theoretically, we find both systems to be insulating, both arising from an orbital ordering at the surface, driven primarily by structural distortions. While SrVO$_3$ favors Jahn-Teller distortions, SrCrO$_3$ favors a ferroelectric ground state, with a large contribution to the energy lowering in the insulating state derived from these distortions. Our detailed analysis shows that the modifications of the crystal field at the surface associated with a missing apical oxygen allow for the observed ferroelectricity in SrCrO$_3$ (and possibly in other non-d^0 transition metal compounds). These distortions at the surface survive even for the thicker films. The calculated polarization is found to be large, comparable to that in bulk d^0 ferroelectrics.

4.2 Methodology

Experimentally films of SrVO$_3$ have been grown on SrTiO$_3$ substrates layer by layer [6]. To make comparison with experiment we mimic the substrate by considering a symmetric slab consisting of 13 layers of SrO - TiO$_2$. The terminal layer of the substrate is taken to be TiO$_2$ on which SrO - MO$_2$ (M=V, Cr) layers are placed alternately. The in-plane lattice constant is fixed to the experimental value for SrTiO$_3$, 3.905 Å. The out of plane lattice constant was allowed to find its minimum energy value. We allowed for tilts of the TiO$_6$ as well as MO$_6$ octahedra, a distortion observed in surface SrTiO$_3$ [39]. The electronic structure of these systems was calculated within a plane wave pseudopotential implementation of density functional theory in VASP[40] using GGA[41] (generalised gradient approximation) for the exchange and correlation. Correlation effects at M were treated within GGA+U scheme using the formalism of Dudarev[42]. A U_{eff} of 2.2 eV was used on V[43] while a value of 2.5 eV was used on Cr. A vacuum of 15 Å was used to minimize interaction between slabs in the periodic supercell geometry. A k-point mesh of $4 \times 4 \times 1$ was used for solving the electronic structure self-consistently, while it was increased to $6 \times 6 \times 1$ for the calculation of the density of states. Internal positions were allowed to relax to their minimum energy value. The ferroelectric polarization was determined with the

use of the shifts of the centers of maximally localized Wannier functions (MLWF). For this purpose, the electronic ground state for the relaxed structure was converged with the Full-Potential Linearized Augmented Planewave Method-based code `FLEUR`[46], in film geometry, on a 7x7 k-points mesh. MLWFs were constructed with the `Wannier90` code[44] and the interface between `FLEUR` and `Wannier90`[45].

4.3 Results & Discussion

We started by calculating the electronic structure of bulk $SrVO_3$ and $SrCrO_3$ within GGA+U. Both compounds were found to be metallic, consistent with experiment. Next, we performed similar calculations for two monolayers of $SrMO_3$ ($M=$ V, Cr) on $SrTiO_3$, and the ground state was in both cases found to be insulating.
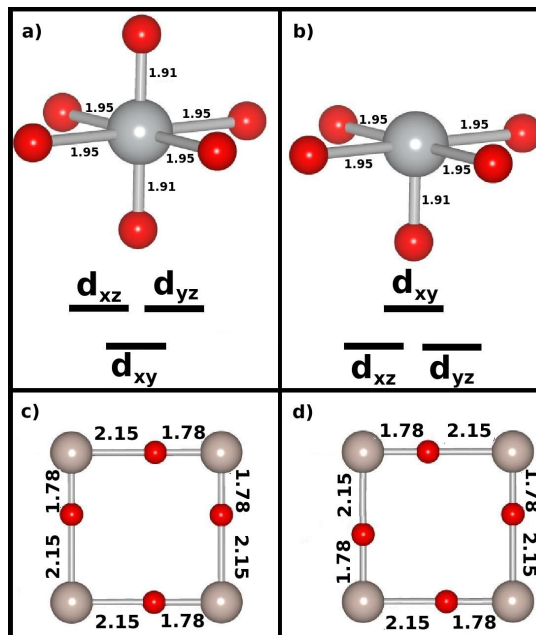
Figure 4.1 Distortions and crystal field splitting of the t_{2g} orbitals for (a) a MO_6 octahedron under tensile strain, (b) a surface MO_5 unit, where M=transition metal atom. The M-O network in the x-y plane found in the presence of (c) Jahn-Teller distortions, (d) pseudo Jahn-Teller distortions. Large(small) and grey(red) spheres denote M (O) atoms.

Let us first examine in more detail the case of $SrVO_3$. Each VO_5 unit at the surface has in-plane V-O bondlengths (1.95 Å) longer than the out of plane one (1.91 Å). This could in principle result in a lower

energy for the d_{xy} orbital than for the doubly degenerate d_{yz} and d_{xz} orbitals Fig. 4.1. As there is just one electron associated with the V^{4+} ion, in this case an insulating ground state is expected. However, since one of the apical oxygens is missing at the surface, this could result in a reversed ordering of the levels leading to a metallic state Fig. 7.6(b). Thus the two apical oxygens give rise to competing effects on the electronic structure and it is not clear which ground state would be favored. Our calculations using the centrosymmetric structure find the scenario discussed in Fig. 4.1(b) realized. However, on performing a complete structural optimization one finds an orbital ordering transition which has a Jahn-Teller origin. The distortion that is favored is of the type shown in Fig. 4.1(c); where two of the V-O bonds are elongated to become 2.18 Å while the other two V-O bonds are contracted to 1.78 Å. This results in a degeneracy lifting of the doubly degenerate d_{xz}, d_{yz} levels with the d_{xz} being occupied at one V site while the d_{yz} orbital is occupied at the next.

To contrast the results for $SrVO_3$ films, we have also considered two monolayers of $SrCrO_3$ on $SrTiO_3$ substrate. Here again the substrate induced strains lead to longer in-plane Cr-O bondlengths than the out of plane bondlengths. However, similar to the case of $SrVO_3$, the degeneracy lifting of the Cr t_{2g} levels is a consequence of the missing apical oxygen at the surface with the d_{xz} and d_{yz} levels at lower energy than the d_{xy} level. As there are two electrons in the d levels of Cr^{4+} ion, they occupy the doubly degenerate d_{xz} and d_{yz} levels, leading to an insulating ground state. Interestingly, we find that carrying out complete structural optimizations results in a strong modification of the in-plane Cr-O bondlengths from their starting values. While two of the bondlengths contract to 1.78 Å, two others extend to 2.15 Å (Fig. 4.1(d)). The effect of this structural distortion is that the system has no inversion symmetry now and possesses a finite electric polarization. While in both $SrVO_3$ and $SrCrO_3$ the dominant energy lowering comes from the in-plane distortions, note the important difference: in $SrCrO_3$, the Jahn-Teller effect is quenched due to one additional electron on Cr^{4+} cation and to the modified crystal field at the surface (with respect to that of the bulk material), so the pseudo-Jahn-Teller effects become operative driving the system ferroelectric/polar. These results put ultrathin films of $SrCrO_3$ in the same category of band insulators turned ferroelectrics where orbital ordering drives the system insulating. We have varied U in a range of 1.0 eV to 3.0 eV and our conclusions remain
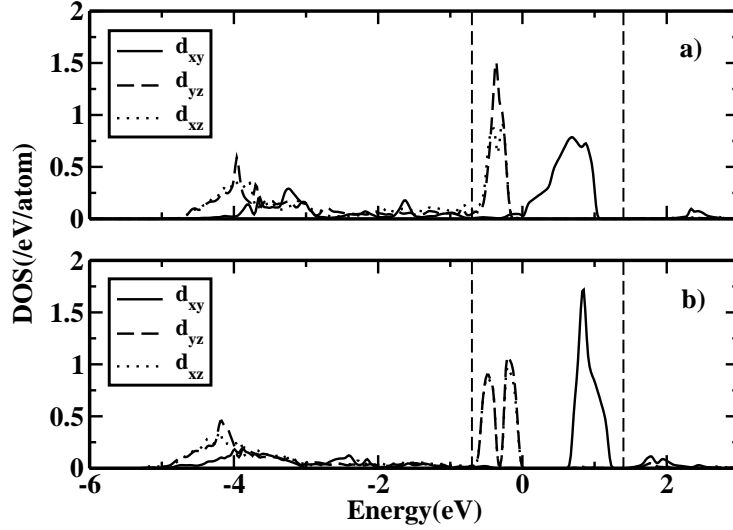
Figure 4.2 The majority spin d_{xz}, d_{yz} and d_{xy} projected partial density of states for a Cr atom in (a) bulk-like geometry, (b) in the optimised ferroelectric geometry for two monolayers of SrCrO$_3$ films on SrTiO$_3$.

same and the insulating state does not depend upon the choice of U. Now every band insulator does not turn ferroelectric, so this immediately brings up the question of the microscopic interactions that are reponsible for ferroelectricity here. In the following, we investigate the origin of the observed ferroelectric distortion.

In Fig. 4.2(a) we have plotted the partial density of Cr-d states for the structure in which the film is constrained to be centrosymmetric. A band gap barely opens up in this structure between the majority spin Cr d_{yz}/d_{xz} states and the d_{xy} states. The bandwidths associated with the d_{xz}, d_{yz} orbitals are a factor of two less than the bandwidths associated with the d_{xy} orbitals as a result of broken periodicity along the positive z-direction.

Allowing for the constraint of centrosymmetry to be relaxed, we find that two of the in-plane Cr-O bondlengths become shorter and are equal to 1.78 Å while two others become longer and are equal to 2.15 Å, in contrast to their undistorted values of 1.95 Å. A part of the energy lowering in the process comes from the increased hopping interaction due to shorter Cr-O bonds. This is clearly seen in the

increased separation of the bonding and antibonding states with dominant contribution from the d_{xy} orbitals (Fig. 4.2(b)).
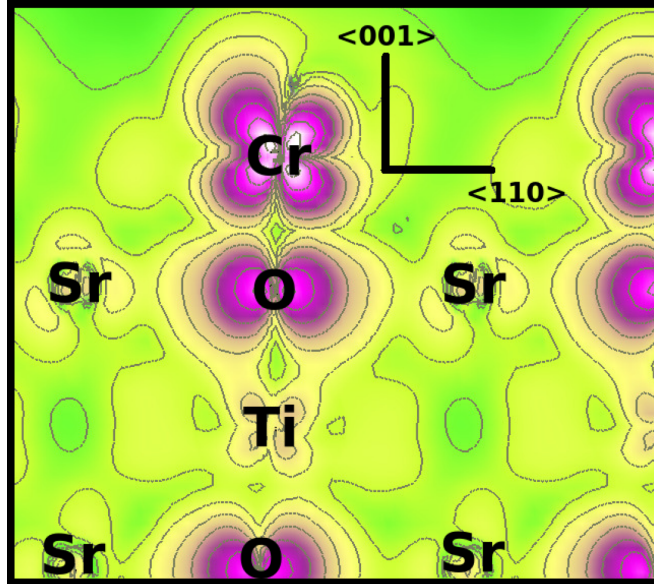
Figure 4.3 Charge density corresponding Cr-d_{xz}/d_{yz} states, and showing the extension into the vacuum region due to shorter Cr-O bond.

The shorter Cr-O bondlengths also results in an increased repulsion between the electrons on Cr and O. This is partly overcome by the presence of the vacuum in the z-direction which allows the d_{xz}, d_{yz} orbitals to extend into the vacuum region. This may be seen from the charge density plot associated with the antibonding states with d_{xz}/d_{yz} character plotted in the Fig. 4.3. One can observe that lobe of the *d* orbital closer to the longer Cr-O bond, extends further into the vacuum to compensate for the increased repulsion associated with the shorter Cr-O bonds. These results also provide us with design principles for generating multiferroic materials in which one has MO_5 octahedra. In-plane distortions as well as larger spacings in one of the *z*-direction in which the oxygen is absent could result in ferroic distortions in transition metal oxides.

In Fig. 4.4 we show the calculated values of the layer-resolved ferroelectric polarization for the case of two monolayers of SrCrO$_3$ on SrTiO$_3$. The bars with vertical, violet pattern show the total (ionic plus electronic) polarization in CrO$_2$/TiO$_2$ layers, while the ones with the horizontal green pattern show the
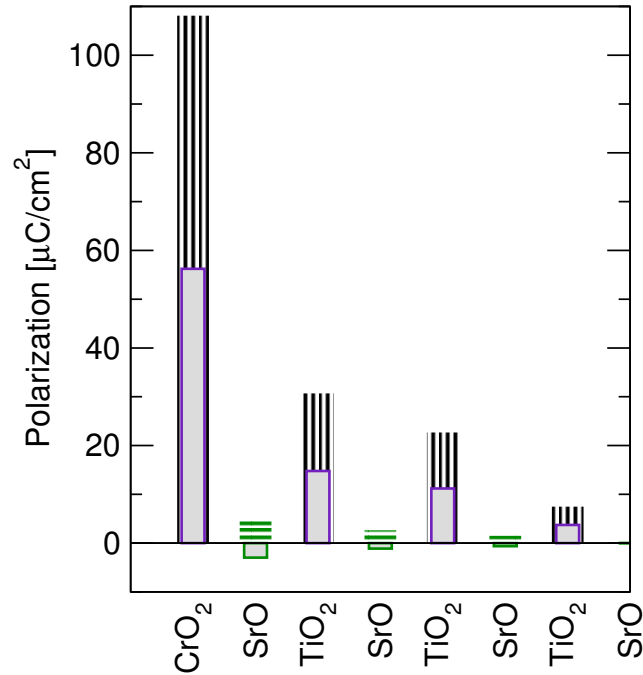
Figure 4.4 The layer resolved polarizations for two monolayers of SrCrO$_3$ on SrTiO$_3$: The bars with vertical, violet pattern show the total (ionic plus electronic) polarization in CrO$_2$ layers, while the ones with the horizontal green pattern show the total polarization in SrO layers. The gray bars outlined with violet (CrO$_2$ layers) or green (SrO layers) indicate the electronic contribution to the total polarization in the respective layers.

total polarization in SrO layers. The gray bars outlined with violet (CrO$_2$/TiO$_2$ layers) or green (SrO layers) indicate the electronic contribution to the total polarization in the respective layers. Note that the electronic contribution in CrO$_2$/TiO$_2$ layers is rather large – it constitutes about 50% of the total polarization, while in SrO layers its contribution is smaller and negative. The polarization points in the <110> direction (in-plane) and is calculated per layer, i.e. instead of the unit cell volume that would be used to evaluate it in a bulk system, we use the volume of each layer, calculated as the product of the area of the in-plane unit cell and the sum of the half-distances to the neighboring layers on either side. The volume of the surface layer is taken to be equal to the one beneath it. While not ferroelectric in bulk, we find that a significant polarization is induced in high-k SrTiO$_3$ by the ferroelectric shifts of Cr^{4+} ions at the surface. Note that the polarization in the center of the film is constrained to zero by the chosen geometry (in the calculation, the Cr^{4+} ions move in the opposite directions on the opposite
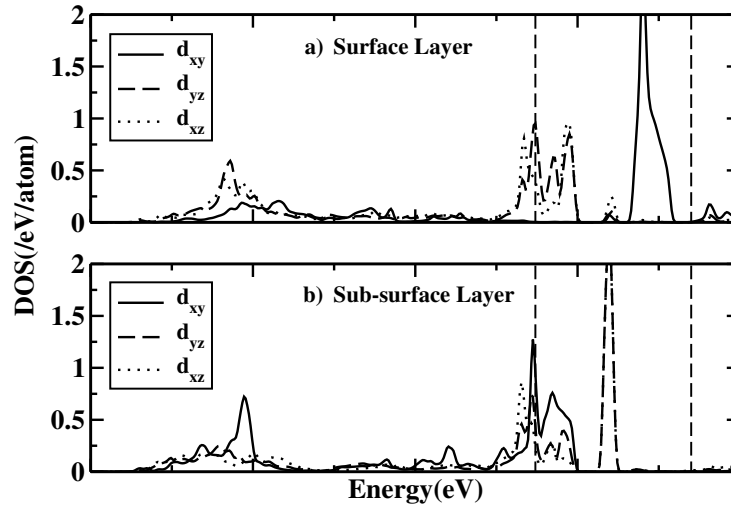
Figure 4.5 The majority spin d_{xz}, d_{yz} and d_{xy} projected partial density of states for a Cr atom belonging to (a) surface, (b) sub-surface layer of 4 monolayer SrCrO₃ films on SrTiO₃.

sides of the film) and its decay with the distance from the surface need not be as rapid in the case of a thicker substrate.

In SrCrO₃ the observed ferroelectric distortions were associated with the two monolayers limit. However when an additional SrO monolayer was added, this led to the out-of-plane distortions becoming *the primary distortions*. The differing environments on either side of the surface CrO₆ octahedra lead to unequal bondlengths of 1.88 Å and 1.95 Å along the positive and negative z-direction. As a result, a finite dipole moment develops (though it is unswitchable by an electric field). Similar observations have been made on other interfaces [16]. The system still remains insulating at this limit. Adding another layer we find that the surface CrO₂ layer sustains a similar ferroelectric distortion as in the two monolayer limit. This is reduced considerably for the sub-surface layer, where although the off-centering survives, the Cr-O bondlengths become 1.94 Å and 1.96 Å. The system still remains insulating with a very similar electronic structure for the surface layer as in the two monolayer case (Fig. 4.5).

The electronic structure of the sub-surface CrO₂ layer is strongly modified as the nature of distortions is different. While the d_{xy} orbital and a combination of d_{xz} and d_{yz} orbitals is occupied, another linear combination is unoccupied. As the bulk is metallic, the insulator-metal transition is expected to

take place beyond the four monolayer limit.

In the preceding discussion the substrate imposed a tensile strain on the $SrCrO_3$ overlayers. It is impressive, however, that one finds that as a consequence of the large stabilization energy for the in-plane ferroelectric distortions, the films can sustain these distortions even for 2% compressive strain.

Having established ferroelectricity at the ultrathin limit, we went on to examine the magnetic properties as a function of thickness. The bulk is found to be an antiferromagnetic metal, consistent with experiment. At the ultrathin limit of two monolayers the antiferromagnetic state is more stable than the ferromagnetic state by 45 meV/Cr atom. This difference is enhanced at the three monolayer limit to 52 meV/Cr atom. At the four monolayers limit various antiferromagnetic configuration that were considered are energetically very close, within the error bars of our calculations. This suggests that long range magnetic order may not be realized at the four monolayer limit, although the system remains insulating.

4.4   Conclusion

Ultrathin films of d^1 and d^2 transition metal oxides have been explored as possible candidates for multiferroicity. Orbital ordering allows one to realize an insulating surface even in systems where the bulk form is metallic. Competing level ordering scenarios involving the out of plane oxygens result in in-plane distortions of the MO_5 octahedra being the dominant structural distortions. While these have a Jahn-Teller origin in the case of $SrVO_3$, pseudo Jahn-Teller effects result in sizeable ferroelectric distortions for $SrCrO_3$ even in the absence of strain, which also turns out to be an antiferromagnetic insulator at this limit of two monolayers. These distortions persist into the substrate and survive for the surface CrO_5 layer even for thicker films of four monolayers opening up new possibilities for non d^0 multiferroics.

Bibliography

[1] A. Ohtomo and H. Hwang, Nature **427**, 6973 (2004).

[2] J.T. Heron *et al.*, Phys. Rev. Lett. **21**, 6973 (2004).

[3] P. B. Allen *et al.*, Phys. Rev. B **53**, 4393 (1996);

[4] G. Cao *et al.*, Phys. Rev. B **56**, 321 (1997).

[5] P. Mahadevan *et al.*, Phys. Rev. B **80**, 035106 (2009).

[6] K. Yoshimatsu, T. Okabe, H. Kumigashira, S. Okamoto, S. Aizaki, A. Fujimori, and M. Oshima, Phys. Rev. Lett. **104**, 147601 (2010).

[7] R. Scherwitzl *et al.*,Appl. Phys. Lett. **95**, 222114 (2009);

[8] R. Scherwitzl *et al.*, Phys. Rev. Lett. **106**, 246403 (2011).

[9] D. Fuchs, C. Pinta, T. Schwarz, P. Schweiss, P. Nagel, S. Schuppler, R. Schneider, M. Merz, G. Roth, and H. v. Lohneysen, Phys. Rev. B **75**, 144402 (2007).

[10] D. Fuchs, E. Arac, C. Pinta, S. Schuppler, R. Schneider, and H. v. LÃűhneysen, Phys. Rev. B **77**, 014434 (2008).

[11] K. Gupta and P. Mahadevan, Phys. Rev. B **79**, 020406 (2008).

[12] I. C. Infante, S. Lisenkov, B. Dupé, M. Bibes, S. Fusil, E. Jacquet, G. Geneste, S. Petit5, A. Courtial, J. Juraszek, L. Bellaiche, A. Barthélémy, and B. Dkhil, Phys. Rev. Lett. **105**, 057601 (2010).

[13] H. Beá, B. Dupé, S. Fusil, R. Mattana, E. Jacquet, B. Warot-Fonrose, F. Wilhelm, A. Rogalev, S. Petit, V. Cros, A. Anane, F. Petroff, K. Bouzehouane, G. Geneste, B. Dkhil, S. Lisenkov, I. Ponomareva, L. Bellaiche, M. Bibes, and A. Barthélémy, Phys. Rev. Lett. **102**, 217603 (2009).

[14] R. J. Zeches1, M. D. Rossell, J. X. Zhang, A. J. Hatt, Q. He, C.-H. Yang, A. Kumar, C. H. Wang, A. Melville, C. Adamo, G. Sheng, Y.-H. Chu, J. F. Ihlefeld, R. Erni, C. Ederer, V. Gopalan, L. Q. Chen, D. G. Schlom, N. A. Spaldin, L. W. Martin, R. Ramesh, Science **326**, 977 (2009).

[15] S. Prosandeev, I. A. Kornev, and L. Bellaiche, Phys. Rev. B **83**, 020102 (2011).

[16] S. Y. Yang, J. Seidel, S. J. Byrnes, P. Shafer, C.-H. Yang, M. D. Rossell, P. Yu, Y.-H. Chu, J. F. Scott, J. W. Ager, L. W. Martin and R. Ramesh, Nature Nanotech. **5**, 143 (2010).

[17] J. Seidel, D. Fu, S.-Y. Yang, E. Alarcón-Lladó, J. Wu, R.Ramesh, and J. W. Ager, Phys. Rev. Lett. **107**, 126805(2011).

[18] I. C. Infante, J. Juraszek, S. Fusil, B. Dupé, P. Gemeiner, O. Diéguez, F. Pailloux, S. Jouen, E. Jacquet, G. Geneste, J. Pacaud, J. Ã■Ãśiguez, L. Bellaiche, A. Barthélémy, B. Dkhil, and M. Bibes, Phys. Rev. Lett. **107**, 237601(2011).

[19] K. T. Ko, M. H. Jung, Q. He, J. H. Lee, C. S. Woo, K. Chu, J. Seidel, B. G. Jeon, Y. S. Oh, K. H. Kim, W. I. Liang, H. J. Chen, Y. H. Chu, Y. H. Jeong, R. Ramesh, J. H. Park and C. H. Yang, Nature Commun. **2**, 567 (2011).

[20] J. C. Wojdel and J. Iniguez, Phys. Rev. Lett. **105**, 037208(2010).

[21] S. Prosandeev, I. A. Kornev, and L. Bellaiche, Phys. Rev. Lett. **107**, 117602 (2011).

[22] N.A. Hill, J. Phys. Chem. B **104**, 6694(2000).

[23] D. I. Khomskii, Bull. Am. Phys. Soc. C 21, 002 (2001).

[24] T. Katsufuji, S. Mori, M. Masaki, Y. Moritomo, N. Yamamoto, and H. Takagi Phys. Rev. B **64**, 104419 (2001).

[25] T. Kimura, Phys. Rev. B **67**, 180401 (2003).

[26] J. H. Haeni*et al.*, Nature **430**, 758 (2004).

[27] M. Ležaić and N. A. Spaldin, Phys. Rev. B **83**, 024410 (2011).

[28] S. Bhattacharjee, E. Bousquet, and P. Ghosez, Phys. Rev. Lett. **102**, 117602, (2009).

[29] E. Bousquet, N. A. Spaldin, and P. Ghosez, Phys. Rev. Lett. **104**, 037601 (2010).

[30] J. M. Rondinelli, A. S. Eidelson, and N. A. Spaldin, Phys. Rev. B **79**, 205119, (2009).

[31] J. H. Lee and K. M. Rabe, Phys. Rev. Lett., **104**, 207204 (2010).

[32] C. J. Fennie and K. M. Rabe, Phys. Rev. Lett., **97**, 267602 (2006).

[33] J. H. Lee, L. Fang, E. Vlahos *et al.*, Nature, **466**,954(2010).

[34] T. Kimura, T. Goto, H. Shintani, Y. Tokura, Nature **55**,426 (2003).

[35] L. C. Chapon *et al.*, Phys. Rev. Lett. **93**, 177402 (2004).

[36] G. Lawes *et al* Phys. Rev. Lett. **95** 087205, (2005).

[37] Yurong Yang, Wei Ren, Massimiliano Stengel, X. H. Yan, and L. Bellaiche, Phys. Rev. Lett. **109**, 057602 (2012).

[38] N. Ogawa *et al.*, Phys. Rev. Lett. **108**, 157603 (2012).

[39] F. W. Lytle, J. App. Phys. **35**, 2212 (1964).

[40] G. Kresse, and J. Furthm*ü*ller, Phys. Rev. B. **54**, 11169 (1996); G. Kresse, and J. Furthm*ü*ller, Comput. Mat. Sci. **6**, 15 (1996).

[41] J. P. Perdew, in Electronic Structure of Solids, edited by P. Ziesche and H. Eschrig (Akademie Verlag, Berlin, 1991), p. 11.

[42] S.L. Dudarev *et al.* Phys. Rev. B **57**, 1505 (1998).

[43] F. Aryasetiawan *et al.* Phys. Rev. B **70**, 195104 (2004).

[44] A. A. Mostofi *et al.*, Comp. Phys. Comm. **178**, 685 (2008).

[45] F. Freimuth *et al.*, Phys. Rev. B **78**, 035120 (2008).

[46] www.flapw.de

[47] G. Singh-Bhalla *et al.* Nature Phys. **7**, 80 (2011).

Chapter 5

A new route to ferromagnetic and ferroelectric insulators

5.1   Introduction

The family of $3d$ transition metal oxides is a typical example of strongly correlated system[1], with most of the members found to be insulators. Existence of ferromagnetic members among the undoped compound has few candidates as the general observation has been that ferromagnetism is accompanied by a metallic state[2]. Ferromagnetic insulators are very rare, and there are very few examples among transition metal oxides which exhibit ferromagnetism along with an insulating character. There has been no general consensus about the mechanism of the rarely observed ferromagnetic insulating state. In lightly doped manganites, $La_{7/8}Sr_{1/8}MnO_3$ to explain the origin of the observed ferromagnetic insulating state many different models have been proposed in the literature, including charged polaron order [3], checkerboard-like charge order [4], orbital order without charge order [5], as well as the electron-phonon coupling induced Peierls instability [6], where the orbital order confines holes to move along quasi-one-dimensional pathways between Mn sites. In another study by Mahadevan *et al* [7], they proposed that charge ordering drives the ferromagnetic insulating behavior in the hollandite system $K_2Cr_8O_{16}$. This system is equivalent to 25% K doping in a polymorph of CrO_2, and charge ordering

arises due to the localization of electrons on certain Cr sites. Lattice distortions associated with the ordering gives rise to a rare example of charge ordering driven ferromagnetic insulator. Another first principle study proposed a coulomb assisted spin-orbit coupling that drives the ferromagnetic insulating state in La_2CoMnO_6 [8].

Ferromagnetic insulators are very important from an application point of view, as they could lead to very rare magnetoelectric multiferroics if one could engineer ferroelectricity in these systems. Multiferroics are the class of materials which exhibit two or all of three types of ferroic order namely ferromagnetism, ferroelectricity and ferroelasticity in the same phase. One could have a handle on the orientation of these three components with externally applied magnetic field, electric field and mechanical stress. Magnetoelectric multiferroics are those materials which have ferromagnetism and ferroelectricity associated with the same phase, while ferroelasticity may or may not accompany them. These are particularly very rare as the basic chemical requirements for these two ferroic components to exist together are mutually exclusive. Basic chemistry requires a ferroelectric to be insulating to screen the charge to create a finite electric polarization, as otherwise the applied electric field would induce the flow of electric current. In most of the examples of conventional ABO_3 type perovskite oxide ferroelectrics, the system has a formal charge which corresponds to a d^0 configuration on B site. If d states are empty, there are no electrons which could result in localized magnetic moments, hence no magnetic ordering is possible. And as soon as there is a partial occupancy in d states, the system starts losing the tendency to distort in a way that removes the centre of symmetry in the structure to stabilize ferroelectricity. So existence of one ferroic component blocks the possbility of another. Ferroelectricity requires an insulating state and on the other hand ferromagnets usually are metallic. As there are not so many ferromagnetic insulators, it could be understood why ferromagnetic and ferroelectric order do not co-exist. If one looks beyond ferromagnetic systems, most of the multiferroics are antiferromagnetic. But ferromagnetic ferroelectrics have better technical possibilities than the antiferromagnetic ferroelectrics. One can change the direction of spins as well as polarization, while on the other hand for an antiferromagnetic ferroelectric, reorienting the magnetic ordering leads to the same configuration because of the alignment of antiparallel spins. Further, the coupling between electrical ($\pm P$) and

magnetic ($\pm M$) order parameters and their control with external parameters in these materials provides a possibility of possessing additional functionalities such as electrical (magnetic) control of magnetization (polarization) [15], and has developed into a very interesting research area[9-19]. Switching of ferromagnetic order by an electric field, for instance, plays an important role in the design of next generation multiple state memory devices[15,20-24]. One can externally apply conjugate magnetic and electric fields to change and reorient the respective cross coupled ferroic components. Therefore ferromagnetic ferroelectrics are potential candidates for future multistate memory devices.

Most of the examples of multiferroics and magnetoelectrics can be sorted out in two categories [25], single component systems [15–17, 26, 27] and two-phase systems. Though they have been predicted to be rare [9, 28, 29]. Two phase systems are mainly artificially grown superlattice heterostructures, composites consisting of more than one materials. Usually the two-phase multiferroics are artificially grown heterostructures. Some of these examples are ferroelectric/ferromagnetic heterostructures such as $BaTiO_3/La_{0.66}Sr_{0.33}MnO_3$[52], $BaTiO_3/SrTiO_3$[41,55] $PbTiO_3/SrTiO_3$[30,43], $BiFeO_3/SrTiO_3$[31,32], nanopillar embedded structures of $BaTiO_3-CoFe_2O_4$[33,34] or $BiFeO_3- CoFe_2O_4$[35], $PbZrO_3/CoPd$, $PbTiO_3/CoPd$ and many others.

Recently, efforts have been made to fabricate artificial layers and tailor their structures for the suitability of multiferroics [36–39]. These materials are in the form of either superlattices, or multilayers. Interestingly, the material made in the form of superlattices, whose structure consists of alternating ferroelectric and ferromagnetic layers, yielded unusual electrical and magnetic transport properties that cannot be obtained in either of their constituents. Ferroelectric superlattices of ABO_3 perovskite oxides have emerged as an important research area of immense scientific interest [40–43]. A diverse range of functional properties can be achieved in these heterostructures, with variation in the choice of the constituent materials [41, 42, 44–46], and the order in which they are fabricated as well as the epitaxial strain [47–50] that is imposed by the substrate. In some cases these properties can be explained by understanding how the electrical and mechanical boundary conditions of the superlattice drive the behavior of the ingredient materials, while in some instances these properties are directly associated with the way the atomic and electronic structure get modified at the interface [51].

Both experimental and theoretical tools are important, in order to design new materials exhibiting novel properties through interface engineering as well as to understand the pivotal role that the interface plays at the atomic level to explain and predict the functional properties in perovskite oxide heterostructures. In heterostructures of $BaTiO_3/La_{0.66}Sr_{0.33}MnO_3$, it was shown that lattice distortions during the structural phase transitions of $BaTiO_3$ can cause changes in the resistivity and magnetic properties of LSMO[52]. In another report these results were confirmed and they also showed that these system exhibit converse magnetoelectric effects [19]. It was shown in experiments that the interface could induce both interfacial magnetoelectric coupling and room-temperature multiferroicity in $Fe/BaTiO_3$ and $Co/BaTiO_3$ heterostructures[53]. First-principles methods also have been extremely useful in providing both qualitative and quantitative characterization of interface effects in superlattices [51, 54]. In most perovskite superlattices combining ferroelectric and paraelectric layers [41–43, 45, 51, 55, 56], the ferroelectric instability and spontaneous polarization are found to be suppressed with increasing interface density for a given composition. Bousquet *et al.* [43] showed that an interface coupling based on rotational distortions that gives rise to improper ferroelectricity in perovskite oxide artificial superlattices of $PbTiO_3/SrTiO_3$, where antiferrodistortive distortions of the substrate $SrTiO_3$ and ferroelectric distortions of $PbTiO_3$ co-exist to stabilize this system. Interfacial multiferroics thus emerge as particularly promising to circumvent the lingering scarcity of single-phase multiferroicity.

Away from the basic requirement of d^0-ness, there are a number of systems which show non-zero polarization in d^n systems. Excluding an exceptional example of $BiFeO_3$ [57], in most of the examples such as, $TbMnO_3$ [15], $YMnO_3$ [29],$Ni_3V_2O_8$ [58] polarization is smaller than the typical cubic oxides $BaTiO_3$ or $PbTiO_3$ by several orders of magnitude. Moreover the mechanism responsible behind ferroelectricity was different from the displacive ferroelectricity. In few systems it was the presence of the lone pair associated with the rare earth atom or some sort of spin spiral magnetic ordering that drives the ferroelectricity in these systems, and they had a very small ionic displacement component. To have a possible route where one can have polarization comparable to the bulk prototypes in d^n systems, Chandra and co-workers [59] studied the ferroelectric behavior of $BaTiO_3$ with dilute doping of transition metals. Surprisingly it was found that ferroelectric distortions were stronger than

the undoped limit. Calculated polarization was found to be $15.3\mu C/cm^2$, though similar ferroelectric distortions in VO_6 octahedra could not be constrained in the bulk. But local polar distortions of VO_6 octahedra were found to be frozen in the two-component superlattice arrangement. Which leads to a new route to design multiferroics.

In this work we consider $BaTiO_3/BaVO_3$ and $BaTiO_3/BaCrO_3$ superlattices. Examining the electronic structure of $BaTiO_3/BaVO_3$ multilayer system, we find the system to be a ferromagnetic insulator. The origin of the ferromagnetic insulating state is traced to the Jahn-Teller distortion driven orbital ordering. However $BaTiO_3/BaVO_3$ heterostructure is found to be an antiferromagnetic insulator. In both the systems, VO_2/CrO_2 layers favor Jahn-Teller distortions in the xy-plane while a polar distortion is favored in the out-of-plane direction, thus rendering a non-zero polarization along the z-direction. Similar distortions persist when one goes from one layer to two layers of $BaVO_3$ and $BaTiO_3$. The calculated values of the polarization for single layer of VO_2 and CrO_2 sandwiched between $BaTiO_3$ layers are found to be $20.61\mu C/cm^2$ and $25.20\mu C/cm^2$, while for two layers it becomes $33.26\mu C/cm^2$ and $25.65\mu C/cm^2$.

5.2 Methodology

We set up a multilayer structure of $BaVO_3/BaTiO_3$ and $BaCrO_3/BaTiO_3$ superlattice with one and two layers of $BaVO_3$ and $BaCrO_3$ sandwiched between 12 monolayers of $BaTiO_3$ as shown in Fig. 5.1(a). The experimental values for the atomic positions and lattice parameters were taken for $BaTiO_3$ [60]. The layers of $BaVO_3$ and $BaCrO_3$ were considered to have the same structure, so as to include the strain effect imposed by $BaTiO_3$. Transition metal oxides in general have a distorted structure which includes rotations and tilts of the transition metal-oxygen octahedra. We also considered both rotations ($a^-a^-c^o$ in glazer notation) as well as rotation plus tilts($a^-a^-c^+$). We performed electronic structure calculations within a plane wave pseudopotential implemenation of density functional theory in VASP using GGA (generalised gradient approximation) to treat exchange and correlation. Correlation effects in V were treated within GGA+U scheme using the formalism of Dudarev. An effective U of 3.0

eV was used on V and Cr, though we have varied U in the range 1.0 to 3.0 for V and Cr and the conclusions remain unchanged. Since Ti in $BaTiO_3$ has no significant occupancy, inclusion of U has hardly any physical consequences and is therefore not included. The electronic structure was solved self consistently using a k-points mesh of $4 \times 4 \times 1$ which was increased to $8 \times 8 \times 1$ to calculate the density of states. The size of the k-point mesh was found adequate to achieve convergence with respect to k-points. Spheres of radii 1.0 Å were considered around V and Cr to calculate the orbital projected partial density of states. Internal positions of atoms were relaxed to find their minimum energy. The polarization was calculated using the Berry phase method.

5.3   Results & Discussion

Let us discuss what one would speculate when a few monolayers of a magnetic material are sandwiched between layers of a ferroelectric material(Fig. 5.2-a). There could be two possible scenarios, first as shown in the Fig. 5.2(b), if the layers of the magnetic material sandwiched between the ferroelectric material could remain insulating and deplete the ferroelectric distortions in the layers of the ferroelectric adjoining the magnetic material. The number of layers that would lose their ferroelectricity would depend on the energy difference between the ferroelectric and paraelectric structure. Alternately as shown in Fig. 5.2(c), the system could gain energy if the ferroelectric layers induced a non-zero polarization in the sandwiched layers. We then switch off the polar distortions in the sandwiched VO_2 layer and calculate the total energy and we find that the structure with the polar distortion has lower energy than the one without any polar distortions by 150 meV/V atom.

We first start by calculating the electronic structure of a single layer of $BaVO_3$ sandwiched between $BaTiO_3$ layers as shown in Fig. 5.1(a), with the V-O bondlengths same as Ti-O above and below. The experimental structure of $BaTiO_3$ has been considered for the calculations in which the in-plane bondlengths are 2.0 Å, while the out-of-plane ones are 1.83 Å and 2.20 Å as shown in Fig. 5.1(c). V in $BaVO_3$ corresponds to a d^1 system and is a Jahn-Teller active ion. Hence the system could gain energy through Jahn-Teller distortions which would also remove the degeneracy of the t_{2g} orbitals. Therefore
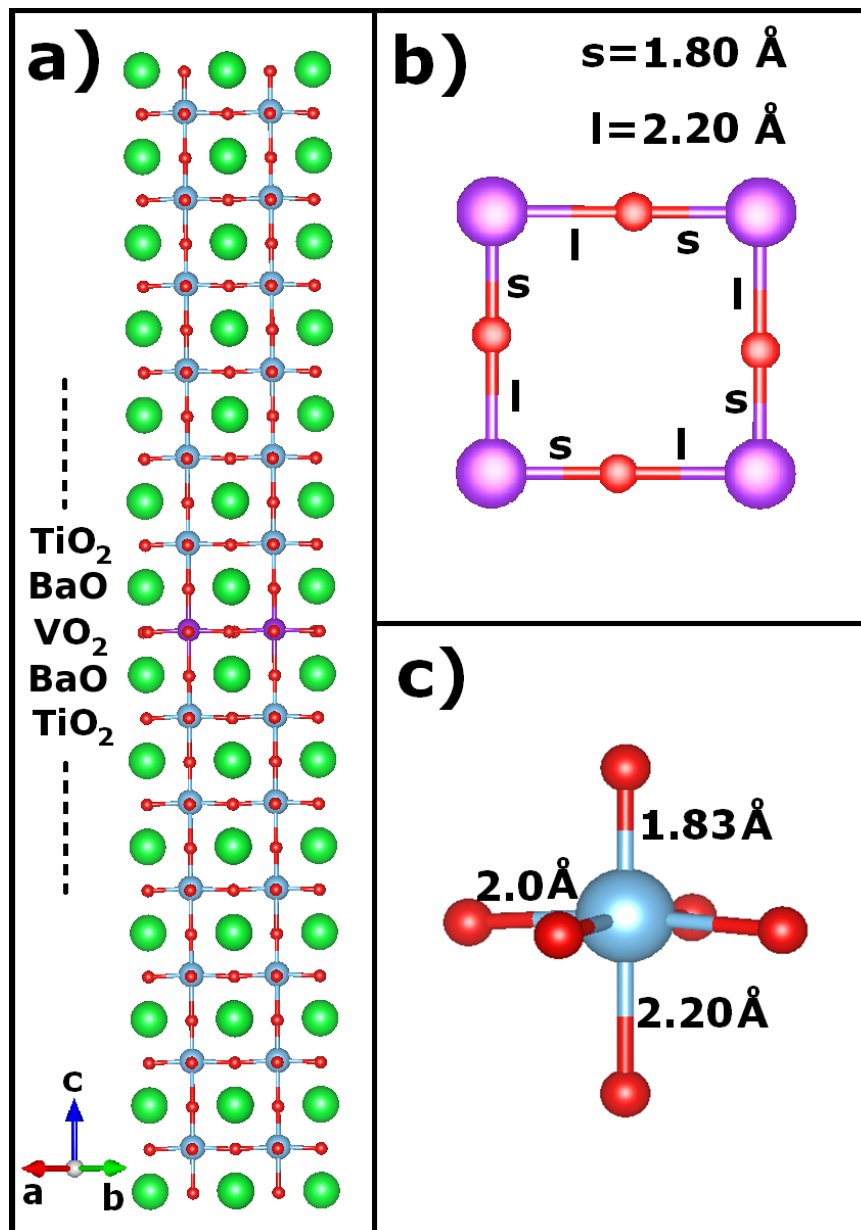
Figure 5.1 a) Superlattice structure set up for the calculations, 2 layers of BaVO$_3$ are sandwiched between 12 monolayer of BaTiO$_3$ b) Jahn-Teller distortions we started with for the V-O bondlengths in the VO$_2$ layers. c) Structure we considered for BaTiO$_3$.

we also considered another case where the symmetry was lowered and the VO$_2$ layer has Jahn-Teller distortions in the xy-plane with V-O bondlengths equal to 1.80 Å and 2.20 Å as shown in Fig. 5.1(b). Atoms in the structure are allowed to relax to find their minimum energy and we find that the Jahn-Teller
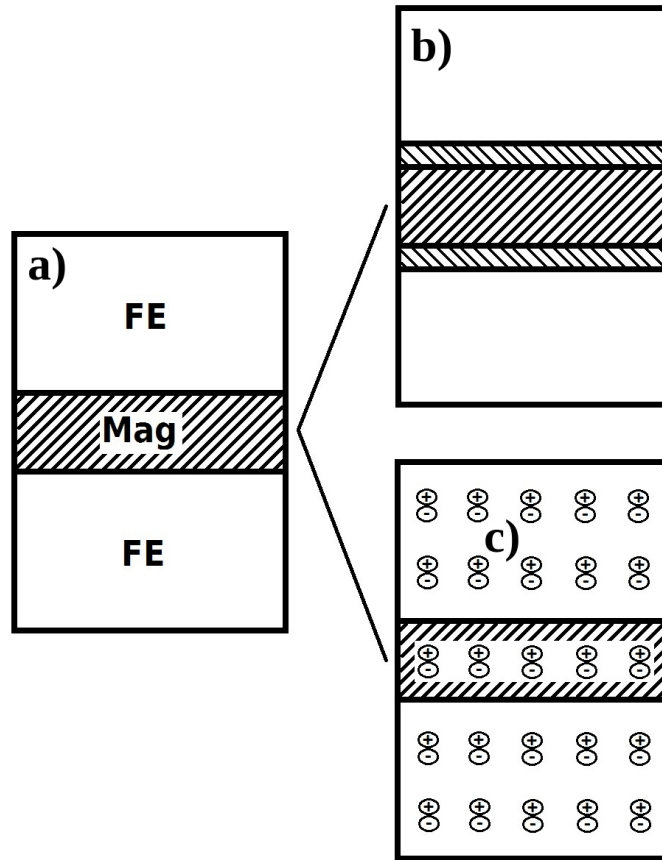
Figure 5.2 Two possible outcomes when a magnetic/metallic material is sandwiched between layers of ferroelectric(FE) material, the sandwiched layers could either a) deplet the polarization in the FE region or b) FE material could induced a non-zero polarization into the sandwiched layers.

distorted structure is indeed stabilized over the other. Let us examine the structure in more detail. On performing complete structural optimization we find that the VO_2 layer is JT distorted in-plane while there is a polar off-centering in the out-of-plane direction. The longer and shorter bondlengths in the xy-plane are found to be 1.89 Å and 2.11 Å respectively after the structural optimization while they are equal to 1.91 Å and 2.14 Å along the z-direction as shown in Fig. 5.3(a). This renders a finite polarization along the z-direction. We consider all possible magnetic configurations and from our total energy calculation we find that the ferromagnetic solution is lower than the antiferromagnetic one by 11 meV/V atom.

Let us next try to understand why Jahn-Teller distortions exist in the xy-plane along with polar
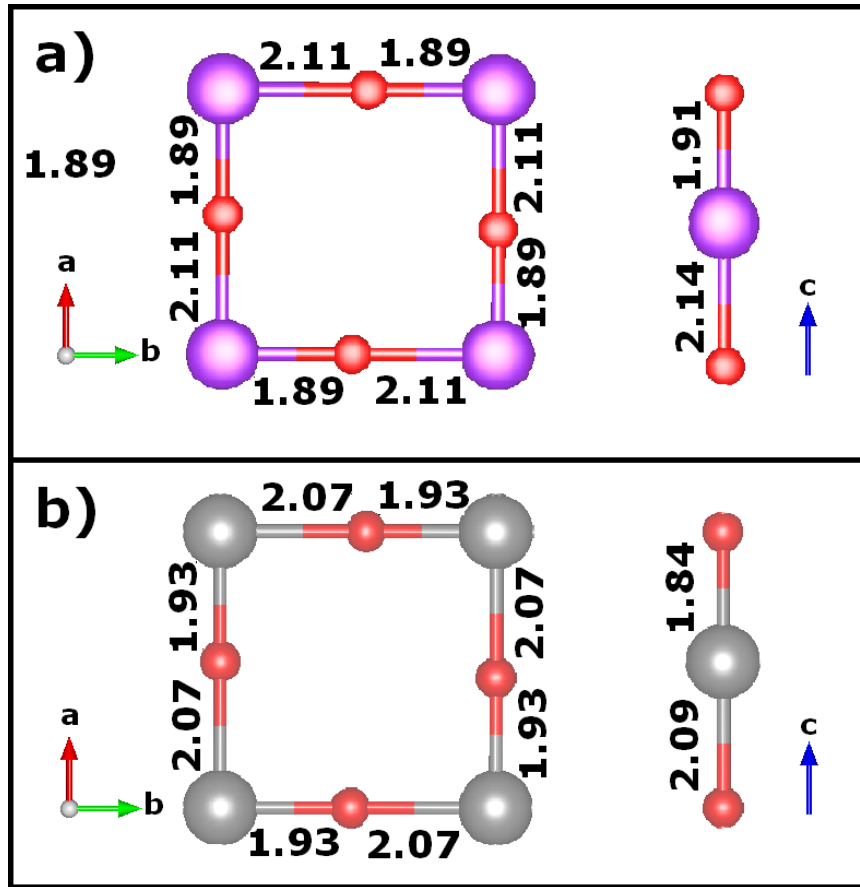
Figure 5.3 a) V-O and b) Cr-O bondlengths in the xy-plane and along the z-direction after full structural relaxation, for the case of one VO_2/CrO_2 layer sandwiched between layers of $BaTiO_3$.

distortions in the out-of-plane direction. In the presence of out-of-plane polar distortions only, the energy of the d_{xy} orbital will be lower than that of d_{xz} and d_{yz}. In VO_2, V has a valence of 4+, which corresponds to a d^1 configuration, now in the ferromagnetic configuration d_{xy} will be occupied at every site as shown in the Fig-5.4(a). In this picture all channels for hopping of the electron are blocked, the single electron can hop to. This rules out the possibility for superexchange to take place between the two V sites, but such a hopping is allowed in the antiferromagnetic state which is stabilized by 60 meV over the ferromagnetic state. However, allowing for in-plane JT distortions, one finds from an analysis of our total energy calculations that system further gains energy by stabilizing Jahn-Teller distortions in the xy-plane. An orbitally ordered ferromagnetic state as shown in Fig. 5.4(b) which is aided by a polar

distortion along z-direction, gets stabilized by 130 meV over the antiferromagnetic state. Because of the in-plane Jahn-Teller distortions, the shortest bondlength around one V site in the xy-plane is along x-axis while it is along the y-axis for another. This anisotropy in the in-plane bondlengths along with
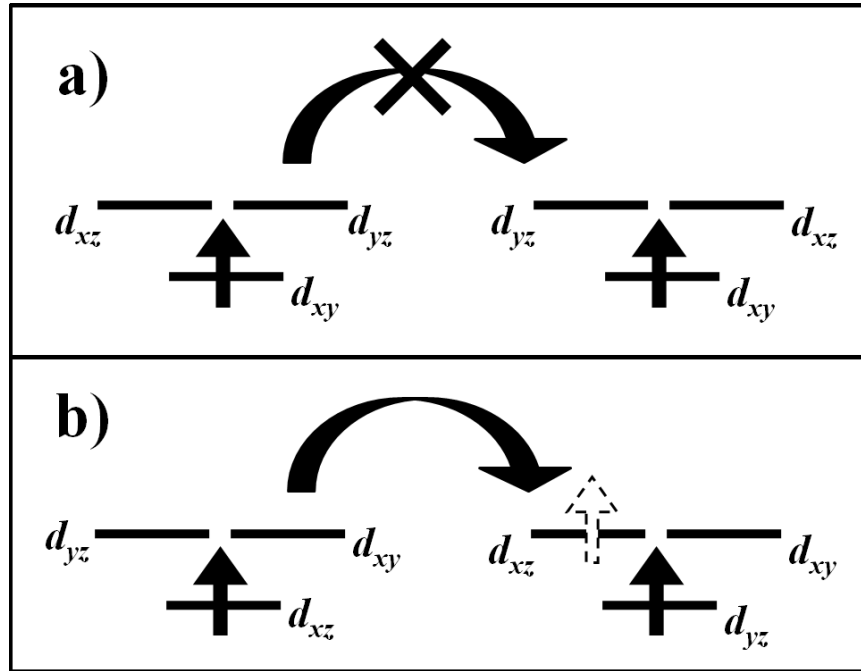
Figure 5.4 Channels for hopping in a ferromagnetic configuration which are a) not allowed if the sandwiched VO_2 layer had only polar offcentring along the z-direction and b) allowed in the presence of both in-plane JT distortions as well as the out-of-plane polar offcentring.

the polar offcentring along z-directions is expected to result in d_{xz} orbital lying lower in energy with respect to the other orbitals, d_{yz} and d_{xy} at one V site while d_{yz} remains lower and d_{xz} and d_{xy} go up in energy on another V site, as shown in the left and right hand side of Fig. 5.4(b). This allows the hopping of the single electron to the orbital of the same symmetry at the neighboring site as shown in the Fig-5.4(b). Hence, as the system gains energy by this process, the Jahn-Teller distortions freeze in the xy-plane. V has a single electron in the d shell and hence an insulating state is expected in this case.

In our attempt to confirm this speculation, we analyse the *V* partial density of states resolved over t_{2g} orbitals in the sandwiched VO_2 layer. And as shown in the Fig-5.5 indeed we find that it becomes very clear that at one V site energy of the d_{xz} orbitals lies lower than that of d_{yz} and d_{xy} while at another,

energy of d_{yz} orbitals lies lower than that of d_{xz} and d_{xy} and the VO_2 layer is insulating. Also since the orbitals are ordered on the alternate sites, this explains the ferromagnetic state that we find in our calculations.
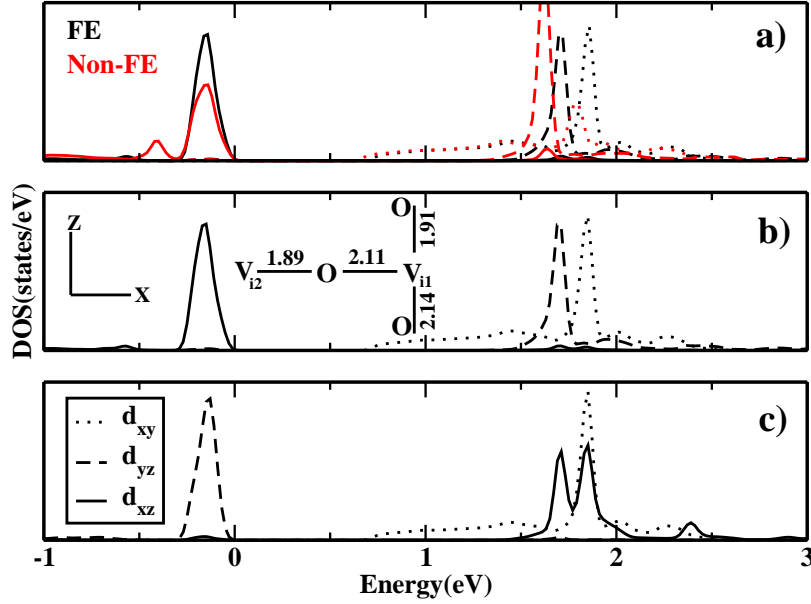
Figure 5.5 V-d partial density of states for the majority spins only showing a) comparison of ferroelectric(black) and non-ferroelectric(red) structure, b) t_{2g} orbitals corresponding to the site V_{i1} c) along the site V_{i2} for the case of single VO_2 layer sandwiched between $BaTiO_3$ layers.

To extend our conclusions, we also consider single monolayer of CrO_2 sandwiched between 13 monolayers of $BaTiO_3$ same as earlier, also shown in the Fig. 5.1. This corresponds to a d^2 configuration. We consider two structures with and without in-plane Jahn-Teller distortions. We calculate the electronic structure of this superlattice in a self consistent manner with the details as discussed earlier. We relax the atomic positions to find their minimum energy. From our total energy calculations we find that similar to the scenario with one VO_2 layer, the structure with in-plane Jahn-Teller distortions is stabilized over the one which does not have Jahn-Teller distortions in the xy-plane. These in-plane distortions exist together with a polar offcentring along z-direction. The Jahn-Teller distorted shorter

Table 5.1 Stabilization energies in meV/V or Cr atom for one and two monlayers thickness of sandwiched layer

	$BaVO_3/BaTiO_3$	$BaCrO_3/BaTiO_3$
Single Monolayer		
FM	-11	17
AFM	0	0
Two Monolayers		
AFM	0	0
FM	-38	-22
FM-AFM	-16	-22
AFM-FM	-11	-95

and longer in-plane bondlengths are found to be 1.93 Å and 2.07 Å, while the polar out-of-plane bondlengths are found to be 1.84 Å and 2.09 Å as shown in Fig-5.3(b). In the environment of the oxygens around Cr ions as in the present case, level ordering could be speculated in a straight forward manner. For one Cr site d_{xz} & d_{xy} orbitals remain lower in energy with respect to the d_{yz} orbitals, while for the other d_{yz} & d_{xy} are lower and d_{xz} goes up in the energy. As analysis of Cr d projected partial density of states as shown in the Fig. 5.6, since we have d^2 configuration, d_{xz} & d_{xy} at one Cr site and d_{yz} & d_{xy} on the other get occupied, as shown in the Fig-5.7.

It is important to note that for the two neighboring Cr sites, spins in the d_{xy} orbital would like to align antiparallel while those in the d_{xz} at one and d_{yz} at another would like to align parallel. So this leads to an interplay between the ferromagnetic and antiferromagnetic couplings. But as we have only single monolayer of CrO_2, in xy-plane the interaction of d_{xy} states which are common to the two neighboring Cr sites would be stronger than the interaction between d_{xz} at one and d_{yz} at another Cr site. Thus antiferromagnetism should prevail over the ferromagnetism. Indeed our analysis of the total energy calculations find the antiferromagnetic solution favored and remains lower than the ferromagnetic one by 17 meV/Cr atom as shown in the Table 5.1.
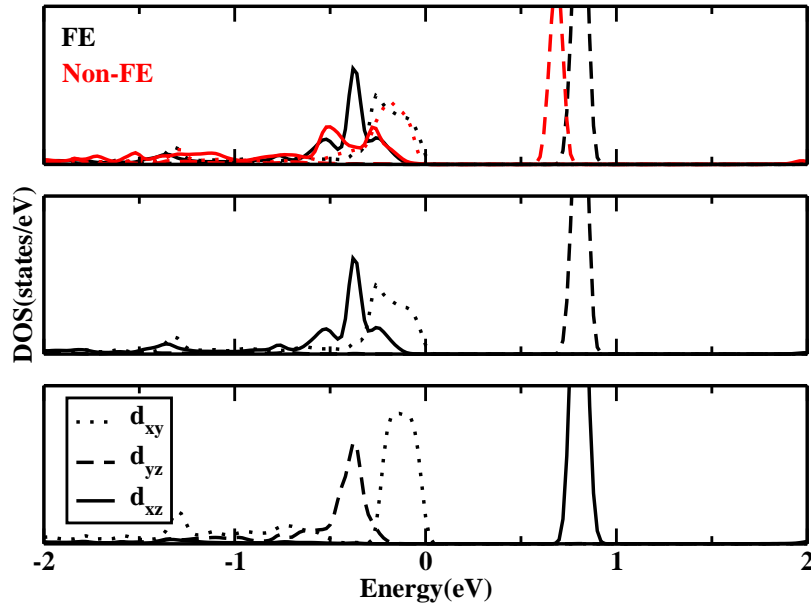
Figure 5.6 Cr-d partial density of states for the majority spins only showing a) comparison of ferroelectric(black) and non-ferroelectric(red) structure, b) t$_{2g}$ orbitals corresponding to one Cr site c) along the next for the case of single CrO$_2$ layer sandwiched between BaTiO$_3$ layers.
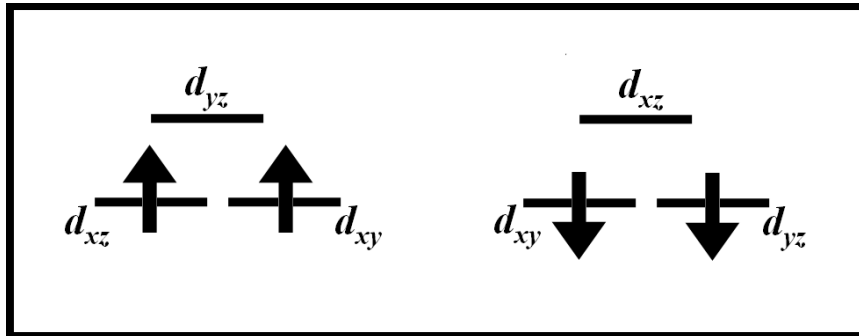
Figure 5.7 t$_{2g}$ orbital ordering for two neighboring Cr site, for the case of single CrO$_2$ layer sandwiched between BaTiO$_3$ layers.

We next go on to examine the behavior of both of these superlattices when more than one monolayer of VO$_2$ or CrO$_2$ are sandwiched between 13 monolayers of BaTiO$_3$. First let us try to understand two monolayers of VO$_2$ sandwiched between layers of BaTiO$_3$. We start with a structure as discussed

earlier (Fig-5.1), but having two monolayes of VO_2. We calculate the electronic structure with the details as discussed above. After full structural relaxation these sandwiched layers are still found to have Jahn-Teller distortions in the xy-plane, while a polar offcentring is found along the z-direction. After relaxation the Jahn-Teller distorted shorter and longer bondlengths in the xy-plane are found to be 1.89 Å and 2.11 Å, the same as in single VO_2 layer, while the polar bondlengths along the z-direction are 1.92 Å and 2.13 Å. In the present scenario, the picture of level ordering remains the same as it was for the single VO_2 layer. So in the xy-plane and along the z-direction both, and orbital ordering is expected where at two alternate neighboring sites, energy of the d_{xz} orbital remains lower than that of d_{xy} and d_{yz} at one site while energy of the d_{yz} orbital remains lower than that of d_{xy} and d_{xz} at other.
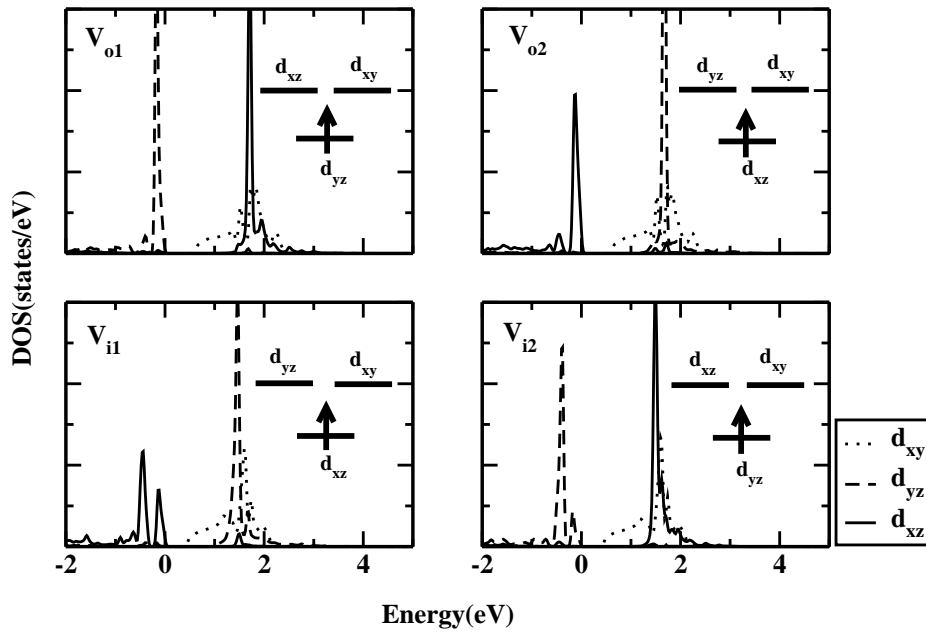
Figure 5.8 V-d partial density of states for the majority spins of t_{2g} states, lower two panels correspond to the two neighboring V sites in the xy-plane while the upper two panels indicate the two V sites above them along the z-direction. The inset shows the respective orbital ordering.

As shown in the Fig-5.8, we plot the partial density of states for the d states on V for two monolayers of VO_2 sandwiched between the $BaTiO_3$ layers. Two neighboring V sites in xy-plane are marked as

V_{i1} and V_{i2} while the two stacked in the z-direction are marked as V_{o1} and V_{o2}. The density of states analysis confirms the speculated ordering of the t_{2g} states. This ordering also gives rise to an insulating state. Due to orbital ordering, spins at each V site would like to align parallel to each other, thus driving the system to stabilize a ferromagnetic solution in its ground state. As shown in the Table-5.1, our total energy calculations found the ferromagnetic state favored over the antiferromagnetic one by 38 meV/V atom. Thus two monolayers of VO_2 sandwiched between $BaTiO_3$ layers are also found to be a ferromagnetic and ferroelectric insulator.

In the limit of two monolayers sandwiched between $BaTiO_3$ layers, we try to understand how does the behavior of the superlattice change on addition of one more electron as we move from VO_2 to CrO_2. From our total energy calculations, the structure with in-plane Jahn-Teller distortions is found to be stabilized over the one without it, by 100 meV/V atom. We consider various antiferromagnetic configurations as well as the ferromagnetic one. We find that the two monolayers of CrO_2 sandwiched between $BaTiO_3$ overlayers favor C-type antiferromagnetic ordering over other magnetic configurations, as shown in the Table-5.1. In the relaxed structure, the in-plane Jahn-Teller distorted shorter and longer bondlengths are found to be 1.93 Å and 2.03 Å respectively while a polar offcentring with bondlengths of 1.85Å and 2.08 Å is found along the z-direction. In Fig-5.8, we plot the Cr d partial density of states for the Cr atoms in both the two layers. The in-plane neighboring Cr sites are marked as Cr_{i1} and Cr_{i2} while those stacked along z-direction are labelled as Cr_{o1} and Cr_{o2}. The System is still found to be insulating at the limit of two monolayers sandwiched between $BaTiO_3$ layers and the level ordering is evident for the density of states.

The ordering of the t_{2g} orbitals is the same as we found in the case of a single CrO_2 layer, as shown in Fig-5.4. As we discussed for the single layer of CrO_2, in the xy-plane antiferromagnetism would prevail while in the out-of-plane direction, d_{xz} and d_{yz} interactions would be stronger than between d_{xy} orbitals at two neighboring Cr sites. Thus as a result of orbital ordering, ferromagnetism wins over the antiferromagnetism in an interplay between the two, along the z-direction. This explains the stabilization of c-type antiferromagnetic solution in the ground state.
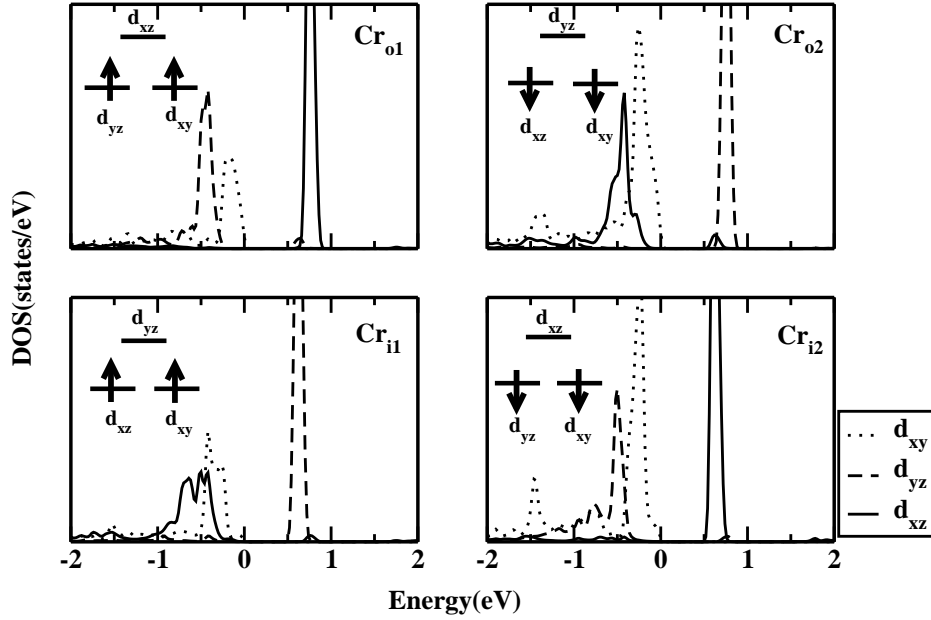
Figure 5.9 Cr-d partial density of states for the majority spins of t_{2g} states, lower two panels correspond to the two neighboring Cr sites in the xy-plane while the upper two panels indicate the two Cr sites above them along the z-direction. The inset shows the respective orbital ordering.

5.4   Conclusion

Starting from a dilute doping into a well known ferroelectric $BaTiO_3$, we arrive at and explore another route to design multiferroics with large value of polarization. We were able to design ferroelectric and ferromagnetic insulators in superlattice geometry. Superlattices of $BaVO_3/BaTiO_3$ where single monolayer of VO_2 is sandwiched between $BaTiO_3$ layers, are found to be ferromagnetic-ferroelectric and remain so upto two monolayers of VO_2 sandwiched between $BaTiO_3$ layers. Superlattices of $BaCrO_3/BaTiO_3$ consisting of single monolayer of CrO_2 sandwiched between $BaTiO_3$ layers are found to be antiferromagnetic-ferroelectric and remain so upto two monolayers of CrO_2 sandwiched between $BaTiO_3$ layers.

Bibliography

[1] M. Imada, A. Fujimori, and Y. Tokura, Rev. Mod. Phys. **70**, 1039 (1998).

[2] J. M. Longo, P. M. Raccah, and J. B. Goodenough, J. Appl. Phys. **39**, 1327 (1968).

[3] Y. Yamada, O. Hino, S. Nohdo, R. Kanao, T. Inami and S. Katano, Phys. Rev. Lett.**77**, 904 (1996).

[4] Y. Yamada, J. Suzuki, K. Oikawa, S. Katano and A. J. Fernandez-Baca, Phys. Rev. B **62**, 11600(2000).

[5] Y. Endoh ,Phys. Rev. Lett. **82**, 4328 (1999).

[6] J H Wei, D Hou and X R Wang, New Journal of Physics,**12**, 053021 (2010).

[7] P. Mahadevan, A. Kumar, D. Chaudhury and D. D. Sarma, Phys. Rev. Lett. **104**, 256401 (2010).

[8] S. Baidya, T. Saha-Dasgupta, Phys. Rev. B **84**, 035131 (2011).

[9] N. A. Hill, J. Phys. Chem. B **104**, 6694 (2000).

[10] C. Ederer and N. A. Spaldin, Nature Materials **3**, 849 (2004).

[11] M. Fiebig, J. Phys. D **38**, R123 (2005).

[12] W. Eerenstein, N. D. Mathur, and J. F. Scott, Nature (London) **442**, 759 (2006).

[13] N. A. Spaldin and M. Fiebig, Science **309**, 391 (2005).

[14] T. Lottermoser, T. Lonkai, U. Amann, D. Hohlwein, J. Ihringer, and M. Fiebig, Nature (London) **430**, 541 (2004).

[15] T. Kimura, T. Goto, H. Shintani, K. Ishizaka, T. Arima, and Y.Tokura, Nature (London) **426**, 55 (2003).

[16] T. Kimura, S. Kawamoto, I. Yamada, M. Azuma, M. Takano, and Y. Tokura, Phys. Rev. B **67**, 180401R (2003).

[17] M. Gajek, M. Bibes, S. Fusil, K. Bouzehouane, J. Fontcubert, A.Barthelemy, and A. Fert, Nature Materrials **6**, 296 (2007).

[18] J. Wang, J. Neaton, H. Zheng, V. Nagarajan, S. B. Ogale, B. Liu, D. Viehland, V. Vaithyanathan, D. G. Schlom, U. Waghmare, N. A. Spaldin, K. M. Rabe, M. Wuttig, and R. Ramesh, Science **299**, 1719 (2003).

[19] W. Eerenstein, M. Wiora, J. L. Prieto, J. F. Scott, and N. D.Mathur, Nature Materials **6**, 348 (2007).

[20] Z. Shi, C.Wang, X. Liu, and C. Nan, Chinese Science Bulletin,**53**, 2135 (2008).

[21] F. Yang, Y. C. Zhou, M. H. Tang et al., Journal of Physics D, **42**, 072004, (2009).

[22] M. Bibes and A. Barthelemy, Nature Materials, **7**, 425 (2008).

[23] X. Chen, A. Hochstrat, P. Borisov, and W. Kleemann, Applied Physics Letters, **89**, 202508 (2006).

[24] J. F. Scott, Nature Mater.**6**, 256(2007).

[25] S. Sahoo, S. Polisetty, C. G. Duan, S. S. Jaswal, E. Y. Tsymbal, and C. Binek, Phys. Rev. B, **76**, 092108 (2007).

[26] C. Thiele, K. Dörr, O. Bilani, J. Rödel, and L. Schultz, Phys. Rev. B **75**, 054408(2007).

[27] T. Zhao, A. Scholl, F. Zavaliche, K. Lee, M. Barry, A. Doran, M. P. Cruz, Y. H. Chu, C. Ederer, N. A. Spaldin, R. R. Das, D. M. Kim, S. H. Baek, C. B. Eom, and R. Ramesh, Nature Materials **5**, 823 (2006).

[28] D. I. Khomskii, Bull. Am. Phys. Soc. **C 21** 002 (2001).

[29] B. B. Van Aken, T. T. M. Palstra, A. Filippetti, and N. A. Spaldin, Nature Mater. **3**, 164 (2004).

[30] M. Dawber, C. Lichtensteiger, M. Cantoni, M. Veithen, P. Ghosez, K. Johnston, K. M. Rabe, and J.-M. Triscone, Phys. Rev. Lett, **95**, 177601 (2005).

[31] R. Ranjith, B. Kundys, and W. Prellier, Appl. Phys. Lett. **91**, 222904 (2007).

[32] S. Bose and S. B. Krupanidhi, Appl. Phys. Lett. **90**, 212902 (2007).

[33] S. Sawamura, N. Wakiya, N. Sakamoto, K. Shinozaki, H. Suzuki, Jap. Journ. Appl. Phys. **47**, 7603(2008).

[34] F. Bai, Huaiwu Zhang, J. Li and D. Viehland, J. Phys. D: Appl. Phys. **43**, 285002(2010).

[35] L. Yan, Z. Xing, Z. Wang, T. Wang, G. Lei, J. Li, and D. Viehland, Appl. Phys. Lett. **94**, 192902 (2009).

[36] K. S. Wang, M. A. Aronova, C. L. Lin, M. Murakami, M. H. Yu, J. Hattrick-Simpers, O. O. Famodu, S. Y. Lee, R. Ramesh, M. Wuttig, I. Takeuchi, C. Gao, and L.A. Bendersky, Appl. Phys. Lett. **84**, 3091 (2004).

[37] H. Zheng, J. Wang, S. E. Lofland, W. Ma, L. Mohaddes-Ardabili, T. Zhao, L. Salmanca- Riba, S.R. Shinde, S. B. Ogale, F. Bai, D. Viehland, Y. Jia; D. G. Schlom, M. Wuttig, A. Roytburd, and R. Ramesh, Science **303**, 661 (2004).

[38] C. W. Nan, N. Cai, L. Liu, J. Zhai, Y. Ye, and Y. Lin, J. Appl. Phys. 94, 5930 (2003).

[39] P. Murugavel, D. Saurel, W. Prellier, Ch. Simon, and B. Raveau, Appl. Phys. Lett. **85**, 4424

[40] N. Sai, B. Meyer, and D. Vanderbilt, Phys. Rev. Lett. **84**, 5636 (2000).

[41] J. B. Neaton and K. M. Rabe, Appl. Phys. Lett. **82**, 1586 (2003).

[42] H. N. Lee et al., Nature (London) **433**, 395 (2005).

[43] E. Bousquet et al., Nature (London) **452**, 732 (2008).

[44] M. Dawber, C. Lichtensteiger, M. Cantoni, M. Veithen, P. Ghosez, K. Johnston, K. M. Rabe, and J.-M. Triscone, Phys. Rev. Lett. **95**, 177601 (2005).

[45] S. M. Nakhmanson, K. M. Rabe, and D. Vanderbilt, Appl. Phys. Lett. **87**, 102906 (2005).

[46] M. Dawber, *et al.*, Adv. Mater. **19**, 4153(2007).

[47] N. A. Pertsev, A. G. Zembilgotov, and A. K. Tagantsev, Phys. Rev. Lett. **80**, 1988 (1998).

[48] O. Diéguez, K. M. Rabe, and D. Vanderbilt, Phys. Rev. B **72**, 144101 (2005).

[49] K. J. Choi, M. Biegalski, Y. L. Li, A. Sharan, J. Schubert, R. Uecker, P. Reiche, Y. B. Chen, X. Q. Pan, V. Gopalan, L.-Q. Chen, D. G. Schlom, and C. B. Eom, Science **306**, 1005(2004).

[50] J. H. Haeni, P. Irvin, W. Chang, R. Uecker, P. Reiche, Y. L. Li, S. Choudhury, W. Tian, M. E. Hawley, B. Craigo, A. K. Tagantsev, X. Q. Pan, S. K. Streiffer, L. Q. Chen, S. W. Kirchoefer, J. Levy and G. Schlom, Nature **430**, 758 (2004).

[51] X. Wu, M. Stengel, K. M. Rabe, and D. Vanderbilt, Phys. Rev. Lett. **101**, 087601 (2008).

[52] M. K. Lee, T. K. Nath, C. B. Eom, M. C. Smoak, and F. Tsui, Appl. Phys. Lett. **77**, 3547(2000). (2004).

[53] S. Valencia, A. Crassous, L. Bocher, V. Garcia, X. Moya, R. O. Cherifi, C. Deranlot, K. Bouze-houane, S. Fusil, A. Zobelli, A. Gloter, N. D. Mathur, A. Gaupp, R. Abrudan, F. Radu, A. Barthélém and M. Bibes, Nature Materials **10**, 753(2011).

[54] X. Wu, O. Diéguez, K. M. Rabe, and D. Vanderbilt, Phys. Rev. Lett. **97**, 107602 (2006).

[55] K. Johnston, X. Huang, J. B. Neaton, and K. M. Rabe, Phys. Rev. B **71**, 100103(R) (2005).

[56] H. Lee, J. Yu, and U. V. Waghmare, J. Appl. Phys. **105**, 016104 (2009).

[57] J. B. Neaton, C. Ederer, U. V. Waghmare, N. A. Spaldin and K. M. Rabe, Phys. Rev. B, 71, **014113**(2005).

[58] G. Lawes, A. B. Harris, T. Kimura, N. Rogado, R. J. Cava, A. Aharony, O. Entin-Wohlman, T. Yildirim, M. Kenzelmann, C. Broholm and A. P. Ramirez, Phys. Rev. Lett. **95**, 087205 (2005).

[59] H. K. Chandra, K. Gupta, A. Nandy and P. Mahadevan, Submitted to Phys. Rev. Lett. (2011).

[60] G. H. Kwei , A. C. Lawson , S. J. L. Billinge , S. W. Cheong, J. Phys. Chem., **97**, 2368 (1993).

Chapter 6

Metal to insulator transition in thin films of SrRuO$_3$

6.1 Introduction

Remarkable advances in the growth techniques has motivated the scientific community to put in considerable efforts to search, develop and exploit technologies which are not primarily based on semiconductors as the main functional material [1, 2]. Major part of this research has been to explore the transition metal perovskite oxides. Having a control over various degrees of freedom drives this class of materials to exhibit robust and novel properties. An important facet of these materials is that they are able to show more than one active property simultaneously [3], the term coined to describe these materials is multifunctional materials. A number of members of transition metal perovskite oxide material exihibit ferroelectricity, charge, orbital and magnetic ordering resulting from an interplay among the charge, orbital, spin or lattice degree of freedom. Another class of these materials which are very important from a device perspective are ones where an externally applied magnetic field could switch or modify the ferroelectric state or an applied electric field could switch the magnetic ordering [4–8]. These oxides are potential candidates for memory devices and have opened up new avenues for oxide based electronics [9, 10]. Conductive oxides are another class which are essential components in composite oxide

heterostructures where they are often used as electrode materials in thin film applications [11, 13, 25].

Reducing the dimensionality is another handle that drives various novel properties which are not observed or expected in their corresponding bulk form. With sophisticated abilites in thin film growth, very fine epitaxy can be obtained for transition metal oxide thin films. Thin films of oxides with perovskite structure are considered to be the most promising material candidates for future dynamic random access memories and for non-volatile ferroelectric random access memories [14]. These oxides generally retain their bulk like properties in two dimensions(in-plane) while they are modified in the direction of growth as a result of confinement, presence of interface or surface, misfit strain, either compressive or tensile due to epitaxial lattice mismatch. Interactions among subsequent overlayers also plays an important role in determining the functionality of these films in comparison to their bulk counterparts. Not only epitaxial thin films can be grown for various oxides but one finds that highly oriented heterostructures could also be grown with atomic level precision [15–17].

SrRuO₃ is empowered with few remarkable features. *Ru* being a $4d$ element, *SrRuO₃* is a moderately correlated material that exhibits several novel physical properties. Strong electron-electron correlation effects in $3d$ transiton metal oxides, drives them to an insulating state, which otherwise should be metallic. In Ruthenates corelation effects are less effective as due to larger spread of wavefunction corresponding to 4d orbitals, and hence increased hybridization results into more effective screening and a reduced coulumb repulsion energy U. In addition as it permits the epitaxial growth of essentially single-crystal films, it is widely studied as a conducting electrode layer in epitaxial heterostructures in conjunction with a range of other oxides.

Bulk *SrRuO₃* undergoes a phase transformation as a function of temperature [18, 19]. It is a ferromagnetic metal upto a curie temperature of 160 K [20,21]. *SrRuO₃* stabilizes in distorted orthorhombic structure(space group *Pnma*) at room temperature. These distortions can be represented by glazer notation(as discussed in chapter 1) $a^- a^- c^+$. The orthorhombic phase can be visualized by rotation of the *RuO₆* octahedra counterclockwise about the $[010]_{cubic}$ and $[001]_{cubic}$ and clockwise rotation about the $[100]_{cubic}$ direction of an *ABO₃* cubic perovskite. These directions become inequivalent upon rotation. With increasing temperature, the degree of the orthorhombic distortion decreases, and the structure

transforms to a higher-symmetry perovskite structure. Around 820 K, the orthorhombic structure transforms into a tetragonal structure with space group I4/mcm [22] In this tetragonal unit cell, the RuO_6 octahedra are rotated only about the $[001]_{cubic}$ direction. Going to higher temperatures around 950 K, tetragonal $SrRuO_3$ transforms into a cubic structure with a standard perovskite space group $Pm3m$, where the RuO_6 octahedra are not rotated [22]. In an alternate route, these structural transition temperatures are influenced by strain, and hence in the case of epitaxial films, they depend on the substrate material [23]. As this structure has orientational anisotropy in its bulk form, where the ferrodistortive rotations of octahedra are along the long axis of the unit cell, which drives thin films of this material to exhibit more complex behaviour. Therefore two orientations are possible for $SrRuO_3$ films; when the long axis of the unit cell points in the plane of epitaxy the films is considered to be ab-oriented while if its out-of-plane films are c-oriented. Obviously films will behave differently between these two possible orientations.

Zayak *et. al.* [30] studied the effect of strain theoretically on rotation and tilts and hence Ru-O-Ru angles in orthorhombic $SrRuO_3$ films, where tuning the strain to these films could put a control over the rotation and tilt angles and consequent Ru-O-Ru angles, in both ab- and c- oriented films. This is very important in functional oxides to engineer novel properties by controlling the electronic band width. They also reported a magnetostructural coupling in both of the orientations of the $SrRuO_3$ films. In another report they also showed a spin state transition from low (S=0) to high (S=1) spin state under bi-axial strain. There are experimental reports confirming such switching of magnetism in these films. The prediction also agrees with isovalent chemical substitution reports, which can be related to the application of pressure, which shows that the ferromagnetic ground state is highly sensitive to the $Ru - O - Ru$ angles.

We make a point here that the slightest of change in the structure of the films by means of substrate strain could drive them to exhibit completely different properties from bulk, as well as the magnitude of the strain imposed could result in modified phase diagram.

The literature is very rich with studies exploring $SrRuO_3$ in the thin films regime, which includes the technology application aspects as well. To name a few are field effect devices, spintronics, multi-

ferroic memory devices [24–27]. Most of the metal oxides when grown in thin film geometry exihibit an increased resistivity compared to the bulk, $SrRuO_3$ is no different. When thin films of $SrRuO_3$ were grown epitaxially on $SrTiO_3$ substrate, films with thickness of four monolayers or less were found to be insulating [28, 29]. There are experimental reports about loss of ferromagnetic order in ultrathin films [28]. $SrRuO_3$ thin films have also been studied in first principle methods. Rondinelli *et.al.* [15] suggested indirect experimental factors or structural defects as a possible reason behind this metal-insulator transition, though they could not reproduce experimentally observed metal-insulator tranisition in their calculation. Zayak *et.al.* [30] studied structural and magnetic behavior as a function of strain, the phenomena of metal-insulator transition was not looked into. Although there is no consensus the importance of the electronic correlation is these systems. Some experimental works suggest that correlations are important even in $4d$ systems and cannot be overlooked [31–33]. While some suggest that correlations are much weaker and are not at all important in this material [34]. So there exist a lack of understanding about the ultrathin film behavior of $SrRuO_3$.

The Mechanism of the experimentally observed metal-insulator transition in thin films of $SrRuO_3$ was succesfully explained in an earlier work on ultrathin films of $SrRuO_3$ by Mahadevan *et. al.*[35] Films grown on SrTiO$_3$ substrate were found to become an antiferromagnetic insulator compared to their ferromagnetic metallic state in bulk from at the few monolayers limit. For thicker films an antiferromagnetic insulating solution coexists with a metallic solution corresponding to an antiferromagnetic surface and a ferromagnetic bulk. Films beyond four-monolayers were found to be metallic as observed in the bulk, though the magnetic state does not evolve to be like the bulk ferrromagnetic state. The bulk shows ferromagnetism while the surface remains antiferromagnetic.

As emphasized in the earlier part, thin film properties are very sensitive to strain imposed and consequent lowering of the symmetry of the structure, in this work we revisit the calculations with two important variations. First, we use the experimental lattice constant (3.905 Å) of $SrTiO_3$ as against the GGA optimized lattice constant (3.94 Å) in the earlier work. Second, as the $Ru - O - Ru$ angles in bulk strongly deviate from $180°$, only $GdFeO_3$ distortions were included in the earlier work. Here we include the rotations of the octahedra about [001] axis also in addition to the $GdFeO_3$ distortions which

are equivalent to what is found in the orthorhombic strcture of *SrRuO₃*.

To probe into the open questions discussed above, we carried out ab-initio density functional calculations for ultrathin films of *SrRuO₃* grown on *SrTiO₃* substrate. We explored how structural, electronic and magnetic properties of these films depend on film thickness.

6.2 Methodology

The electronic structure of bulk as well as of thin films of *SrRuO₃* was calculated within a planewave pseudopotential implementation of density functional theory within VASP. Exchange and correlation functionals were approximated with GGA (generalized gradiednt approximation). Correlation effects on Ru were treated within the GGA+U method using formalism of Dudarev. A value of U=2.5 eV and J=0.4 eV was applied on Ru atom as deduced from a constrained random phase pproximation based formalism as it was used in earlier work. A k-point mesh of $6 \times 6 \times 6$ and $6 \times 6 \times 2$ was used to calculate the electronic structure of the bulk form and thin films respectively, in a self consistent manner. It was increased to $8 \times 8 \times 8$ and $8 \times 8 \times 2$ to calculate the density of states. Spheres of radii 0.9 Å were considered to calculate the partial density of states for the Ru *d* levels.

From our calculations we find that correlation effects are necessary to correctly interpret the insulating state in this system in the GGA+U picture. Thin films with this magnitude of U are found to be insulating. *SrRuO₃* in the bulk form occurs in the orthorhombic structure, with unit cells containing 20 atoms arising from four formula units. We perform calculations considering the experimental structure for bulk *SrRuO₃*. After full structural relaxation we find the in-plane and out-of-plane angles to be 158° and 160° respectively. The substrate material *SrTiO₃* occurs in the cubic structure with experimental lattice constant of 3.905 Å which is smaller than the pseudocubic lattice constant of *SrRuO₃* 3.94 Å, thus imposing a compressive strain on the thin film layers due to lattice mismatch between the substrate and the thin film material. In our calculations a symmetric slab consisting of a total of 15 layers with *TiO₂* and *SrO* layers on the both sides of a central *SrO* layer along $< 001 >$ direction is used to mimic the *SrRuO₃* films grown on *SrTiO₃*(001) substrate as shown in the Fig. 6.1. We consider the case

where the substrate terminates with a TiO_2 layer and on that SrO/RuO_2 layers are placed alternaltively. We consider the substrate to terminate at the TiO_2 surface as this is usually the layer exposed in the experiments on which the $SrRuO_3$ films are grown. We use periodic boundary conditions in the implementation of density functional theory that we use. In order to minimize the interaction between the images of the slab, we use 15 Å of vacuum. The in-plane lattice constant of the $SrRuO_3$ films is set to be equal to the cubic lattice constant of $SrTiO_3$ substrate, while out-of-plane one is allowed to find its minimum energy during structural optimization. As stated earlier rotations of Ru-O octahedra about [100], [010] and [001] directions are allowed, as $Ru - O - Ru$ angles strongly deviate from $180°$.
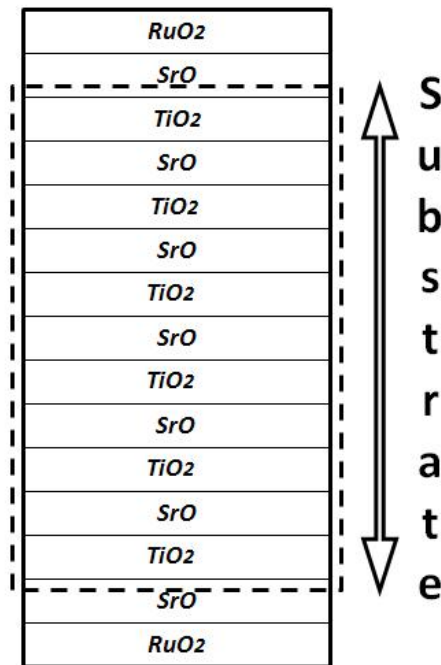
Figure 6.1 Symmetric slab setup we considered for the calculations consisting of alternate SrO/TiO₂ layers and at both of the ends monolayers of SrRuO₃ are considered.

6.3   Results and Discussion

We consider the experimental orthorhombic structure of SrRuO₃. Which has a long axis along the b direction. In the experimental structure, the bondlengths are 1.99 Å in the ac plane, while 1.97 Å along

the *b* direction. The Ru-O-Ru angles are 160° and 170° in *ac* plane and along *b* direction respectively. We then optimize the experimental structure within GGA+U calculations with U=0 eV and U=2.5 eV. Without any addition of U the relaxed bondlenghts in the *ac* plane and along the *b* direction become 2.0 Å and 1.99 Å respectively, while the angles become 158° and 160°. With U=2.5 eV though the Ru-O-Ru angles, and Ru-O bondlength along the *b* direction remain the same as in the case of U=0 eV, bondlengths in the ac plane become Jahn-Teller distorted with short and long bondlengths being 1.99 Å and 2.0 Å. A full comparion is shown in Table-6.1.

Let us understand the bulk behavior of $SrRuO_3$ in more detail. Ru in $SrRuO_3$ has a valence of +4, hence having four electrons in the d shell. Generally the five fold degenerate d orbitals on the transition metal ion, under octahedral environment of the six oxygens around them, split into triply degenerate t_{2g} and doubly degenerate e_g orbitals. Ru being a 4d transition metal ion, the crystal field splitting should be larger than the exchange splitting due to the extended nature of the 4d orbitals. Therefore, they are usually in the low spin configuration, in which all of t_{2g} bands are lower than the e_g bands. As the crystal-field splitting is quite large, the electrons occupy the t_{2g} down-spin states after occupying the t_{2g} up-spin states. As shown in the Fig. 6.2, the system appears to be at the brink of a transition to a half-metallic state with a weak shoulder due to the up-spin states at the Fermi level.

While going to GGA+U from simple GGA at U=2.5 eV and J=0.4 eV, system become half metallic for finite U calculations. On the application of non-zero U the spin-up states move deeper into the valence band while spin-down states remain pinned to the fermi energy, as shown in the Fig-6.2. So essentially the effective splitting between spin-up and down stated is increased that drives the system to half metallic state.

After having a knowledge of the bulk electronic structure, let us examine the thin films of $SrRuO_3$ over $SrTiO_3$ substrate. As we have seen, both rotations of the RuO_6 octahedra as well as tilts of the RuO_6 are found in the bulk $SrRuO_3$. We consider two cases of the structure; one with rotations of the octahedra only and second with both, the rotations and tilts of the RuO_6 octahedra. Total energy calculations for different number of monolayers show that structures with both tilt and rotations of octahedra have lower energy than that with only rotations of octahedra as shown in Table 6.2. This
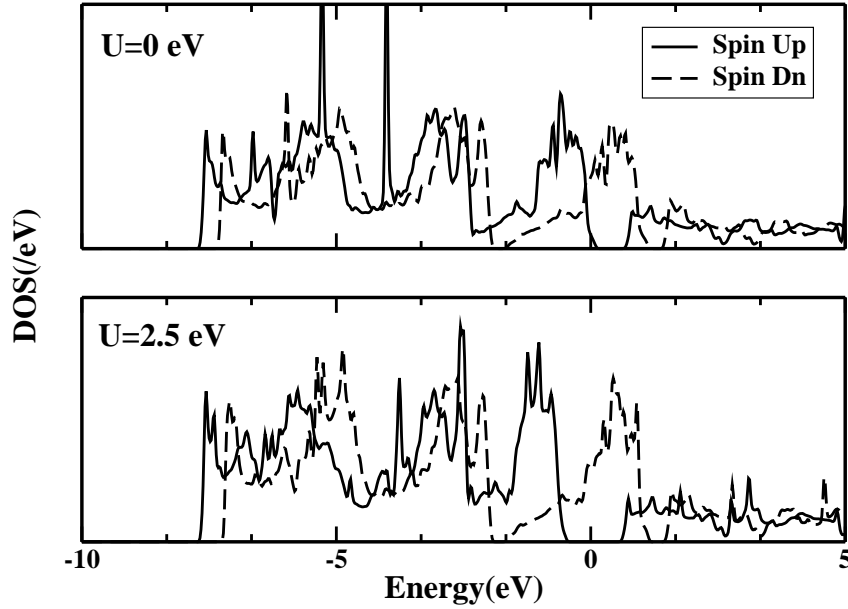
Figure 6.2 The up-spin solid line and down-spin dashed line Ru d partial density of states for bulk SrRuO$_3$ in the ferromagnetic state. The zero of energy corresponds to the Fermi energy.

energy difference is within the error bars of our calculations for antiferromagnetic configuration in the two monolayer case, though it becomes significant for all other cases. If not specified explicitly, now onwards we describe our results for structures having both rotations and tilts of the octahedra.

We performed the calculations with details discussed above, and we found the films to be insulating at the two monolayers limit unlike their bulk counterpart. As *SrRuO$_3$* films are imposed with a compressive strain by the substrate *SrTiO$_3$*, in-plane lattice constant is smaller and to keep the volume of the unit cell, out-of-plane lattice constant is expected to increase than in bulk. More over the broken coordination at the surface leads to a strong crystal field anisotropy and hence results in the level ordering of doubly degenerate d_{yz} and d_{xz} levels followed by d_{xy} levels. An insulating state can be expected if the four electrons from Ru ion resides in d_{xz} and d_{yz} states, rendering a zero moment which is possible in low spin state of Ru in *SrRuO$_3$*.

To find out the ground state of these films we considered various possible magnetic(both ferromag-

Table 6.1 Ru-O bondlengths in Å and Ru-O-Ru angles in degree for experimental and calculated relaxed structure.

	Expt.	U=0, J=0 eV	U=2.5, J=0.4 eV
Bondlengths			
ac-plane	1.99/1.99	2.0/2.0	2.00/1.99
b-direction	1.97	1.99	1.99
Angles			
ac-plane	160°	158°	158°
b-direction	170°	160°	160°

netic and antiferromagnetic) and nonmagnetic configurations within the scope of our calculations. The structure is optimized to relax the internal atomic positions and to achieve their minimum energy. We find that two monolayers of SRO are insulating unlike their bulk counterpart, and the antiferromagnetic solution is lower than the ferromagnetic by 157 meV/Ru atom, as shown in the Table-6.2. So magnetism survives at this ultrathin film limit. In all $SrRuO_3$ here undergoes a transition from metal to insulator, accompanied by a change in the magnetic state from ferromagnetic to antiferromagnetic while going from bulk to thin film regime. We next look at the in- and out-of-plane Ru-O bondlengths for two monolayers of $SrRuO_3$ having single RuO_2 layer with one of the two apical oxygens missing at the surface, corresponding to the fully relaxed structure in its minimum energy. The in-plane bondlengths are 1.95/1.97 Å and out-of-plane bondlength become 2.15 Å.

To understand the origin of this insulating nature, next we look into the DOS for two monolayers of $SrRuO_3$. In Fig. 6.3, we plot the Ru partial density of states resolved over spins and orbitals, for this case. As shown in the top three panels of Fig-6.3, electronic states corresponding to the spin-up of the orbitals with t_{2g} symmetry have significant weights at fermi level and deeper at lower energy in the valence band, thus one can not directly determine the ordering of the d_{xz}, d_{yz} and d_{xy} orbitals. On the other hand level ordering of the t_{2g} orbitals becomes straight forward, having a look at the spin-down channel. Very clearly states to d_{xz} and d_{yz} states lie lower, while the d_{xy} goes up in the energy. Strong

Table 6.2 Total energies in meV/Ru for all magnetic configurations with a) rotations only b) both of the rotations and tilts of the RuO$_6$ octahedra

		GdFeO$_3$ rotations	GdFeO$_3$+001 rotations
two-mono	FM	0	0
	AFM	-175	-157
three-mono	FM	0	0
	AFM	-45	-35
four-mono	FM	0	0
	AFM	-69	-110
	FM-AFM	-82	-129

modifications in the crystal fields at the surface of these films also yields a significant splitting of the e_g orbitals. Panel (d) and (e) of the Fig. 6.3, show that earlier unoccupied $d_{3z^2-r^2}$ level is now occupied unlike to the bulk scenario. Also clearly the states corresponding to $d_{x^2-y^2}$ lie above the d_{xy} derived spin-down states. Here we have the shortest bond-length in the *ab* plane while the longest bondlength is along the *c* direction. Therefore in such a geometry the crystal fields are expected to determine the ordering of these orbital resulting in the d_{xz}, d_{yz} being lower than the d_{xy}, and the $d_{3z^2-r^2}$ orbital getting occupied unlike the bulk as discussed above. The transition into the high-spin state at the surface from a low-spin state in bulk, is accompanied by a strong Jahn-Teller type distortion associated with a d^4 configuration with a partially filled e$_g$ states, which drives the system to an insulating state.

As shown in the Fig. 6.4 the in-plane distortions are ferroelectric in nature locally. Though on a macroscopic scale with the periodic boundary condition along x- and y-directions, the net effect of dipoles is zero, as they cancel each other out. As described earlier the strain effects and the symmetry lowering plays an important role in the functionality of this system in the thin films regime, and the role of substrate material becomes very crucial. We take care of the same by cross checking our calculations with the inclusion of antiferrodistortive rotations in *SrTiO$_3$*, exploring any possibility of symmetry lowering of substrate which could bring such an observed anisotropy in the in-plane Ru-O
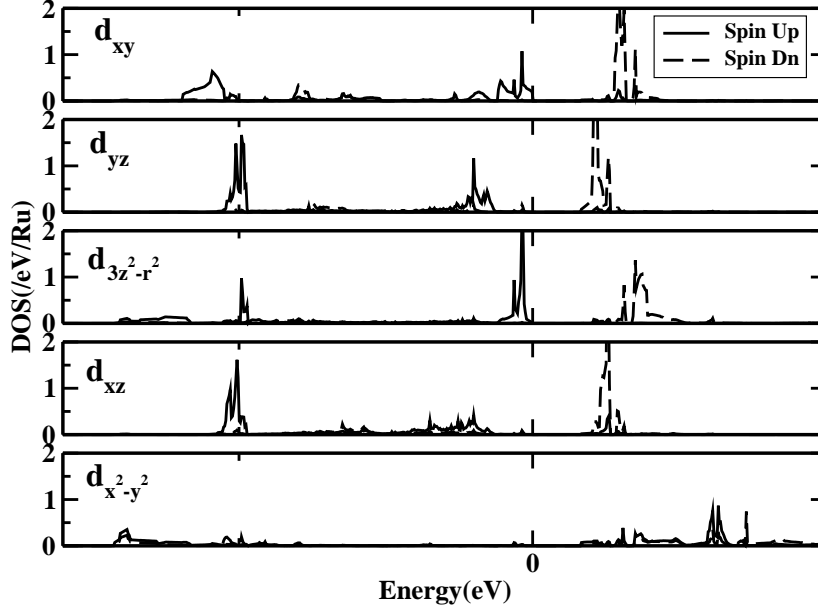
Figure 6.3 The spin-up and spin-down (solid and dashed lines respectively),spin and orbital-projected Ru d partial density of states for the surface Ru atom for two monolayers of *SrRuO₃* grown on *SrTiO₃* calculated for the antiferromagnetic ground state. The zero of energy corresponds to the top of the valence band.

bondlengths. These antiferrodistortive distortions occur in the low temperature structure of *SrTiO₃* and could be represented in glazer notation $a^0a^0c^-$. We calculate the electronic structure with such variations and find no role of AFD distortions of substrate on the in-plane bondlength anisotropy, and the ground state is almost degenerate with the earlier calculated antiferromagnetic insulating solution.

Next we tried to understand what are the energetics that can drive such unconventional level ordering in these films? As a result of spin-state transition from low to high spin state there is an additional Hund's intra atomic exchange present which we argue, could possibly compensate the huge strain energy required to bring in the large crystal distortions in these films. We would like ti stress here that interestingly the crystal field distorted structure exists only for the antiferromagnetic state. Such distortions are absent in solutions corresponding to the nonmagnetic and ferromagnetic states.

We go on to examine the films with more number of overlayers, to reach the threshold point of
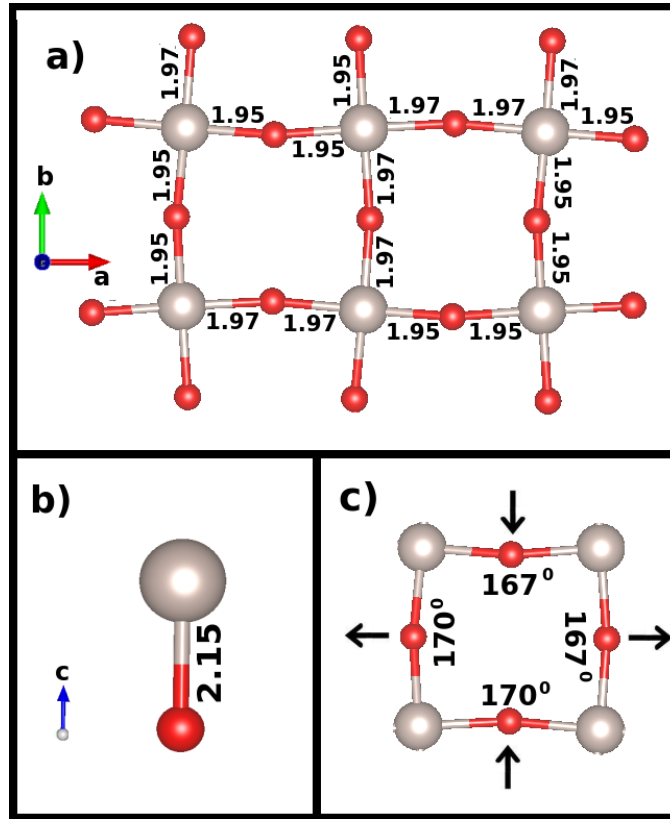
Figure 6.4 Relaxed in-plane a)Ru-O bondlengths in Å and b) angles in degree for the RuO$_2$ layer of two monolayers of *SrRuO$_3$* grown on *SrTiO$_3$*.

metal-insulator transition. As mentioned earlier *SrRuO$_3$* films have been reported to be insulating at the limit of four monolayers in experiment, so it is important to see if the insulating state still survives with the thicker films. On adding *SrO* layer on top of the *RuO$_2$* layer, we find that the ground state is still antiferromagnetic and the solution is lower than the ferromagnetic one by 35 meV/Ru atom(Table 6.2).

Adding a layer of SrO on the two monolayers of SrRuO$_3$ results in the in-plane Ru-O network to adopt the structure shown in Fig. 6.5. Each Ru atom has a small Jahn-Teller distortion with the long and short Ru-O bonds differing by 0.01 Å. The in-plane Ru-O-Ru angles now at this limit of three monolayers are 6-8° less than the values found in bulk. This trend, however is expected in the case of compressive strain. The out-of-plane bondlengths are found to be 2.0 Å and 2.05 Å. The longer Ru-O bondlength in the z-direction results in a degeneracy lifting of the t$_{2g}$ orbitals with the d$_{xz}$ and d$_{yz}$ levels
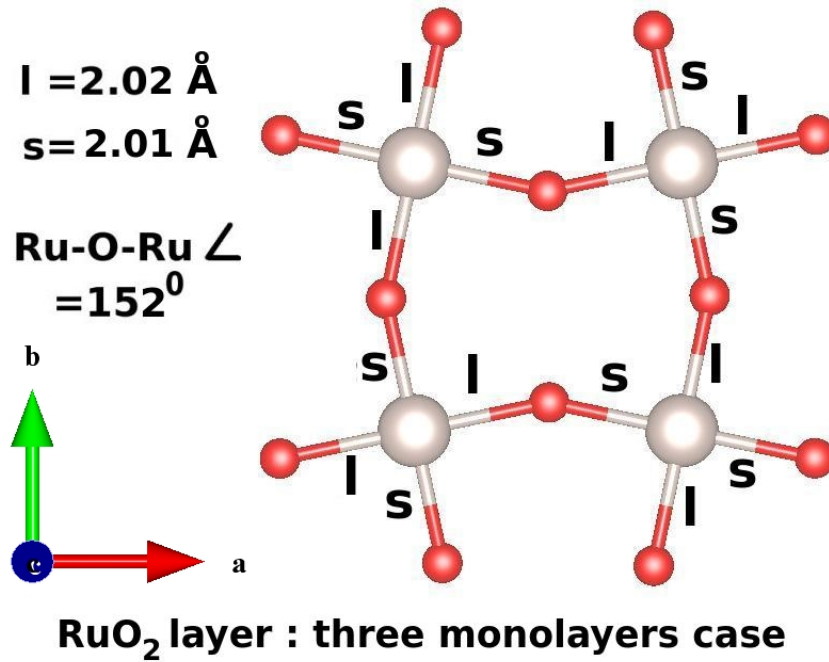
Figure 6.5 Relaxed in-plane a)Ru-O bondlengths in Å and b) angles in degree for the RuO$_2$ layer of three monolayers of *SrRuO$_3$* grown on *SrTiO$_3$*.

found at lower energies compared to the d$_{xy}$ orbitals, as seen for the Ru d projected partial density of states for the up spin channel in Fig. 6.6. However one finds a change in the level ordering in the down spin channel. The fourth electron goes into the down spin d$_{xy}$ orbitals. This could be understood in terms of an orbital dependent exchange splitting. The d$_{xy}$ orbitals delocalize in the xy-plane forming wide bands, while the d$_{xz}$ and d$_{yz}$ orbitals interact with other d$_{xz}$ and d$_{yz}$ orbitals only along the x- and y-axis respectively and form narrower bands. The interaction in the z-direction is very weak, as the corresponding Ti orbitals with which they can interact are much higher in energy. As a result the effective intra-atomic exchange interaction strength for the d$_{xy}$ orbitals is small compared to the d$_{yz}$ and d$_{xz}$ orbitals and hence the former gets occupied.

We then went on to examine whether the system would remain insulating under additional compressive strain. This was simulated by changing the lattice parameter of the SrTiO$_3$ substrate. Shorter Ru-O bonds in the 1% and 2% compressed SrTiO$_3$ substrate, resulted in an increased gain in bonding energy for the *d$_{xy}$* orbitals. As a result, one had a competition between the intra-atomic exchange
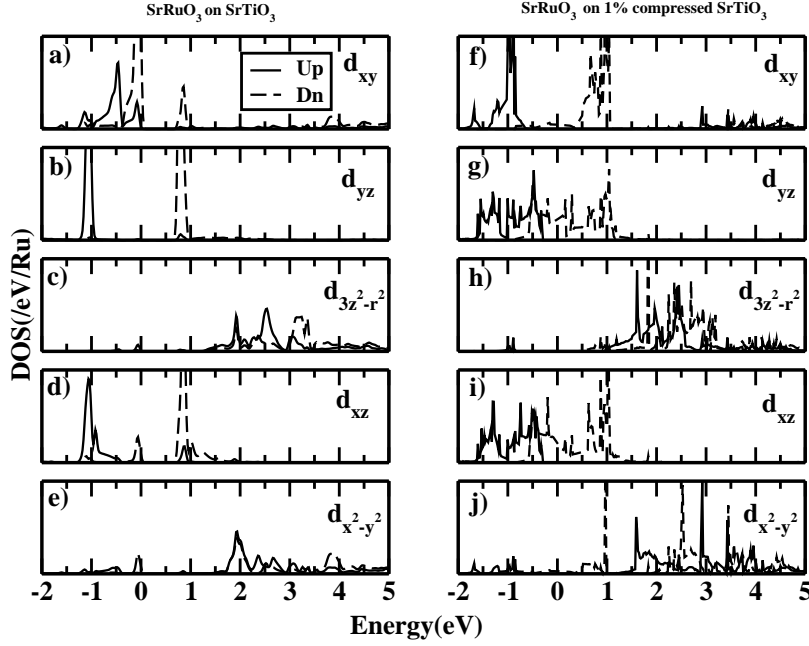
Figure 6.6 The spin-up and spin-down (solid and dashed lines respectively),spin and orbital-projected Ru d partial density of states for the RuO_2 layer of three monolayers of *SrRuO₃* grown on *SrTiO₃*(left panels) and 1% compressed *SrTiO₃* (right panels). The zero of energy corresponds to the top of the valence band.

and the bonding energy to determine the orbitals into which the fourth electron went into. From the calculated density of states one found that the electron went into the d_{xz} and d_{yz} orbitals. Allowing for different magnetic configurations one finds that the ferromagnetic configuration is metallic while the antiferromagnetic solution is insulating. Comparing the energy in each case, one finds that the ferromagnetic solution has lower energy than the antiferromagnetic solution, though this would depend on the degree of localization. Interestingly as is evident from the charge density plotted in the energy interval upto 1.0 eV below E_f, ine finds that this metallic state is strongly confined to just one monolayer and is in addition 100% spin polarized. This could have a lot of applications, one of them being in thermoelectrics as suggested by Ohta *et al* [36]. Further the metal-insulator transition driven by a modest strain could have applications in two state devices. The work by Verissimo-Alves *et al* [37] found a spin polarized strongly confined metallic state in heterostructures of SrRuO₃ and SrTiO₃. Here

we show that just one monolayer of SrO is sufficient to result in this metallic state. The competing state with an energy 35 meV/Ru higher for the films grown on 1% compressed SrTiO$_3$ substrate is found to be the antiferromagnetic state. In this case, however, one finds that the d$_{xz}$ and d$_{yz}$ states are more localized. This drives a Jahn-Teller distortion in the system, with in-plane bondlengths now found to be equal to 1.98 and 2.0 Å. As a result one finds that the down spin d$_{xz}$ orbital gets occupied at one site, while it is the d$_{yz}$ orbital that is found to be occupied at ther other Ru site. This orbital ordering also drives system insulating.

Let us now examine electronic structure of the four monolayer arrangement, after adding another *RuO$_2$* layer on top of three monolayer. We perform total energy calculations for the four-monolayers structure and it is important to notice from the Table-6.2, that antiferromagnetic solution is stabilized over ferromagnetic with an energy difference of 110 meV. And the films are insulating at the thickness of four monolayers. This seems to be in constrast with experiments. We examine other experimental results.

It has been observed experimentally that thin films of *SrRuO$_3$* exhibit an exchange bias behaviour. Exchange bias effect or exchange anisotropy usually occurs between ferromagnetic and antiferromagnetic regions in contact. This effect has technological importance as the hard magnetic behaviour of antiferromagnetic region could tune the soft magnetic behaviour of ferromagnetic region. In our attempt to explain this phenomena observed in experiments we chose to consider a magnetic configuration in four monolayer thickness with an antiferromagnetic surface and ferromagnetic bulk. And interestingly we find this solution to become lower than the antiferromagnetic solution by 20 meV/Ru atom(Table-6.2). Though the antiferromagnetic surface and ferromagnetic bulk solution is accompanied by a metallic state. Thus making our results compatible with experiments. Performing full structural optimization, the surface layer Ru-O bondlengths follow the same distortion pattern as was the case for two monolayers of *SrRuO$_3$*. Though the sub-surface has different Ru-O bondlengths than the surface layer. Sub-surface layer shows Jahn-Teller type of distortion in the xy-plane, with long and short bondlengths of 2.02 Å and 1.98 Å, while apical bondlengths along plus and minus z-direction are found to be 2.04 Å and 2.06 Å respectively, as shown in the Fig-6.8. We rely on the density of states to
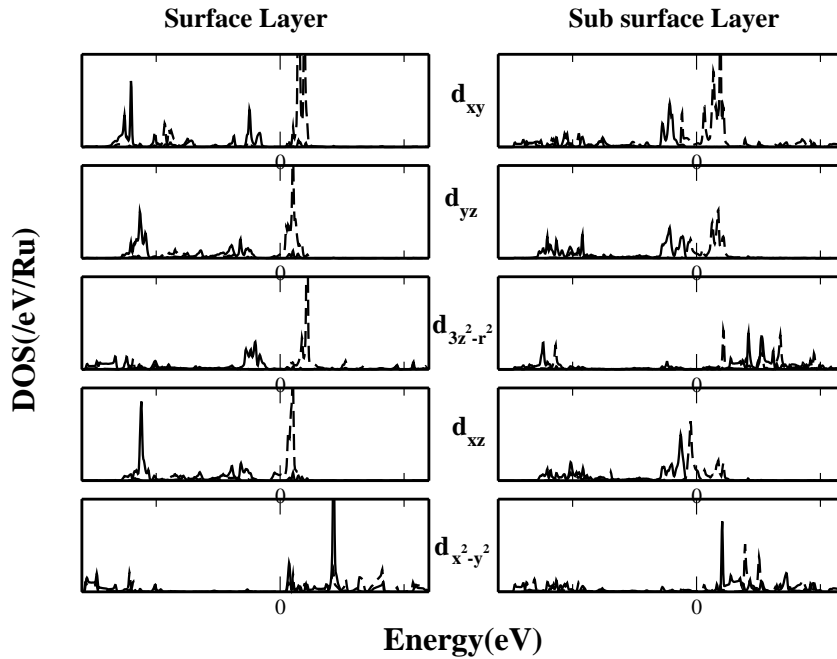
Figure 6.7 The spin-up and spin-down (solid and dashed lines respectively), orbital-projected Ru d partial density of states for the surface(left) and sub-surface(right) RuO_2 layer of four monolayers of *SrRuO₃* grown on *SrTiO₃*. The zero of energy corresponds to the top of the valence band.

understand the behavior of these layers. The surface layer shows similar level ordering as was the case for two monolayers, as the Ru-O bondlength distortions are same as in the two monolayers case. On the other hand for the sub-surface layer two of the shortest bondlengths are in the xy-plane, as a result d_{xy} states go up in energy with respect to the d_{xz} and d_{yz} states. This is confirmed from our calculated Ru d partial density of states for surface and sub-surface layer as shown in the Fig-6.7. Electronic states for the surface layer are more localized than in the sub-surface layer. Ru shows a high-spin state for the surface layer similar to the two monolayer case. Surface layer shows almost insulating character. For the sub-surface layer d_{xz} in spin-down channel gets occupied after the t_{2g} states in the spin-up channel are filled. This leads to a low-spin state accompanied by metallic character.
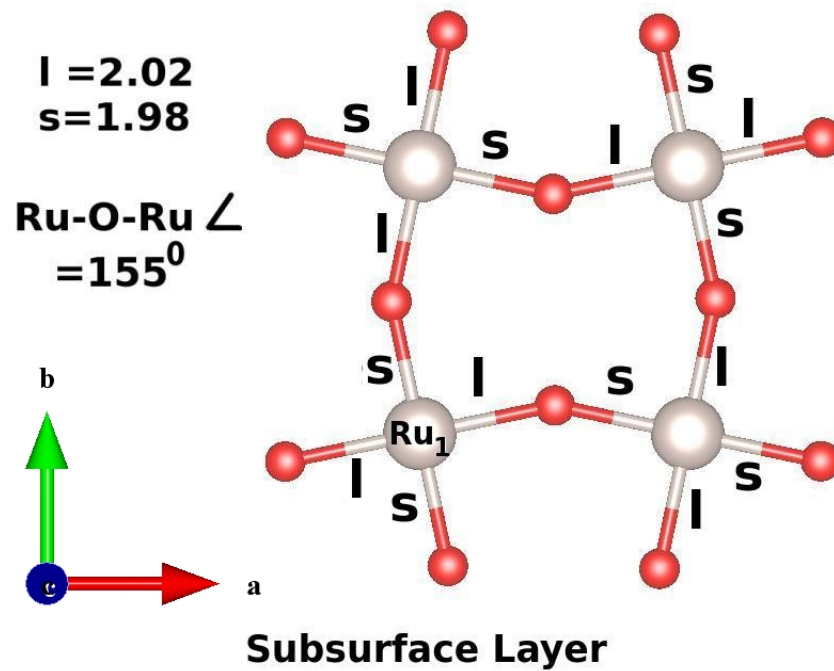
Figure 6.8 Relaxed in-plane a)Ru-O bondlengths in Å and b) angles in degree for the RuO_2 layer of four monolayers of *SrRuO₃* grown on *SrTiO₃*.

6.4 Conclusion

To summarize, ultrathin films of *SrRuO₃* with thickness less than four monolayers are found to be insulating. This metal to insulator transition is accompanied by a change of magnetic state from ferromagnetic to antiferromagnetic. High spin-state of Ru ion is stabilized on the surface, which stabilizes an antiferromagnetic solution for two monolayer case. Insulating state is driven by the antiferromagnetic ordering. Though films of four monolayer thickness have antiferromagnetic surface and ferromagnetic bulk. Metal to insulator transition occurs as a function of thickness at four monolayers.

Bibliography

[1] A. Ohtomo, D. A. Muller, J. L. Grazul, and H. Y. Hwang, Nature (London) **419**, 378 (2002).

[2] A. Ohtomo and H. Y. Hwang, ibid. **427**, 423 (2004).

[3] N. Hur, S. Park, P. A. Sharma, J. S. Ahn, S. Guha, and S. W.Cheong, Nature (London)**429**, 392(2004); J. Wang, J. B. Neaton, H. Zheng, V. Nagarajan, S. B. Ogale, B. Liu, D. Viehland, V. Vaithyanathan, D. G. Schlom, U. V. Waghmare, N. A. Spaldon, K. M. Rabe, M. Wuttig, and R. Ramesh, Science **299**, 1719(2003); T. Kimura, T. Goto, H. Shintani, K. Ishikawa, T. Arima, and Y. Tokura, Nature(London) **426**, 55(2003).

[4] G. A. Prinz, Science, **282**,1660(1998).

[5] C. Chappert, A. Fert, and F. N. Van Dau, Nature Materials, **6** 813(2007).

[6] S. X.Wang and A. M. Taratorin, Magnetic Information Storage Technology, Academic Press, San Diego, Calif, USA(1999.

[7] Z. Shi, C.Wang, X. Liu, and C. Nan, Chinese Science Bulletin,**53**, 2135(2008).

[8] F. Yang, Y. C. Zhou, M. H. Tang et al., Journal of Physics D, **42**, 072004(2009).

[9] A. P. Ramirez, Science **315**, 1377(2007).

[10] Z. Yang, C. Ko, and S. Ramanathan, Annu. Rev. Mater. Res. **41**, 337(2011).

[11] F. L. Marrec, A. Demuer, D. Jaccard, J.-M. Triscone, M. K. Lee, and C. B. Eom, Appl. Phys. Lett. **80**, 2338(2002).

[12] K. S. Takahashi, A. Sawa, Y. Ishii, H. Akoh, M. Kawasaki, and Y. Tokura, Phys. Rev. B **67**, 094413(2003).

[13] W. J. Gallagher and S. S. P. Parkin, IBM J. Res. Dev. **50**, 5(2006).

[14] N. Setter, R. Waser, Acta Mater. **48**, 151(2000).

[15] J. Rondinelli, N. Caffrey, S. Sanvito, N. Spaldin, Phys. Rev. B ,**78**, 155107(2008).

[16] R. Ramesh and D. G. Schlom, Science **296**, 1975 (2002).

[17] H. N. Lee et al., Nature (London) **433**, 395(2005).

[18] B. C. Chakoumakos, S. E. Nagler, S. T. Misture, and H. M. Christen, Physica B **358**,241(1998).

[19] F. He, B. O. Wells, Z.-G. Ban, S. P. Alpay, S. Grenier, S. M.Shapiro, W. Si, A. Clark, and X. X. Xi, Phys. Rev. B **70**, 235405(2004).

[20] J. M. Longo, P. M. Raccah, and J. B. Goodenough, J. Appl. Phys. **39**, 1327(1968)

[21] A. Kanbayasi, J. Phys. Soc. Jpn. **41**, 1876(1976).

[22] B. J. Kennedy, and B. A. Hunter, Phys. Rev. B **58**, 653(1998).

[23] G. Koster, G. Koster, L. Klein, W. Siemons, G. Rijnders, J. Dodge, C. B. Eom, D. Blank, M. Beasley, Rev. Mod. Phys. **84**, 253(2012)

[24] C. H. Ahn, R. H. Hammond, T. H. Geballe, M. R. Beasley, J.-M. Triscone, M. Decroux, O. Fischer, L. Antognazza, and K. Char, Appl. Phys. Lett. **70**, 206(1997).

[25] K. S. Takahashi, M. Gabay, D. Jaccard, K. Shibuya, T. Ohnishi, M. Lippmaa, and J.-M. Triscone, Nature(London) **441**, 195(2006).

[26] I. Zutic, J. Fabian, and S. D. Sarma, Rev. Mod. Phys. **76**, 323 (2005).

[27] N. A. Spaldin and M. Fiebig, Science **309**, 391(2005).

[28] D. Toyota, I. Ohkubo, H. Kumigashira, M. Oshima, M. Lipmaa,M. Takizawa, A. Fujimori, K. Ono, M. Kawasaki, and H. Koinuma, Appl. Phys. Lett. **87**, 162508(2005).

[29] J. Xia, W. Siemons, G. Koster, M. R. Beasley, and A. Kapitulnik, Phys. Rev. B **79**, 140407 (R) (2009).

[30] A. T. Zayak, X. Huang, J. B. Neaton, and Karin M. Rabe, Phys. Rev. B, **74**, 094104(2006).

[31] H. D. Kim, H. J. Noh, K. H. Kim, and S. J. Oh, Phys. Rev. Lett. **93**, 126404(2004).

[32] P. B. Allen, H. Berger, O. Chauvet, L. Forro, T. Jarlborg, A. Junod, B. Revaz, and G. Santi, Phys. Rev. B **53**, 4393(1996).

[33] P. Kostic, Y. Okada, N. C. Collins, Z. Schlesinger, J. W. Reiner, L. Klein, A. Kapitulnik, T. H. Geballe, and M. R. Beasley, Phys. Rev. Lett. **81**, 2498(1998).

[34] K. Maiti and R. S. Singh, Phys. Rev B **71**, 161102(R)(2005).

[35] P. Mahadevan, F. Aryasetiawan, A. Janotti, and T. Sasaki, Phys. Rev. B, **80**, 035106 (2009).

[36] H. Ohta, S. Kim, Y. Mune, T. Mizoguchi, K. Nomura, S. Ohta, T. Nomura, Y. Nakanishi, Y. Ikuhara, M. Hirano, H. Hosono, K. Koumoto, Nature Mat. **6**, 129(2007).

[37] M. Verissimo-Alves, P. Garcia-Fernandez, D. I. Bilc, P. Ghosez, J. Junquera, Phys. Rev. Lett. **108**, 107003(2012).

Chapter 7

Strong Jahn-Teller distortions in ultrathin films of cubic SrVO$_3$

7.1 Introduction

Modification of electronic properties of transition metal oxides in reduced dimensionality such as thin films, heterostructures and superlattices with very precise interfaces at atomic level is one of the foremost areas of material research at present [1–3]. A systematic tuning of various phenomena, such as ferroelectricity, magnetic order and superconductivity has been achieved by several control parameters which includes the overlayer thickness, composition along with the substrate imposed epitaxial strain. The role played by static lattice distortions occuring at the interface affect some of these phenomena and this has been studied already in literature [4–7]. It is not just the physical properties of systems that evolve as a function of thickness, one finds that the structure also evolves as a function of thickness. The substrate constrains the lattice constant of the overlayers and this in turn results in the realization of crystal structures which have not been observed in the bulk. An additional dimension comes in when one has few monolayers. This is an increase in the degree of localization of the electrons as the full bandwidth is not formed. This takes the system which is metallic in the bulk in addition to having full cubic symmetry to one in which electron-phonon couplings get enhanced, resulting in structural distor-

tions not observed in the bulk. The dynamical electron-phonon interaction tuned electronic properties of artificial layered structures and thin films have not been studied in detail yet. Though their crucial role in phase behavior of bulk transition metal oxides has been suggested [8–10].

High temperature superconductor YBa$_2$Cu$_3$O$_7$ and ferromagnetic metal La$_{1-x}$Ca$_x$MnO$_3$, both in their bulk form have been studied and it has been found that electron-phonon interaction and its interplay with electronic correlations dictates the competing superconducting behavior and the charge density wave states in YBa$_2$Cu$_3$O$_7$ [10–12], while metallic and polaronic insulating behavior of La$_{1-x}$Ca$_x$MnO$_3$ [8, 13, 14]. But in the bulk form, one does not have a substantial control over this interplay. As it has been discussed in the introduction, reduced dimensionality as possible in thin films and superlattices hold a lot of promises in order to have a control over electronic interaction strengths. Driza *et. al.* [15] did the Raman scattering studies of lattice dynamics of superlattices of YBa$_2$Cu$_3$O$_7$/La$_{1-x}$Ca$_x$MnO$_3$. They found that MnO$_6$ octahedra in La$_{1-x}$Ca$_x$MnO$_3$ undergo line-shape anamolies which are induced by the superconducting behavior of YBa$_2$Cu$_3$O$_7$. In addition to the elecron-phonon coupling associated with the rotational modes of MnO$_6$ octahedra was found to scale linearly with the thickness of YBa$_2$Cu$_3$O$_7$ layers over several tens of nanometers.

Not only superlattice geometries but transition metal oxides in the thin film regime have also been found to exhibit completely different behavior from their bulk counterparts. For instance an antiferromagnetic insulating phase is found in SrRuO$_3$ [16] which is otherwise metallic and ferromagnetic in the bulk. LaCoO$_3$ which does not exhibit any type of long-range order in the bulk form, is found to exhibit ferromagnetism in epitaxially grown thin films of the material [17, 18]. The bulk nickelates which have a very interesting phase diagram which can be tuned with a change in the Ni-O-Ni angle [19], also are an interesting system in the thin film form where they exhibit metal insulator transitions [20–23] as a function of thickness.

The metal-insulator transition in transition metal oxides is a very important phenomena from fundamental solid state physics as well as an application point of view [24]. From Mott-Hubbard theory [25, 26], one can have a handle on this metal-insulator transition by tuning the magnitudes of the on-site Coulumb correlation strength U as well as the d orbital bandwidth W. In most of the examples

of the bulk systems metal-insulator transition has been studied in a great deal by chemical substitution of constituent ions with ones having a smaller ionic radii. The bandwidth W can be controlled by the distortion that arises from the substitution and consequent changes in the transition metal-oxygen-transition metal bond angles [24].

Ultrathin films of $SrVO_3$ where V has a valence of 4+ and corresponds to $3d^1$ configuration. This system is an ideal system for studying the dimensional-crossover-driven metal-insulator transition. This is because of the robust metallic states found in bulk $SrVO_3$. The bandwidth controlled metal-insulator transition has been discussed in the case of $SrVO_3$. With Ca substitution ($Ca_{1-x}Sr_xVO_3$), $SrVO_3$ remains metallic in the entire range of x and V-O-V angles change from $180°$ to $160°$ [27,28]. Yoshimatsu *et. al.* [28] grew thin films of $SrVO_3$ on $SrTiO_3$ substrate and they found that the $SrVO_3$ overlayers undergo a metal-insulator transition with the decreasing film thickness(Fig. 7.1). And the origin they offered for this metal-insulator transition at the thickness of two monolayer was the reduction in the bandwidth resulting from the dimensional crossover.

In this work we re-examine the origin of metal-insulator transition that has been observed experimentally by Yoshimatsu *et. al.* [28]. Where a metal-insulator transition was observed with decreasing thickness. In spite of bulk $SrVO_3$ being a bulk metal which has a cubic crystal structure, one finds significant Jahn-Teller distortions in $SrVO_3$ at the few monolayers limit. We examine the origin of these distortions as well as discuss their depth dependence.

7.2 Methodology

Experimentally films of $SrVO_3$ [28] have been grown on $SrTiO_3$ substrates layer by layer. To make comparison with experiment we mimic the substrate by considering a symmetric slab consisting of 11 layers of SrO/TiO_2. The terminal layer of the substrate is taken to be TiO_2 on which SrO/VO_2 layers are grown alternately. The in-plane lattice constant is fixed to the experimental value for $SrTiO_3$ which is 3.905 Å. The out of plane lattice constant was allowed to find its minimum energy value. We did allow for tilts of the TiO_6 as well as the VO_6 octahedra, a distortion observed (see Fig.7.2) in the low
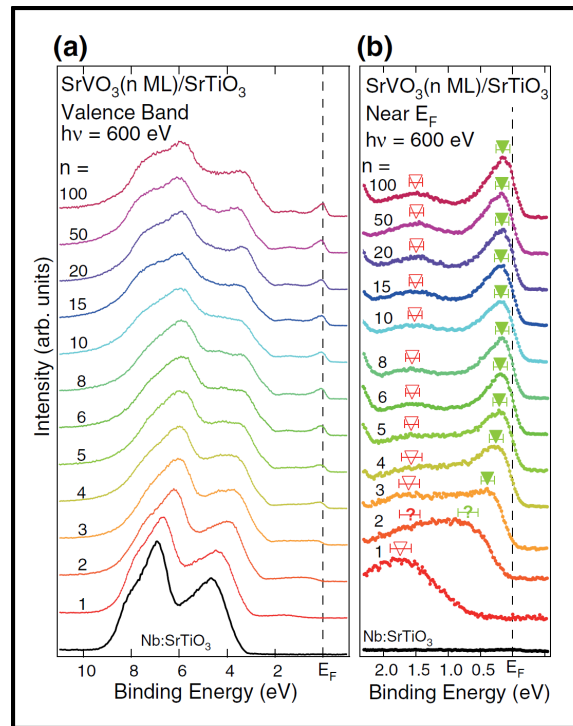
Figure 7.1 (a) In situ valence band spectra(photo emission) of SrVO$_3$ thin films grown on SrTiO$_3$ substrates by digitally controlling the film thickness. (b) Photo Emission Spectra spectra near E$_F$.

Fig. ref: Phys. Rev. Lett., **104**, 147601 (2010).

temperature structure of SrTiO$_3$ [29].
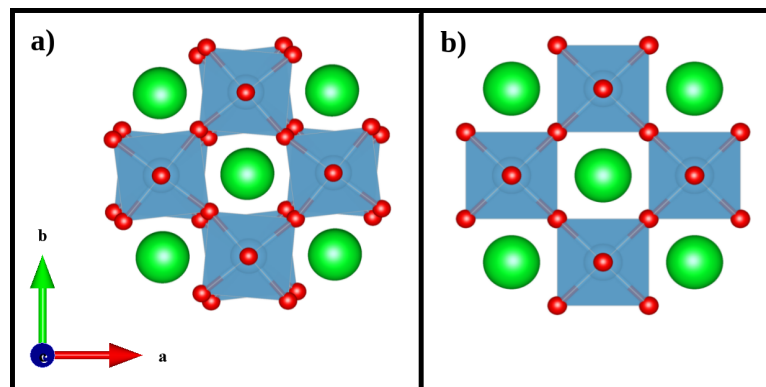
Figure 7.2 SrTiO$_3$ structure a) at low temperature, denoted by $a^0a^0a^-$ and b) at growth temperature (cubic).

Internal positions were allowed to relax in the structure considered to their minimum energy value.

The electronic structure of these systems was calculated within a plane wave pseudopotential implementation of density functional theory in VASP [30] using GGA [31] for the exchange correlation. Correlation effects at V were treated within GGA+U scheme using the scheme of Dudarev [32]. A U_{eff} of 2.2 eV [33] was used on V. A vacuum of 15 Å was considered to minimize interaction between slabs in the periodic geometry of slabs that we were forced to consider within the implementation of DFT that we use. A k-point mesh of $4 \times 4 \times 1$ was used for solving the electronic structure self-consistently, while it was increased to $6 \times 6 \times 1$ for the calculation of the density of states.

7.3 Results & Discussion

The electronic structure of bulk $SrVO_3$ was examined within GGA and GGA+U. Within GGA, $SrVO_3$ is found to be a nonmagnetic metal as shown in the Fig. 7.4(a), which is consistent with the experiments [28]. In Fig. 7.3, we show the total density of states as well as V-d and O-p orbital projected density of states. The system is found to be a nonmagnetic metal and the three t_{2g} orbitals are degenerate. But with U=2.2 eV on V ion within GGA+U, $SrVO_3$ is barely metallic. V ions are ferromagnetic in xy-plane, while stacked antiferromagnetically along z-direction *i.e.* A-type antiferromagnetism. These results suggest that $SrVO_3$ even in the bulk form is at the brink of a magnetic instability and future experiments should be carried out to examine this hypothesis.

Similar calculations were performed for two monolayers of $SrVO_3$ on $SrTiO_3$, and the ground state was found to be insulating. These results are consistent with recent experiments [28] that find a thickness dependent insulator metal transition. An unusual aspect that emerges from the present set of calculations is that a large contribution to the energy lowering in the insulating state comes from large structural distortions which allow the stabilization of Jahn-Teller distortions in the overlayers of $SrVO_3$.

Let us first examine the $SrVO_3$ films in two monolayers limit. The origin of observed metal-insulator transition is traced to the competing distortions that the surface V atoms encounter. As we are growing the films on $SrTiO_3$ which has a larger lattice constant, the in-plane lattice constant is fixed by
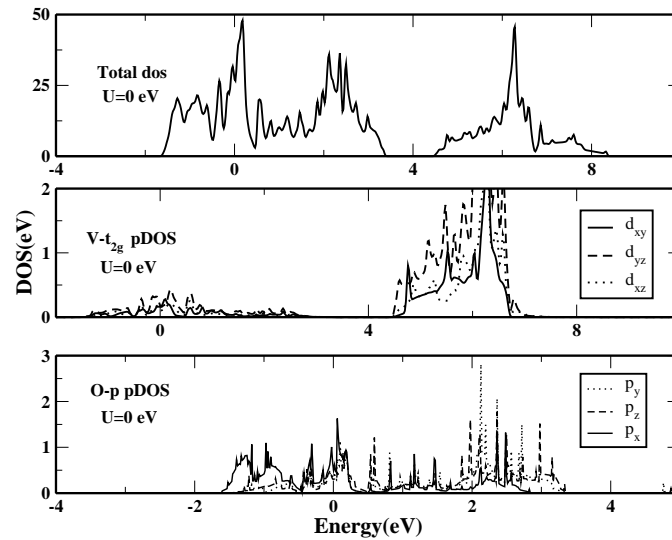
Figure 7.3 a) Total Density of states for SrVO$_3$ b) partial density of states for V-t$_{2g}$ and for c) O-p orbitals, with U=0 eV on V ion.
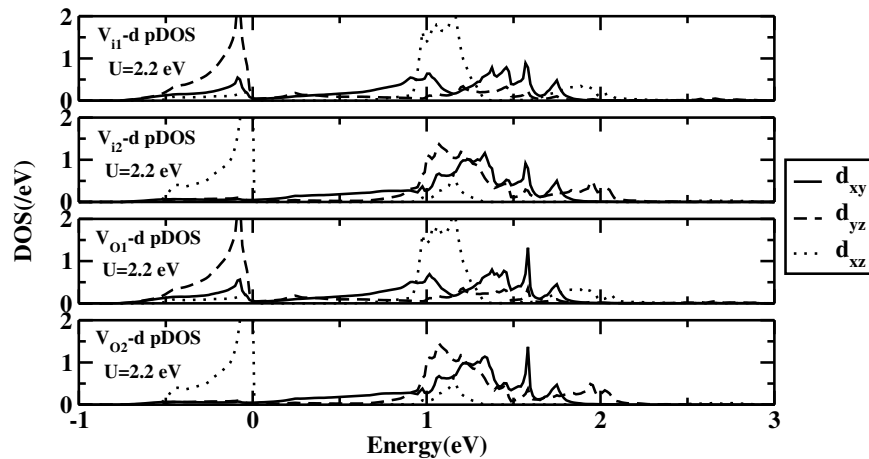
Figure 7.4 Partial density of states with U=2.2 eV for V-t$_{2g}$ in xy-plane(Vi1,Vi2) and along z-direction(Vo1,Vo2).

the substrate and is larger than that found in bulk SrVO$_3$, where it is 3.84 [34]. The out of plane lattice constant is therefore compressed. This results in a shorter V-O bond in the z-direction as shown in Fig. 7.5(a). This effect alone would result in a lifting of the degeneracy of the d orbitals with d_{xy} orbital having a lower energy than the d_{yz} and d_{xz} orbitals. On the other hand the coordination of the surface

V atom is reduced from 6 to 5 as shown in Fig. 7.5(b).
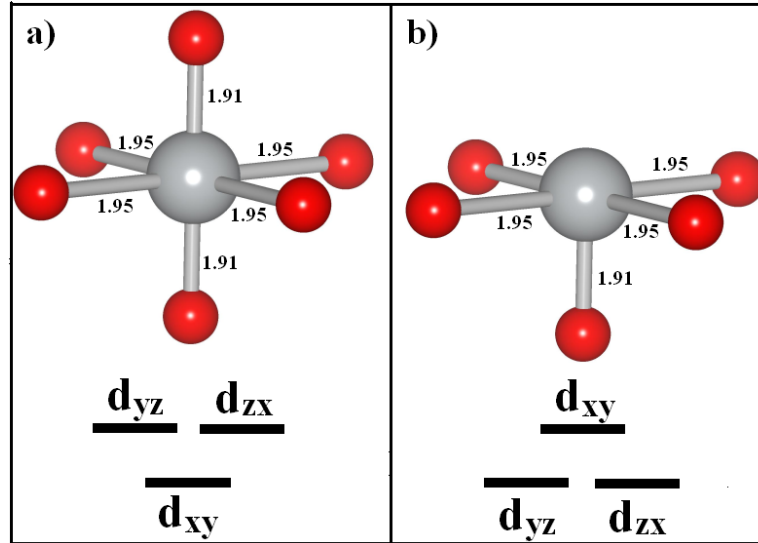
Figure 7.5 Distortions and crystal field splitting of the t_{2g} orbitals for (a) a VO_6 octahedron under tensile strain, (b) a surface VO_5 unit, Large(small) and grey(red) spheres denote V (O) atoms.

As also discussed in the chapter-4, the oxygen atom above the V atom in the positive z-direction is missing. This would result in a lifting of degeneracy of the three-fold degenerate d orbitals with t_{2g} symmetry to doubly degenerate levels comprising of d_{xz} and d_{yz} orbitals that are found lower in energy, and d_{xy} orbital found higher in energy. So the lifting of degeneracy of the d orbitals has opposing effects from the missing surface oxygen atom and the compressed V-O bond. V in $SrVO_3$ is 4+, so there is just one electron associated with the V^{4+} ion. An insulating state is expected in the case as discussed in Fig-7.5(a) while a metallic one as in the case shown in Fig-7.5(b). We performed calculations considering the centrosymmetric structure and an analysis of V-d partial density of states (see Fig. 7.6) finds the scenario as discussed in Fig-7.5(b).

However on performing a complete structural optimization, we find an orbital ordering transition driven by Jahn-Teller distiortions. V^{4+} ion in $SrVO_3$ corresponds to d^1 configuration, and thus is Jahn-Teller active ion. The system gains energy by stabilizing Jahn-Teller distortions and by removing the degeneracy of d_{xz} and d_{yz} orbitals. Stabilized distortions are of the type as shown in Fig-7.7(b), where two of the V-O bondlengths are elongated to become 2.08 Å and two of them are contracted
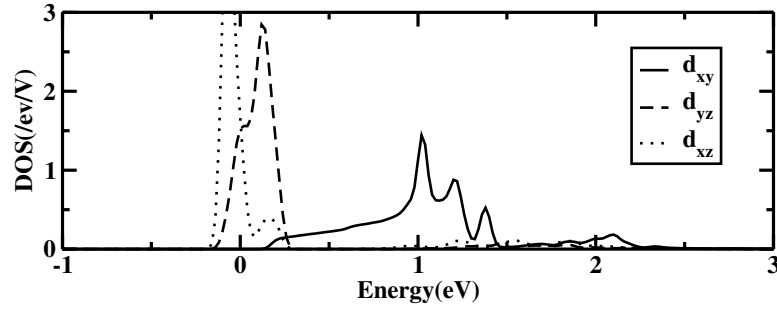
Figure 7.6 Partial density of states for V-t_{2g} states in surface VO_2 layer with broken oxygen octahedra.

to become 1.82 Å. This distortion would lead to a degeneracy lifting of d_{xz} and d_{yz} orbitals with d_{xz} getting occupied at one site and d_{yz} at other. The observed Jahn-Teller distortions drives the system insulating. While there is no report of magnetism in bulk SrVO₃, one finds that as a result of reduced dimensionality, V atoms at the surface favor magnetic ground state with exchang splittings as large as 3.0 eV. As a result of the Jahn-Teller distortions, d_{xz} orbital at one V site while d_{yz} at the next holds one electron. While one of the two orbitals is occupied, the effect of coulumb interaction move the states associated with the unoccupied orbitals to higher energies, thereby opening up a gap. Examining for long range magnetic order, we find that for the two monolayer case, the ferromagnetic state is stabilized by 60 meV/V atom. In Fig. 7.8 we show, V-d partial density of states where only majority spin channels for t_{2g} orbitals are plotted. An analysis of DOS, clearly shows that at one V site d_{xz} orbital lies lower in energy with respect to the d_{yz} and d_{xy} orbitals (Fig-7.8a), while at next it is d_{yz} orbital which is lower in energy than the d_{xy} and d_{xz} orbitals. So Jahn-Teller distortions found in V-O bonglenghts in the xy-plane leads to an orbital ordering which could explain the stabilization of ferromagnetic configuration over the antiferromagnetic one.

We went on to examine SrVO₃ films by increasing the film thickness to three monolayers by an addition of SrO layer. After performing full structural relaxation with other computational details as discussed above, the Jahn-Teller distorted V-O bondlengths become 1.88 Å and 2.02 Å, as shown in Fig. 7.7(c). Increasing the SrVO₃ film thickness to three monolayers we find that still ferromagnetism is stabilized, however the energy difference between the ferromagnetic and the antiferromagnetic con-
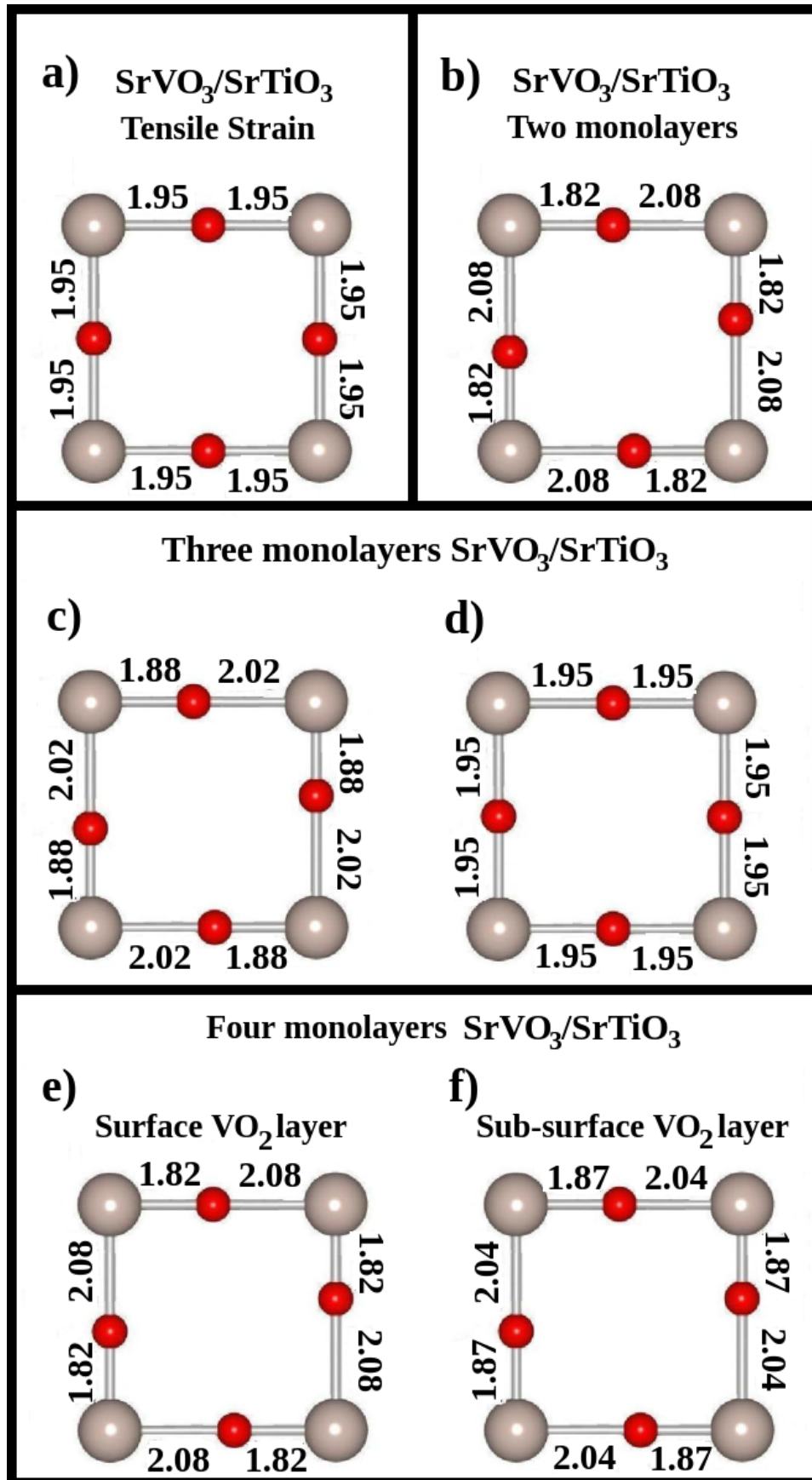
Figure 7.7 V-O bondlengths in SrVO$_3$ films for: a) tensile strain b) two monolayers c) three monolayers with AFD SrTiO$_3$ substrate d) three monolayers on cubic SrTiO$_3$ substrate, and e) Surface VO$_2$ layer f) Sub-surface VO$_2$ layer of four monolayers case.
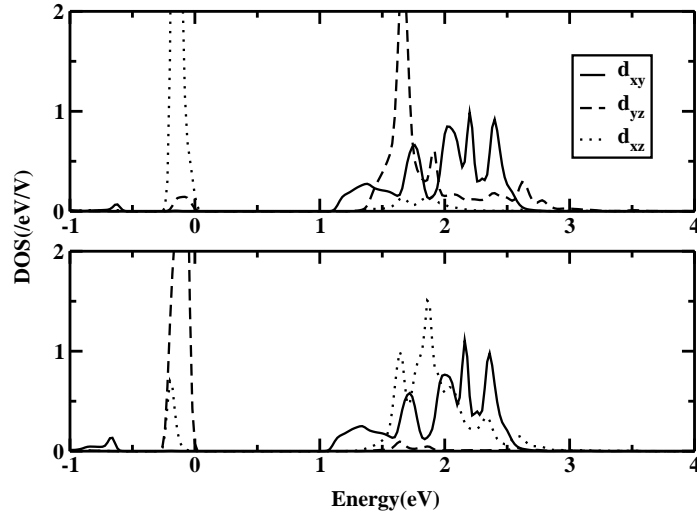
Figure 7.8 Partial DOS for t_{2g} states on two neighboring V sites, in two monolayers of SrVO₃ on SrTiO₃ case.

figuration is reduced to 25 meV/V atom. As shown in the Fig. 7.9 similar to the case of two monolayers, Jahn-Teller distortions leads to an orbital ordering in the xy-plane, at neighboring V sites in the VO₂ layer, and hence a ferromagnetic ground state is stabilized.

In the four monolayers thickness limit, after structural optimization, the Jahn-Teller distorted V-O bondlengths are found to be 1.82 Å and 2.08 Å for the surface VO₂ layer, while 1.87 Å and 2.04 Å for the sub-surface VO₂ layer (see Fig. 7.7e, 7.7f). One notices that as we go for thicker films of SrVO₃, the electron-phonon coupling associated with these distortions decays when the system has not yet evolved to the bulk. In addition, the terminating layer of the films also dictates these distortions, as the presence of a SrO layer at the surface gives rise to a non-monotonous trend for the decay of electron-phonon coupling associated with the Jahn-Teller distortions with the increment in film thickness.

We also explore if the substrate structure could influence these distortions in SrVO₃ overlayers. The low temperature structure of SrTiO₃ has antiferrodistortive distortions of TiO₆ octahedra, denoted by $a^0a^0a^-$ in Glazer notation, as discussed in the introduction. While at the growth temperature SrTiO₃ is cubic. For the VO₂ layer terminated ultrathin films of SrVO₃, we found that structure of the SrTiO₃
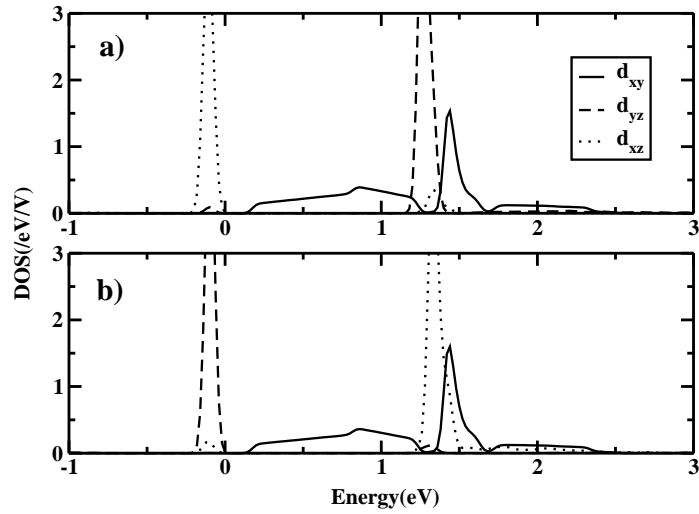
Figure 7.9 Partial DOS for t_{2g} states on two neighboring V sites, in two monolayers of $SrVO_3$ on $SrTiO_3$ case.

substrate does not influence the observed Jahn-Teller distortions in the VO_2 layer. But for the SrO layer terminated ultrathin films of $SrVO_3$, as we have considered the case of three monolayers of $SrVO_3$ on cubic structure of $SrTiO_3$ substrate, surprisingly Jahn-Teller distortions in the VO_2 layer vanishes with V-O bonglengths to become 1.95 Å. So these results suggest that at the growth temperatures one could have a different structure for the $SrVO_3$ overlayers which could change as a function of temperature.

7.4   Conclusion

To Summarize, we have explored the dimensional crossover driven metal to insulator transition in the ultrathin films of a metallic oxide $SrVO_3$, and we find strong structural modifications arising from the surface effects. Which decay with increasing film thickness. Additionaly the terminating layer as well as the substrate structure plays an important role in the structural effects in the $SrVO_3$ overlayers.

Bibliography

[1] J. Mannhart and D. G. Schlom, Science, **327** 1607 (2010).

[2] H. Y. Hwang, Y. Iwasa, M. Kawasaki, B. Keimer, N. Nagaosa and Y. Tokura, Nature Materials, **11**, 103 (2012).

[3] P. Yu, W. Luo, D. Yi, J. X. Zhang, M. D. Rossell, C.-H. Yang, L. You, G. Singh-Bhalla, S. Y. Yang, Q. He, Q. M. Ramasse, R. Erni, L. W. Martin, Y. H. Chu, S. T. Pantelides, S. J. Pennycook and R. Ramesh, PNAS, **109**, 9710 (2012).

[4] S. A. Pauli, S. J. Leake, B. Delley, M. Björck, C. W. Schneider, C. M. SchlepÃijtz, D. Martoccia, S. Paetel, J. Mannhart, and P. R. Willmott, Phys. Rev. Lett., **106**, 036101 (2011).

[5] V. Y. Butko, Natasha Bozovic, Z. Radovic and I. Bozovic, Advanced Materials **21**, 3644(2009).

[6] J. Hoppler, J. Stahn, Ch. Niedermayer, V. K. Malik, H. Bouyanfif, A. J. Drew, M. Rössle, A. Buzdin, G. Cristiani, H.-U. Habermeier, B. Keimer and C. Bernhard, Nature Materials, **8** 315(2009).

[7] R. Pentcheva, and W. E. Pickett, Phys. Rev. Lett. **102** 107602 (2009).

[8] D. M. Edwards, Adv. Phys., **51** 1259 (2002).

[9] E. Dagotto, T. Hotta, and A. Moreo, Phys. Rep., **344**, 1-153 (2001).

[10] O. Gunnarsson, and O. Rösch, J. Phys. Condens. Matter **20**, 043201 (2008).

[11] T. Wu, H. Mayaffre, S. Kramer, M. Horvatic, C. Berthier, W. N. Hardy, R. Liang, D. A. Bonn and M. Julien, Nature 477, **191**(2011).

[12] M. Raichle, D. Reznik, D. Lamago, R. Heid, Y. Li, M. Bakr, C. Ulrich, V. Hinkov, K. Hradil, C. T. Lin, and B. Keimer, Phys. Rev. Lett., **107**, 177004 (2011).

[13] F. Rivadulla, M. Otero-Leal, A. Espinosa, A. de Andres, C. Ramos, J. Rivas, and J. B. Goodenough, Phys. Rev. Lett. **96**, 016402(2006).

[14] M. B. Saloman and M. Jaime, Rev. Mod. Phys., **73**, 583(2001).

[15] N. Driza, S. Blanco-Canosa, M. Bakr, S. Soltan, M. Khalid, L. Mustafa, K. Kawashima, G. Christiani, H-U. Habermeier, G. Khaliullin, C. Ulrich, M. Le Tacon and B. Keimer, Nature Materials **11**, 675(2012).

[16] P. Mahadevan, F. Aryasetiawan, A. Janotti and T. Sasaki, Phys. Rev. B **80**, 035106 (2009).

[17] D. Fuchs, C. Pinta, T. Schwarz, P. Schweiss, P. Nagel, S. Schuppler, R. Schneider, M. Merz, G. Roth, and H. v. Lohneysen, Phys. Rev. B **75**, 144402 (2007).

[18] D. Fuchs, E. Arac, C. Pinta, S. Schuppler, R. Schneider, and H. v. LÃűhneysen, Phys. Rev. B **77**, 014434 (2008).

[19] Jian Liu, M. Kareev, B. Gray, J. W. Kim, P. Ryan, B. Dabrowski, J. W. Freeland, and J. Chakhalian, Appl. Phys. Lett. **97**, 142110 (2010).

[20] J. L. Garcia-Munoz, J. Rodriguez-Carvajal and P. Lacorre, Phys. Rev. B **50**, 978 (1994).

[21] J. L. Garcia-Munoz, J. Rodriguez-Carvajal, P. Lacorre and J. B. Torrance, Phys. Rev. B **46**, 4414 (1992).

[22] X. Obradors, L. M. Paulius, M. B. Maple, J. B. Torrance, A. I. Nazzal, J. Fontcuberta and X. Granados, Phys. Rev. B **47**, 12353 (1993).

[23] P. C. Canfield, J. D. Thompson, S-W. Cheong and L. W. Rupp, Phys. Rev. B **47**, 12357(1993).

[24] M. Imada, A. Fujimori, and Y. Tokura, Rev. Mod. Phys. **70**, 1039 (1998).

[25] J. Hubbard, Proc. R. Soc. A **276**, 238 (1963).

[26] A. Georges, G. Kotliar, W. Krauth, and M. J. Rozenberg, Rev. Mod. Phys. **68**, 13 (1996).

[27] I. H. Inoue, O. Goto, N. E. Hussey and M. Ishikawa Phys. Rev. B **58**, 4372 (1998).

[28] K. Yoshimatsu *et al.*, Phys. Rev. Lett. **104**, 147601 (2010).

[29] F. W. Lytle, J. App. Phys. **35**, 2212 (1964).

[30] G. Kresse, and J. Furthm*ü*ller, Phys. Rev. B. **54**, 11169 (1996); G. Kresse, and J. Furthm*ü*ller, Comput. Mat. Sci. **6**, 15 (1996).

[31] J. P. Perdew, in Electronic Structure of Solids, edited by P. Ziesche and H. Eschrig (Akademie Verlag, Berlin, 1991), p. 11.

[32] S.L. Dudarev *et al.* Phys. Rev. B **57**, 1505 (1998).

[33] F. Aryasetiawan *et al.* Phys. Rev. B **70**, 195104 (2004).

[34] J. G. Jaea *et al.* **34**, 289 (1999).

Chapter 8

Future direction and outlook

Transition metal oxides exhibit a range of remarkable properties as a result of very strong interplay between charge, orbital and spin degrees of freedom and consequent modification and variation in the associated electronic interaction strengths. Reduced dimensionality such as in thin films and heterostructures provides one with additional handle to have a control over this interplay which has been discussed in various preceeding chapters. In this thesis we have considered few examples of transition metal oxides, which show completely different behavior in reduced dimensionality compared to their bulk form. In the following we discuss the future direction and outlook of this thesis.

- In **chapter-3** we have examined the origin of ferromagnetism in epitaxially grown films of $LaCoO_3$, considering both compressive and tensile strain. The experimental observation of ferromagnetism is reproduced and the development of ferromagnetic order with thickness are aspects which have not been examined theoretically and future work should consider these aspects also.

- In **chapter-4** we have examined the nature of distortions in ultrathin films of a metallic oxide $SrCrO_3$. These theoretical predictions must be examined experimentally and we hope the experiments will stimulate activity in this area. Limited by the computational demands of the calculations, we have calculated the electronic structure only upto four monolayers. Further work should examine the evolution of structure, magnetism and electronic structure as a function of

film thickness.

- In **chapter-5** we have examined superlattices of $BaTiO_3$ in which sandwich layers of $BaVO_3$ and $BaCrO_3$ are introduced. Surprisingly we find the possibility of a ferromagnetic and ferroelectric insulator in $BaVO_3$ sandwiched superlattices. This claim has to be verified experimentally. Further microscopic analysis of the electronic structure of these systems would help us to identify other possible candidates.

- In **chapter-6** we have examined the unusual insulating state in $SrRuO_3$ grown on $SrTiO_3$ substrate at the three monolayer limit as well as the two dimensional electron gas realized when the films are subjected to further compressive strain. These have important implications on device physics using oxides.

- In **chapter-7** we have examined the strong structural modifications in ultrathin films of $SrVO_3$. Further experimental verification is needed as well as additional theoretical modelling to understand the thickness dependence of the electron-phonon coupling.